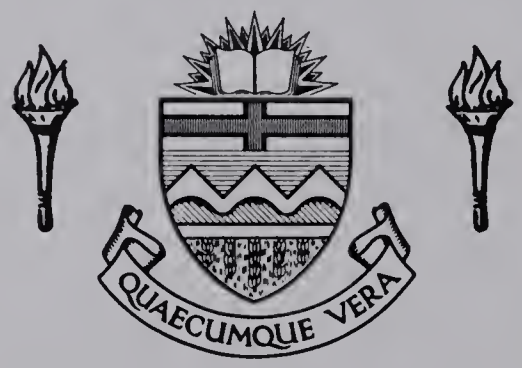

THE UNIVERSITY OF ALBERTA

BEAM-FOIL STUDIES OF THE OXYGEN SPECTRUM

BY

© CHII-CHAN LIN

A THESIS

SUBMITTED TO THE FACULTY OF GRADUATE STUDIES AND RESEARCH

IN PARTIAL FULFILLMEMT OF THE REQUIRMENTS FOR THE DEGREE

OF DOCTOR OF PHILOSOPHY

DEPARTMENT OF PHYSICS

EDMONTON, ALBERTA

FALL, 1971

UNIVERSITY OF ALBERTA

FACULTY OF GRADUATE STUDIES AND RESEARCH

The undersigned certify that they have read, and recommend to the Faculty of Graduate Studies and Research for acceptance, a thesis entitled BEAM-FOIL STUDIES OF THE OXYGEN SPECTRUM submitted by Chii-Chan Lin in partial fulfillment of the requirements for the degree of Doctor of Philosophy.

ABSTRACT

The beam-foil technique has been used to study the spectrum in the wavelength range 370-5000 Å, produced by an O_2^+ beam of energy between 0.6 and 1.5 MeV. Radiative lifetimes of the excited electronic states which have been measured are compared with other experimental values and theoretical calculations wherever available. Seventeen new lines have been observed, which are identified by the use of a computer program. The possibilities of cascading from higher levels for each multiplet and blending for each line are discussed. The systematic trends of absorption oscillator strengths in isoelectronic sequences involving some of the observed oxygen transitions are discussed.

The beam velocity has been measured directly from the radiating beam by observing the Doppler shifts produced in the emitted spectrum lines. The variation of line intensity with incident beam energy has been used for the charge state identifications. The charge deflection method has also been attempted for more rigorous charge identifications in the visible region. Photon-counting techniques have been used for most of the experimental work.

ACKNOWLEDGEMENTS

I would like to thank my supervisor, Dr. E. H. Pinnington, for the initiation of and his participation in this project. His guidance and encouragement through the past several years have been especially instructive.

I also wish to thank Dr. J. A. Kernahan for many suggestions and assistance in the data acquisition, and Dr. D. J. G. Irwin for many valuable discussions, which have greatly improved the results of this project.

I would also like to express my gratitude to Dr. G. R. Freeman of the Radiation Research Committee for the use of the Van de Graaff accelerator. Special thanks are due to Messrs. R. J. Gardner and F. W. Bach for their technical assistance in the operation of the accelerator.

I am particularly grateful to Mr E. A. Foster for the construction and modification of the various chambers used in these experiments. Mr. N. Riebeek is also to be thanked for his help in such matters.

My gratitude also extends to Messrs. A. E. Livingston and G. Finley and Miss S. Dorper for their enthusiastic help in taking data.

Finally, I thank Mrs. A. Pang for her patience in typing this thesis.

TABLE OF CONTENTS

LIST OF TABLES

LIST OF ILLUSTRATIONS

LIST OF ILLUSTRATIONS (Continued)

CHAPTER I

INTRODUCTION

1.1 Necessity for Radiative Lifetime Measurements

In the determination of the composition of plasmas, stellar atmospheres and nebulae it is necessary to know the oscillator strengths, or f-values, of radiative transitions from excited states of neutral and ionized species of atoms. The f-value is determined by the quantum mechanical wavefunctions of the two states involved in the transition. For a transition from a state i to a state j, the f-value for the transition, f_{ij}, is given by (Di 63a)

$$f_{ij} = \frac{8\pi^2}{3h} m\nu_{ij} \vec{r}_{ij} \vec{r}^{*}_{ij} \qquad (1.1)$$

where h = Planck's constant

m = electron mass

ν_{ij} = frequency of the transition $i \rightarrow j$

and $\vec{r}_{ij} = \int \psi_i \vec{r} \psi_j^* d\tau$ (for electric dipole transitions)

The intensity of the spectrum line is then given by

$$I = \int I_\nu d\nu = \frac{1}{4\pi} N_i A_{ij} \ell h\nu_{ij} \qquad (1.2)$$

where N_i = number density of atoms in state i

ℓ = thickness of emitting layer (supposed optically thin)

A_{ij} = Einstein transition probability.

The Einstein transition probability, A_{ij}, is related to the f-value by the relation (Di 63b)

$$A_{ij} = \frac{8\pi^2 \nu_{ij}^2 e^2}{mc^3} f_{ij} \qquad (1.3)$$

Many methods have been tried to determine experimentally the f-values of important spectrum lines, and an excellent review has been given by Foster (Fo 64). Few accurate measurements have been attained because of difficulty in the determination of the number density of atoms, N_i ; and in general only neutral atoms have been excited in the source.

To avoid the necessity of measuring the number density of atoms, the lifetimes of the excited states can be determined and the oscillator strengths calculated according to the equation,

$$\frac{1}{\tau_i} = \sum_j A_{ij} = \frac{8\pi^2 e^2}{mc^3} \sum_j \nu_{ij}^2 f_{ij} \qquad (1.4)$$

If one of the transitions is dominant (denoted by $i \rightarrow j$)

then $$\frac{1}{\tau_i} = \frac{8\pi^2 e^2}{mc^3} \nu_{ij}^2 f_{ij} \qquad (1.5)$$

1.2 Earlier Methods for Radiative Lifetime Measurements

Before the development of beam-foil spectroscopy, two major techniques were used for lifetime measurements: the phase shift technique and the delayed coincidence technique.

In the phase shift technique (Ma 29, Ma 31, Br 62, Br 63), the excitation of the atoms is achieved by exposing the gas or vapor to a sinusoidally pulsed source of ultraviolet light, electrons or protons. The resulting fluorescence has modulation of the same form as the exciting signal with the same frequency but is delayed by a phase angle, θ, which is related to the lifetime, τ, by (Br 63, Fo 64)

$$\tan \theta = 2\pi f\tau \qquad (1.6)$$

where f = modulation frequency of signal. Thus, the lifetime can be obtained by measuring the phase shift between the excitation and the fluorescence.

The time resolution of the technique is limited by the resolution of the oscilloscope used in the observation; Smith (Sm 70) reported a ± 0.2 nsec resolution. No highly ionized atoms have been excited significantly in the fluorescence and hence lifetime measurement for highly ionized species has been unsuccessful by this technique.

The delayed coincidence technique (Kl 66, Ka 67, Ni 68) uses pulses of very short duration to excite the electronic

states of interest. The distribution of the fluorescence signal as a function of time after the excitation signal represents the decay of the upper level involved in the transition. To measure the time distribution of the fluorescence signal, the excitation and fluorescence signals are fed to a time-to-pulse-height converter. The excitation is used to start, and the fluorescence signal to stop, a signal in the converter. The time which the fluorescence signal occurs after the excitation is converted to pulse-height and a multichannel-pulse-height analyzer is then used to analyze and display the results.

Again the measurement of lifetime for highly ionized atoms is difficult by this technique. The time resolution is limited by the capability of the coincidence circuit.

1.3 The Beam-Foil Technique

The use of beam-foil excited radiation as a new source of spectra was proposed by Kay in 1963 (Ka 63). Bashkin et al. developed the technique further, measured mean lifetimes and the dependence of spectral line intensity upon beam energy, using various gas sources, such as hydrogen, deuterium, helium and neon (Ba 64, Ba 65, Ba 66a, Ba 66b, Bi 66, Bi 67a, Bi 67b, Bi 68a, Fi 68).

The beam-foil technique has so far been employed primarily for measuring radiative lifetimes of excited

energy levels. The element of interest is accelerated by a Van de Graaff accelerator to energies ranging from 0.1 to several MeV. The energetic ion beam is then deflected by an analyzing magnet and the ions of interest are led into the vacuum chamber and impinge on a carbon foil, usually of 10 or 20 $\mu g/cm^2$ thickness. The energetic ions are excited into a variety of ionization states and energy levels. Spontaneous decays of the excited states produce a faint source of light on the downstream side of the foil. A study of the variation of the intensity of a spectral line as a function of the distance from the foil yields the radiative lifetime of the upper level responsible for the transition.

For a cascade-free upper level, the decay of the spectral line intensity follows the equation,

$$I(x) = kA_{ij}N_o e^{-\frac{x}{\tau v}} \qquad (1.7)$$

where k is a constant depending upon geometrical factors and detection efficiency of the monochromator and photomultiplier.

and A_{ij} = the Einstein coefficient,

N_o = the number of atoms in the initial state excited by traversing the foil,

x = the distance from the foil,

τ = the mean lifetime for the upper level

and v = the velocity of the beam particles.

The beam velocity, v, is determined either by theoretical estimation from the incident beam energy or by direct measurement using the Doppler effect (see section 3.3 and 5.1). Then the decay of a spectral line intensity as a function of distance from the foil can be used to evaluate the lifetime of the upper level.

Two types of observational techniques are possible for detecting the signals: photographic detection and photoelectric detection. For both methods the speed of the instrument is a main concern. In the photographic detection the slits are, in general, parallel to the image of the excited beam. The spectrum is recorded with a high speed plate. The observed lines are slanted and broadened due to the fast moving source. In photoelectric detection, a monochromator coupled with a suitable photon detector is employed to record the signals. The slits are in general perpendicular to the image of the beam.

Photoelectric detection was employed for the observations in this project. There are two approaches: the direct current and photon counting methods. The direct current method records continuously the current output from the photomultiplier as a function of wavelength or of the distance from the foil. The photon counting method records the number of photons arriving in a certain time interval at various successive positions of interest, either spectral or spatial.

Aside from the simplicity of lifetime measurements for excited levels, the beam-foil technique has the following points of interest:

(1) the purity of the source is, in general, very high. It is achieved by using an analyzing magnet which will bend the particles of different mass-energy product into different directions. However, it is not always possible to separate impurities from ions of interest, e.g., N_2^+, CO^+ and Si^+ can not be separated by a magnet.

(2) the de-excitation takes place in a high vacuum (about 10^{-5} torr or lower), thus recombination and secondary collision processes are absent. An evacuable monochromator can be connected directly to the target chamber so that studies can be extended into the far ultraviolet region. This is particularly important for highly ionized atoms.

(3) this technique is capable of obtaining highly ionized atoms by increasing the beam energy. It also produces lines which are not observed from other light sources. Some of the new lines can be identified by computing all the allowed transitions between the tabulated energy levels (Mo 49); whereas some remain unidentified.

(4) the charge state of the ion responsible for a transition can be easily determined by studying the line intensity as a function of the beam energy or more rigorously by applying a transverse electric or a magnetic field

to deflect and split the beam. The beams, one for each charge state, may not be well separated before the spectral line intensity has decayed to an undetectable value, but due to their different transverse components of velocity along the electrostatic field (or perpendicular to the magnetic field) the charge state for the ions responsible for a line can be determined by measuring the Doppler shifts induced by the fields.

(5) the place of excitation is exactly located and is very well defined. With the high velocity of the radiating ions, the time required to traverse the carbon foil is of the order of 10^{-15} sec for a foil of thickness 10 $\mu g/cm^2$.

The beam-foil technique does have some drawbacks as well. Firstly, the light is faint and thus a high speed spectrometer is essential. Somewhat wide spectrometer slits must be used, resulting in wide line profiles. In general, the uncertainty in wavelength measurements is not better than about ± 0.3 Å for lines in the visible region. Secondly, the Doppler shifts introduce a broadening of the spectral line (see also section 4.4) which hinders the measurement of wavelength as well as the resolution of closeby spectral lines. These disadvantages often make it difficult to identify the foil-excited spectral lines.

In practice, the beam particles can not be exactly

monoenergetic. Besides the unstability of the accelerating voltage and the analyzing magnet current, the ions suffer a straggling while traversing the carbon foil. The ejection of the target atoms which has been observed in this project as well as by other workers (Be 70a, Oo 70) and the scattering of the ions by the target may present problems which will limit the accuracy attainable in future investigations.

CHAPTER II

EQUIPMENT

2.1 The Target Chambers

Five target chambers, including the charge deflection chamber which will be illustrated in section 4.2, have been built and used in this project. Fig. 2.1 illustrates the target and focusing-scanning chamber used in the 1969 experiment. The components in the chambers, some common to all and some specific for the particular chamber, will be briefly described as follows.

In each chamber there is a foil wheel with a capacity of 6 to 20 foils. Any one of the foils can be selected for use with an external control mechanism so that the vacuum remains undisturbed when a new foil is brought into position. The aluminum foil holders have 0.5" diameter holes in most cases except those for the charge deflection experiment which have 3/8" apertures. A collimating aperture is in front of the foil to prevent superfluous beam from reaching the area of observation.

Viewing windows, generally of quartz, in the chamber wall are designed to allow observation of the beam either by the monochromator or by eye. At least one window of width larger than 1.5" is required for the reloading of the foil holder.

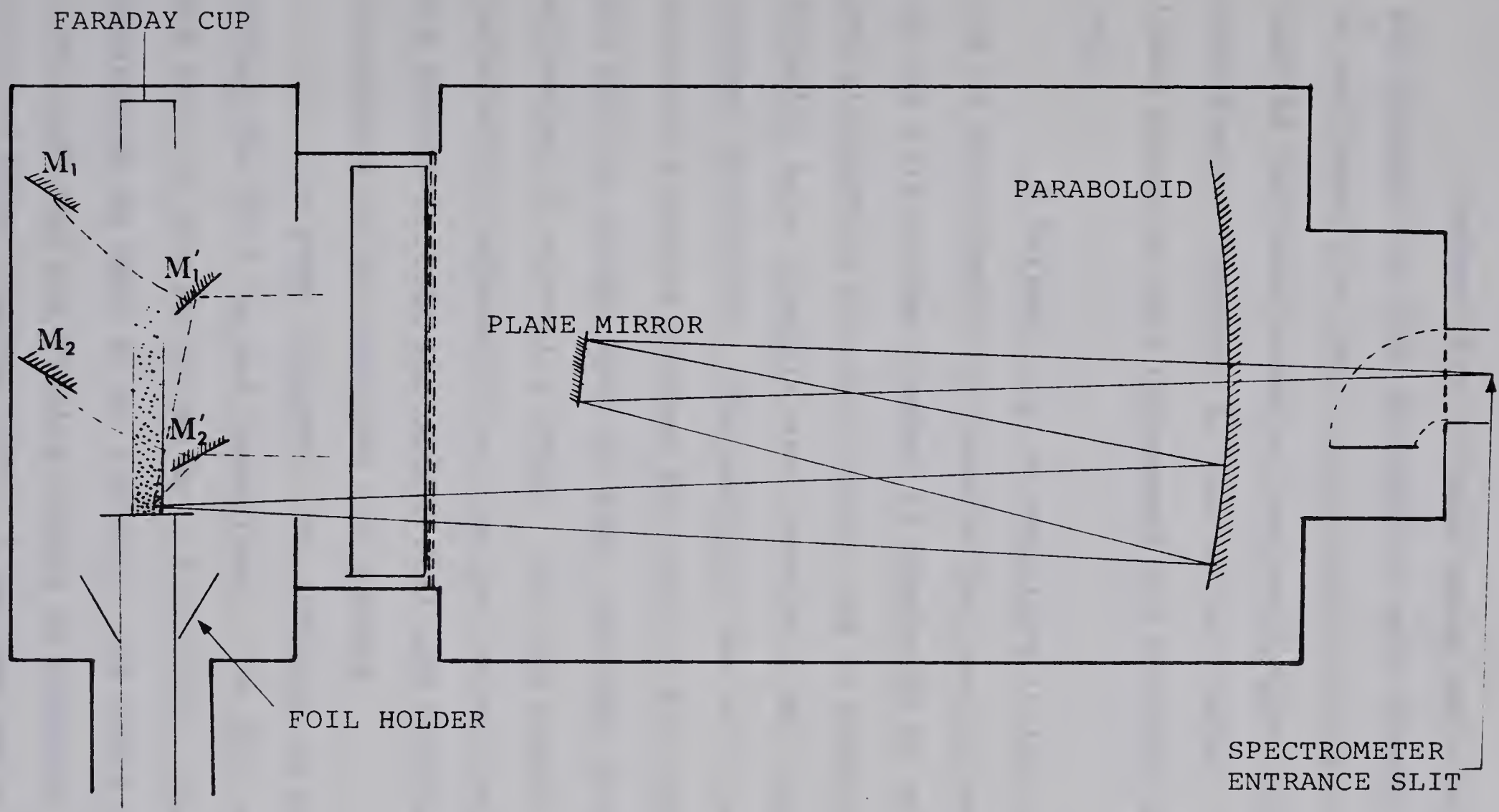

FIG. 2.1 SCHEMATIC DIAGRAM OF THE TARGET AND FOCUSING-SCANNING CHAMBER

Outlets for a vacuum gauge and auxiliary pumping systems are also provided on each chamber. However, it was found that the vacuum system of the accelerator (and of the monochromator) was sufficient to maintain a satisfactory pressure in the target chamber. A cold cathode gauge is used to measure the pressure in the chamber.

A Faraday cup is installed at the downstream end of each chamber to measure the beam current. The cup in the 1971 vacuum chamber is supported by an insulating rod attached to the foil holder and is connected electrically by a flexible wire through a BNC connector to a current integrator. The modification is to maintain a constant distance between the cup and the carbon foil as the foil is moved, step by step, upstream during the observation of a level's decay. The cup current does not necessarily represent the true ion current because secondary electrons from the carbon foil and residual gas also contribute to the observed cup current.

In some chambers, the scanning is performed by moving the foil up-and downstream. The foil wheel or the foil in use is driven by a screw which can be turned externally by hand or by a motor. The drive screw has a 1 mm pitch and the turning handle is designed to give a click at every quarter turn. A pointer and a scale are also provided to indicate the position of the foil.

Two small front surface mirrors (M_1' and M_2') can be seen in Fig. 2.1. They reflect light at 10° and 30° to the beam direction, respectively, into the spectrometer. They are moved to the M_1 and M_2 positions when not in use.

Two field plates separated by about 1.5 cm are installed in the charge deflection chamber. Slots are made in the plates to permit observation at a suitable position along the plates. Electrodes through which high voltage can be supplied to the field plates from outside, and the polarity of the field can be changed, are located at the bottom of the chamber.

2.2 The Focusing-Scanning Device

The focusing-scanning chamber shown in Fig. 2.1 was designed by Dr. E. H. Pinnington and has been in use since 1969. The plane mirror, 0.8" x 1.5", is situated at the focus point of the paraboloid. The axis of the paraboloid is set perpendicular to the ion beam and crosses the beam at about 2" from the foil. As the plane mirror rotates, different sections of the beam are focused at the entrance slit of the monochromator. A paraboloid is required because the radiation is to be observed at a direction perpendicular to the ion beam. The width of the plane mirror must be small so that little nonperpendicular light is accepted and hence less Doppler broadening of the spectral line results.

The rotation of the mirror is made by a lead-screw which drives a lever attached to the rotation axis of the plane mirror. Both the lead-screw and the lever are outside the chamber and scales are installed so that the amount of rotation, that is, the position of observation on the beam, can be readily obtained. Adjustment to the tilt of the mirror is performed by rotating a knob at the bottom of the chamber which has a rod connected to one end of the mirror.

The paraboloid has a pivot and can be tilted for the alignment of the optics. The adjustment is made by turning a screw which is in touch with the bottom end of the paraboloid. Two masks have been designed for the paraboloid: one gives a 3" x 3" section for the scan of lines which decay to noise level within 5 cm; the other one gives a 1" x 5" section for the scan of strong or long-lived lines at one third the intensity.

The optical alignment is done by shining a laser beam normally into the center of the exit slit of the monochromator. The beam, emerging from the entrance slit, is automatically incident on the center of the plane mirror. The tilt of the mirror is then adjusted so that the laser beam hits the center of the paraboloid. Finally the paraboloid is tilted to reflect the light on to the ion beam.

The departure of the paraboloid from a sphere has to be sufficiently small so that horizontal focus re-

mains sharp, i.e., a vertical section through the beam is focused to a vertical image at the slit. This is essential because the decay of intensity is to be measured as a function of distance from the foil. On the other hand, the lack of a sharp vertical focus is not so critical as the slits of the monochromator are considerably longer than the beam image. The small departure of the paraboloid from a sphere leads to the relation that the distance scanned across the beam is proportional to the angle of the rotation of the plane mirror.

Flap valves are installed between the focusing-scanning chamber and the monochromator and between the focusing-scanning chamber and the target chamber. This is to isolate one component from the others when that component has to be vented to the air. For instance, when new foils are to be loaded on the foil wheel, the two flap valves mentioned above can be closed thus maintaining the focusing-scanning chamber and the monochromator under good vacuum.

2.3 The Photon-Counting Electronics

A schematic diagram of the photon-counting equipment is shown in Fig. 2.2. The output from the photomultiplier is fed to a preamplifier through a short cable and then to a pulse generator. Working as a discriminator, the pulse generator produces an appropriate pulse to be recorded

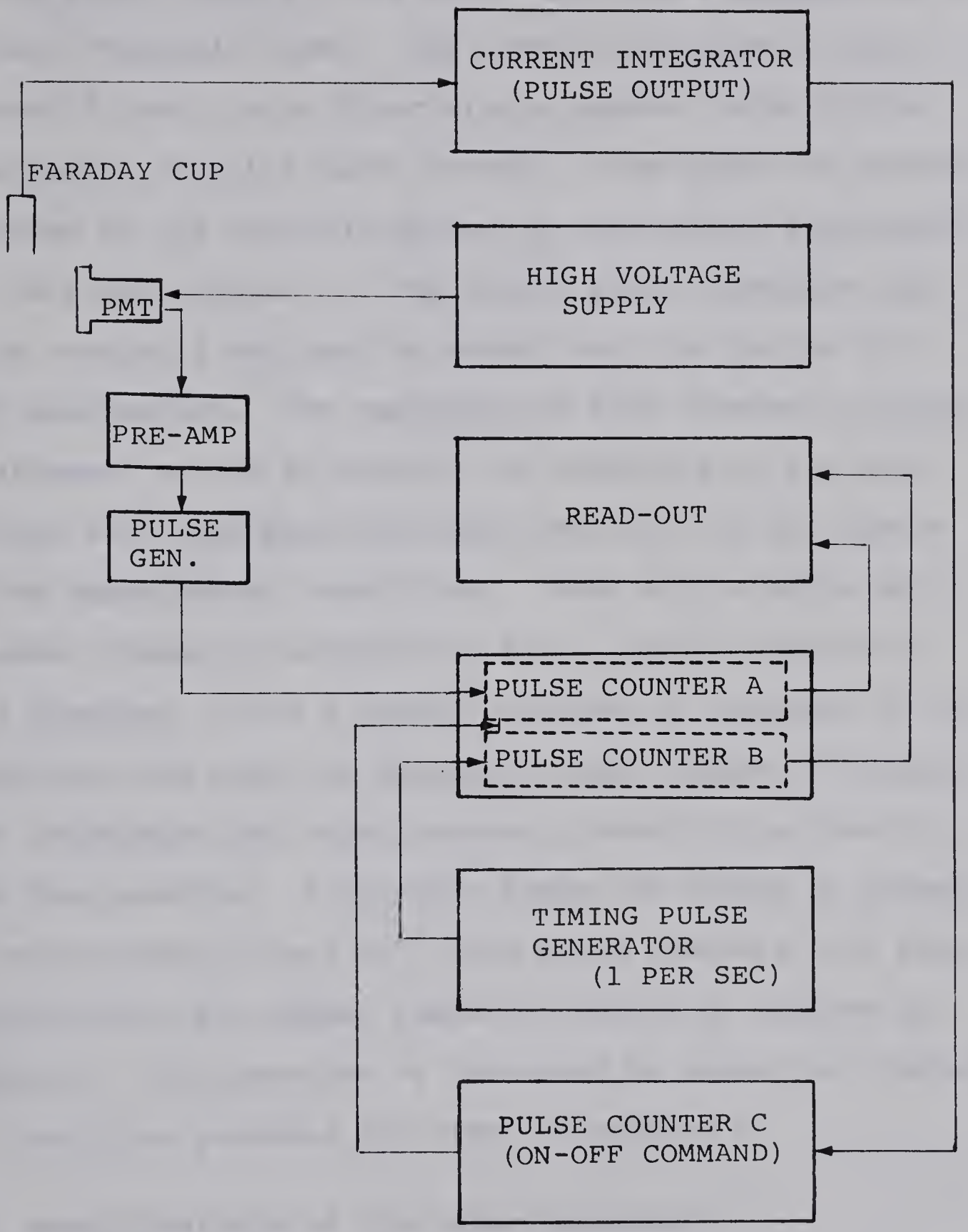

FIG. 2.2 SCHEMATIC DIAGRAM OF THE ELECTRONICS USED IN THE PHOTON-COUNTING TECHNIQUE

by the pulse counter A for each input pulse larger than a certain threshold level. The proper adjustment of the threshold level is to discriminate against noise pulses originating from the later dynodes. The number of photons detected by the photomultiplier is, therefore, registered by the pulse counter A. The timing pulse generator and pulse counter B are used to record the time period for each measurement. The recording of time elapsed for each measurement served to monitor the stability of the beam current and often provided good indication of any change of the experimental conditions. Among such changes were a sudden change in integration time, usually because of foil breakage, while a gradual increase or decrease of integration time might be because of poor vacuum. The current integrator and pulse counter C control the time to stop the counting. A suitable number of counts is preset on pulse counter C and all three pulse counters will stop counting when the preset number of counts is reached in counter C. The counting is restarted by resetting counter A, B and then pressing the reset of counter C.

2.4 Specifications of the Other Equipment

Van de Graaff Accelerator

Model: High Voltage Engineering Corp. AK 60

Ion Source: Radio frequency ion source

Energy range: 0.5 - 2.0 MeV

Analyzing Magnet

Model:	High Voltage Engineering Corp. AK/H
Maximum Field:	9.6 kilogauss

Monochromators

Model:	Spex 1500	McPherson 225
Mounting:	Czerny-Turner	Normal incidence
Focal Length:	0.75 m	1.0 m
Speed:	f/6.8	f/10.4 (Masked to f/50)
Dispersion: (600 g/mm grating)	10 Å/mm	16.6 Å/mm

Gratings

Obs. Range:	370-1000Å	1000-2000Å	2000-3500Å	3500-5000Å
Grooves/mm:	600	600	1200	1200
Blaze (Å):	900	1500	1500	5000
Ruled Area: (mm x mm)	56 x 96	56 x 96	120 x 120	120 x 120

Photon Detectors

Model:	EMI 6256S	EMR 542-G	Bendix 4219X
Response Range:	1650-6800Å	1050-2000Å	2-1500Å
No. of Dynodes:	13	18	-
Operation V.:	-1750	-3000	+2200

CHAPTER III

OBSERVATION

3.1 General Procedure and Experimental Conditions.

The experimental arrangement for the beam-foil measurements is shown in Fig. 3.1. The element of interest was stored in the ion source at the high voltage end of the Van de Graaff accelerator. The highly-energetic ion beam, mainly singly-charged molecules, was magnetically deflected by about 7° and split into beams of differing mass-energy product. Only the ions of interest were admitted to the target chamber which was about 2 meters from the analyzing magnet (see also section 4.3). The pressure of the residual gas in the target chamber was of the order of 10^{-5} torr. The beam impinged on a carbon foil of thickness 10 ± 4 $\mu g/cm^2$ and was excited to various charge and energy states. The beam charge was collected in Faraday cup at the end of the target chamber and measured with a current integrator which can indicate either the current intensity or the total integrated charge received by the Faraday cup.

The radiation was, in general, observed in a direction perpendicular to the ion beam. The detecting systems employed were a 0.75 meter spex 1500 monochromator

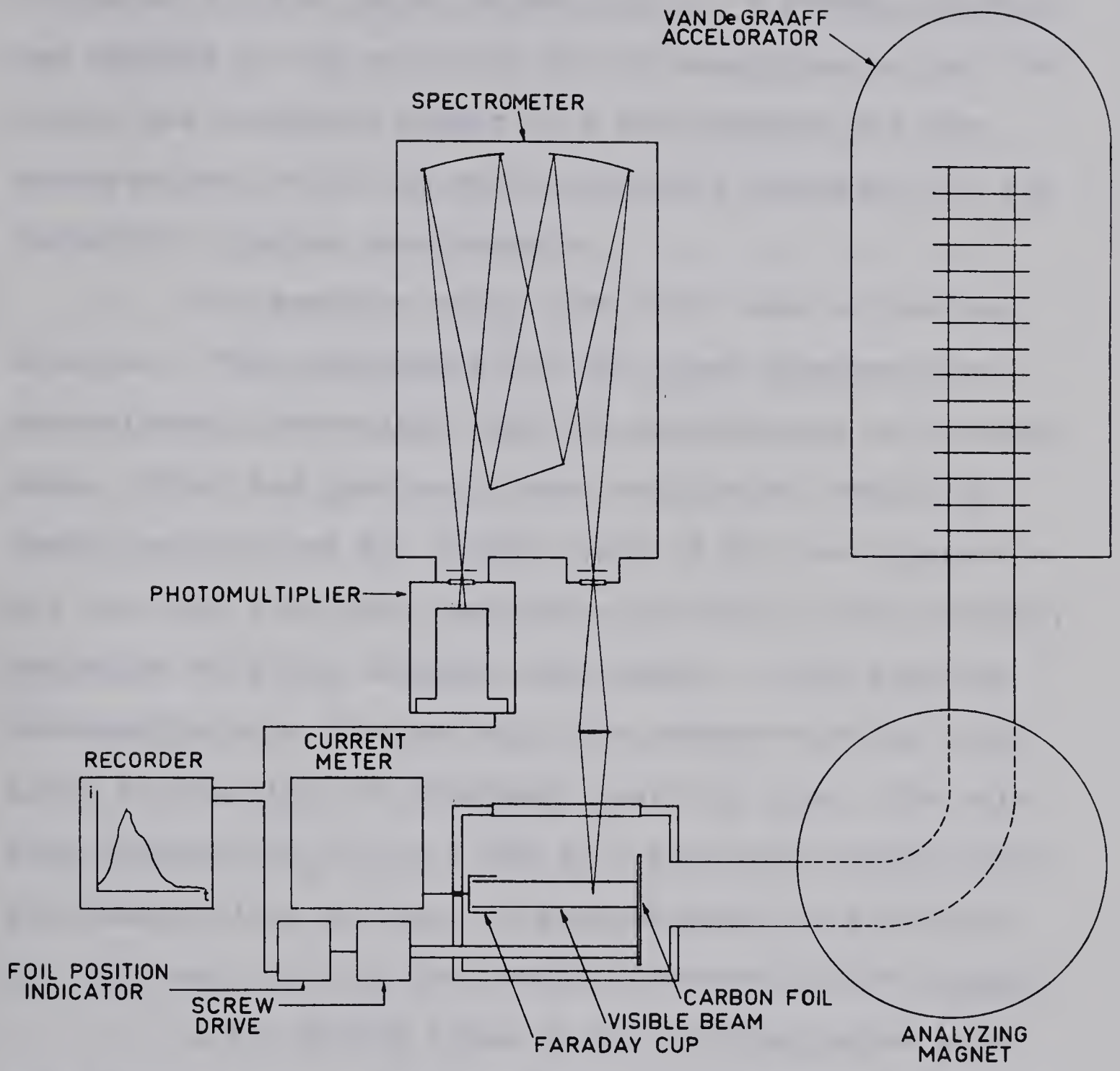

FIG. 3.1 SCHEMATIC DIAGRAM OF THE BASIC ARRANGEMENT OF THE BEAM-FOIL TECHNIQUE

for the region above 2000 Å and a 1-meter McPherson monochromator for the region below 2000 Å. A photon detector was coupled to the exit slit of the monochromator and the output was connected either to a microammeter for the spectrum scan or to the photon counting equipment for the radiative lifetime measurements.

The spectrum scans were first made at various energies. The wavelengths for the lines observed were approximately determined from the spectrometer wavelength scale (which had previously been calibrated from an external source) and the charge state of the ions responsible for each line were assigned according to the intensity variation with the incident beam energy. More accurate wavelengths were obtained with the photon-counting technique by counting the intensity near the line. The relative intensities of the lines at a particular energy were then measured by setting the monochromator on each line in turn and counting the photons detected by the system.

A few strong lines in the visible region were then selected for the measurements of the beam velocities. The Doppler shifts for these lines at 10° and 30° from the beam direction were measured and the beam velocities evaluated. A spectrum observed at 30° from the direction of the beam was also obtained to determine whether all the lines had originated from ions with the same velocity (See also section 4.3).

For the radiative lifetime measurements, the photon detector output was connected to the photon-counting equipment. The decay of the line intensity as a function of distance from the foil was measured at a suitable incident beam energy by counting the number of photons at a sequence of points along the beam, for a predetermined Faraday cup charge.

The beam employed in the measurements was O_2^+. The lifetimes for levels in OI-II were measured at 0.6 MeV, levels in OIII were measured at 1.0 MeV and levels in OIV-V at 1.4 MeV. The beam currents were, in general, 0.5 μA or less. The scanning speeds for taking the spectrum were 50 Å/min. The slit widths of the monochromator used were either 200 μ or 400 μ depending upon the intensity of the signal. The pressure in the McPherson monochromator was less than 10^{-7} torr and in the target chamber 5×10^{-5} torr or less. Each carbon foil was used for no longer than two hours or for the lifetime measurements of no more than four lines. The signals obtained ranged from 1 to several orders of magnitude greater than the background noise, except in the vuv region where some of the strong lines gave a signal-to-noise ratio of many orders of magnitude.

3.2 The Spectrum

Three different arrangements were used to observe

the spectrum:

1. direct current chart recording,
2. pulse rate chart recording,
3. pulse rate computer recording.

The block diagram of the arrangements are given in Fig. 3.2. The third method mentioned above is complicated but the most sensitive. Several scans over the same region can be made, stored and superposed through the manipulation of the instrument computer to obtain an improved signal-to-noise ratio. Some of the results taken with this method are presented in Chapter VI.

Since some lines had very short lifetimes and decayed to the noise level within a few milimeters, extra care was taken to focus the brightest portion of the beam on to the monochromator. Furthermore, the spectra were taken at, at least, three different energies: the lowest available, highest available and 1 MeV. Since all of these methods are equivalent to photon counting over short time intervals (typically 1 sec /channel), it was necessary to use higher beam currents than were used for recording the decay curves.

The determination of the wavelength of the line observed relied on the calibration of the monochromator or in the visible region a reference spectrum could be superimposed on the spectrum. The instrumental wavelengths of the lines observed with the chart recording method were

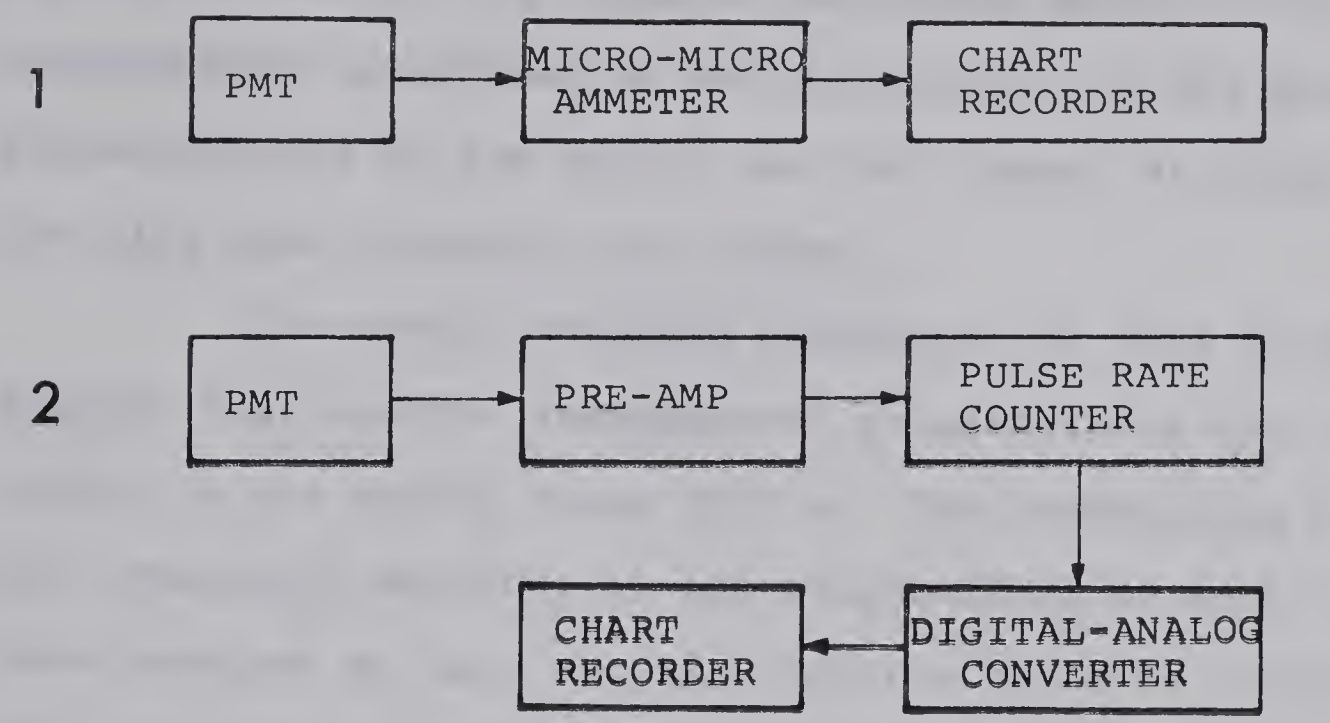

FIG. 3.2 ELECTRONIC ARRANGEMENTS FOR SPECTRAL SCANS

obtained with reference to the side event marker spikes which were imposed on the chart at every 5 Å. For the lines observed by the computer recording method, the wavelengths were determined by the correlation of the exact region covered by the memory and the channel at which the line peak intensity was stored.

The photon-counting technique was used to determine the accurate instrumental wavelength of the lines except in the region below 1000 Å. The intensities at the wavelength settings in the neighborhood of each line were measured so that the line profile could be plotted and the line center be determined more accurately.

3.3 Beam Velocity Measurements.

A small section of the spectrum which included several strong lines was recorded from a direction perpendicular to the beam with a much slower scanning speed (20 Å/min or less) so that the wavelength could be accurately determined. Then the scanning device was set to collect the light reflected by the small mirrors (Fig. 2.1) consecutively and the shifted spectra were taken at the same scanning speed. All of the arrangements mentioned in section 3.2 could be used for the velocity measurement purpose.

The photon-counting technique was also tried to acquire the data needed and proved to be both more accu-

rate and efficient. It was more time consuming in the observation but more convenient in the determination of the amount of the shifts. This technique would be even more useful when weaker, sharper spectral lines are chosen for measurement.

3.4 Radiative Lifetime Measurements.

This project began by making the lifetime measurements with the direct current method. The decay in intensity of the spectral line as a function of the distance from the foil was recorded through a strip chart recorder onto chart paper. The lifetime for the upper level responsible for the line was then deduced from the decay.

In an attempt to reduce the noise level, a different approach was tried in the 1969 experiment. The scanning action was achieved by rotating the plane mirror mentioned in section 2.2 with a synchronous motor and the signals fed to an instrument computer. For each revolution of the plane mirror, a simple electronic device produced a pulse to trigger the computer and thus the signals from many successive sweeps could be superimposed and stored. The noise was then subtracted from the signals and the resulting decay curve and its logarithm displayed on an oscilloscope. The signals displayed on the oscilloscope were photographed for later analysis. This approach was not satisfactory because of its low efficiency, result-

ing from an effective duty-cycle of only about 5%.

The photon-counting technique was then employed and proved to be much more satisfactory. The number of photons coming from discrete sections along the beam was counted for a certain amount of charge collected in the Faraday cup. The distances from the foil, signals, background noise and the time elapsed for measurement were recorded for the analysis.

The semilog plot for each line was made while the photon counting was in progress. This made it possible to decide at what position to make the next measurement and the data in doubt could be repeated so that some errors might be avoided. Estimation of the lifetime could be made from the plot and comparison with the values obtained by other workers or theoretical calculation was then possible.

The accuracy of the lifetime measurements depends upon the line intensity, hence it is desirable to observe the decay at the beam energy at which the spectral line has maximum intensity. The charge state of the ions responsible for each line were, in general, identified and suitable beam energy was chosen for the observation.

The peak intensity observed ranged from several hundreds to about ten thousands counts. The time required for counting were typically 45 sec in the visible region, 25 sec in the region between 1000 Å and 2000 Å

and 15 sec for the region below 1000 Å. The number of data taken for the decay of each line were in the range of 20-40. The decays were followed for about three lifetimes or longer after the excitation. In the vacuum region some of the lifetimes were very short, and more than one set of measurements were made for better accuracy.

It is to be noted that associated with a photon-counting signal, S, there is a standard deviation $\sigma = \pm\sqrt{s}$. This is a fluctuation of the true signal; another independent measurement may result in any value but the probability of lying between $S+\sigma$ and $S-\sigma$ is 68% (see, for example, reference (Ev 55b)). In the measurements of the decay of a spectral line, the intensities go down and hence the fluctuations go up as the measurements are made farther and farther from the foil. There is a position at which measurements will be too inaccurate for inclusion in the analysis of the mean life. On the other hand, if the measurements are discontinued too early, some useful data will be missed. The optimum duration of the observation of the decay depends upon the initial signal-to-noise ratio. According to Peierls' calculation (Pe 35), the time of observation should last three lifetimes for lines of initial signal-to-noise ratio of 5 and four lifetimes for lines of initial signal-to-noise ratio of 30.

The counting loss due to the resolving time of the system is negligible because the counting rate is, in ge-

neral, low. Let p be the resolving time of the system and s be the observed counting rate, then the true counting rate S is given by (see, for example, reference (Ev 55a))

$$S = s(1+sp) \qquad (2.1)$$

when $Sp << 1$. With a system of resolving time shorter than 10 nsec no consideration of the counting loss will be necessary unless the counting rate is larger than 5000 cps.

The photon-counting technique has the following advantages over the direct current method in the measurements of the radiative lifetimes:

(1) more sensitive and flexible intervals of observation. The measurements at the brighter portion of the beam are more reliable; the spatial interval of observation, corresponding to the speed of scan in the direct current method, can be smaller so that more accurate results can be expected.

(2) different integrated beam charge can be used for different line intensities.The statistical fluctuation of a weak line can be reduced by increasing the preset integrated beam charge. On the other hand, the integrated beam charge can be reduced for strong lines to shorten the time of observation.

(3) suppression of low amplitude noise. Noise originating from the dynodes, either due to thermionic

emission or secondary emission or other cause, contribute to the noise with anode pulses of lower amplititude which can be suppressed by appropriate adjustment of the threshold level of the discriminator.

(4) no scale problem involved. The intensity scale has to be changed for different line intensities in the direct current method. Furthermore, in some cases, one scale is too small and the next one is too large. The photon-counting technique can measure a wide range of intensity accurately.

CHAPTER IV

LINE IDENTIFICATION

4.1 Charge Identification: Intensity Variation Method

The beam-foil technique has produced new lines which can not be found in the literature, and has generated highly-ionized species which have not been fully investigated by the more conventional methods of spectroscopy. For this reason, and the relatively wide linewidths that make the comparison of the listed and observed wavelengths in many cases ambiguous, charge state identification becomes more necessary in the beam-foil work.

Two methods can be used to identify the charge state of the ion responsible for a given spectral line: (a) measurements of intensity variation with the incident beam energy (Ka 65, De 69a, De 69b, Dr 70); (b) either a magnetic or an electrostatic field can be applied transversely to the beam (Fi 68a, Fi 68b, Ca 70, Ba 70).

The intensity-variation method was suggested by Kay (Ka 65) in 1965. The technique is to correlate the relative intensities with the velocity of the ions or, as modified by other workers (Du 70), the normalized intensity with beam energy. The charge state of the ion responsible for a spectral line can be identified by comparing

the intensity variation as a function of beam energy with that of well identified lines. The normalized intensities and the energy for the maximum intensity are good indicators for the charge state to be identified.

The intensity-variation method has the advantage of simplicity. A comparison of relative intensity at five different energies would, in general, provide good information for charge identification. However, the following difficulties limit the reliability of the method.

(a) Normalization of the beam current is difficult at different beam energies. Furthermore, the beam current as monitored by the Faraday cup at different energies may not represent the same number of ions per second crossing the carbon foil because both the charge state distribution after crossing the foil and the number of secondary electrons ejected from the foil per impinging ion are energy-dependent. Scattering of the beam by the carbon foil presents an extra difficulty in the normalization of the beam current.

(b) The intensity depends also on the lifetime because the observation is, in general, made laterally and covers only a small section of the beam. The observed intensity is not proportional to the initial population of the

upper level unless all the lifetimes of all the observed transitions are the same. If axial observations are employed, it is necessary to collect the light from the entire radiating length of beam.

(c) Blended lines of different charge states give an intensity variation which is difficult to analyze.

(d) The available accelerator energy range may limit the identification to only certain ionization stages. For instance, the machine used in this project can be operated stably only in the range of 0.5 - 1.5 MeV when heavy ions are accelerated. Both OIV and OV populations peak at higher than 1.5 MeV incident beam energy and these populations rise at essentially the same rate as the energy increases (Sm 69), hence no confident identification of OIV or OV is possible. On the other hand with a high energy machine which can not be operated at energy lower than 1 MeV, it would be difficult to distinguish OI from OII.

In order to avoid the difficulty of normalization of the beam current, the method employed in this project was to plot the normalized relative intensity against the beam energy. The intensities were normalized

at 1 MeV and the relative intensities were calculated with respect to an averaged identified OIII line. Fig. 4.1 shows some of the results. Fairly certain assignments were found for most of the lines, but in few cases it was difficult to distinguish OI from OII , and O*V* from OIV. The energy range of observation was centered at 1 Mev which is about the optimum energy for OIII lines, and the relative intensities were with respect to an identified OIII line, which optimizes the identification of OIII lines. The identification of lines due to other ionization stages could be optimized by centering the observational energy at the optimal energy for that charge state and the relative intensities calculated with respect to the identified line of the same charge state.

4.2 Charge Identification: Charge Deflection Method

A more direct approach in charge identification is by the charge deflection method. Observation of the emitted spectra can be made on each of the spatially separated beams (Ma 65) or the Doppler shifts due to the transverse velocity can be measured for each line and hence the charge state can be identified (Ca 70, Ba 70). The experimental arrangement is shown in Fig. 4.2. Doppler shifts are observed along the direction of the electrostatic field.

Suppose the field is applied as shown in Fig. 4.2. The displacement of the ions along the direc-

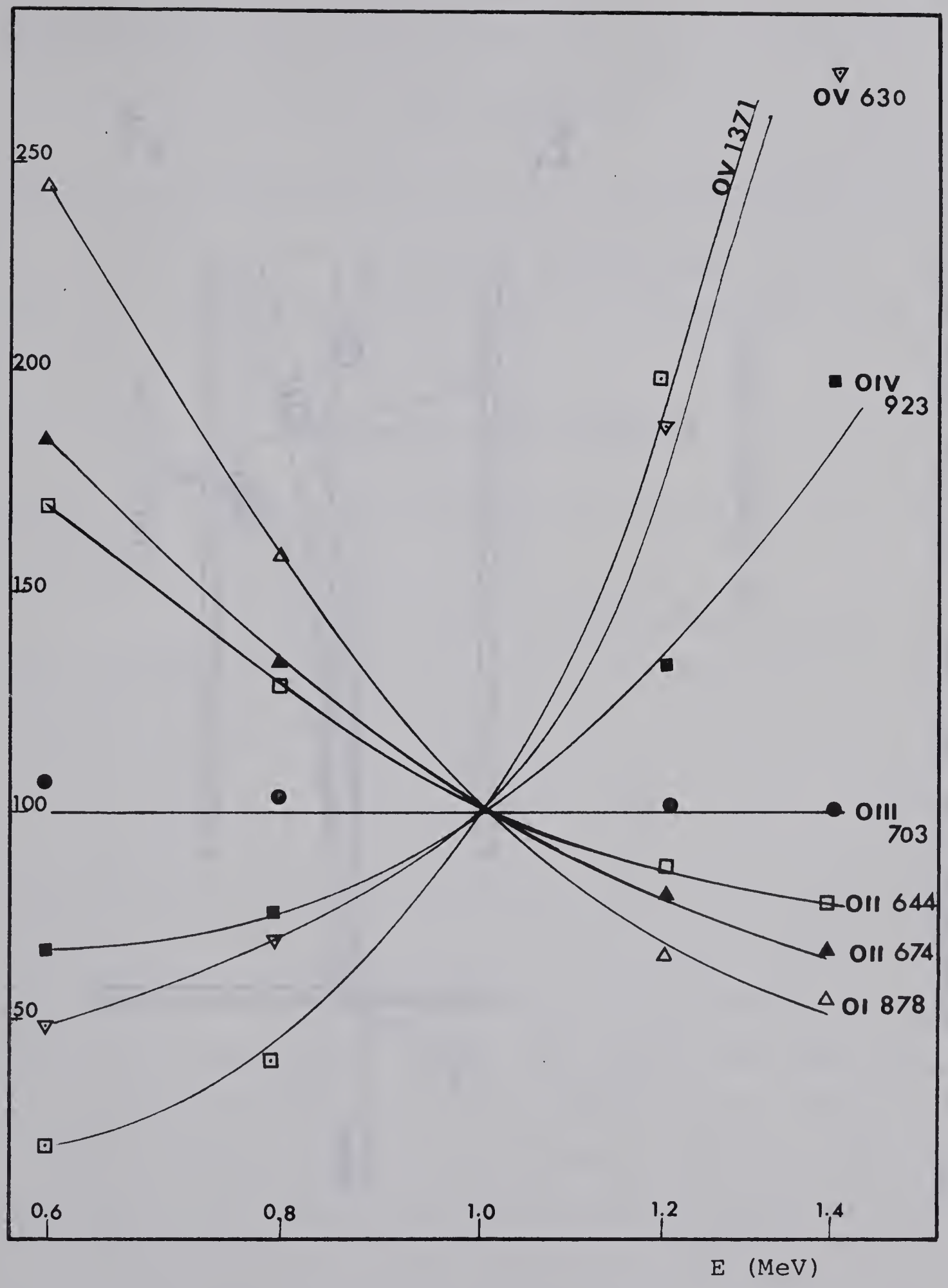

FIG. 4.1 RELATIVE VARIATIONS OF LINE INTENSITY WITH INCIDENT BEAM ENERGY

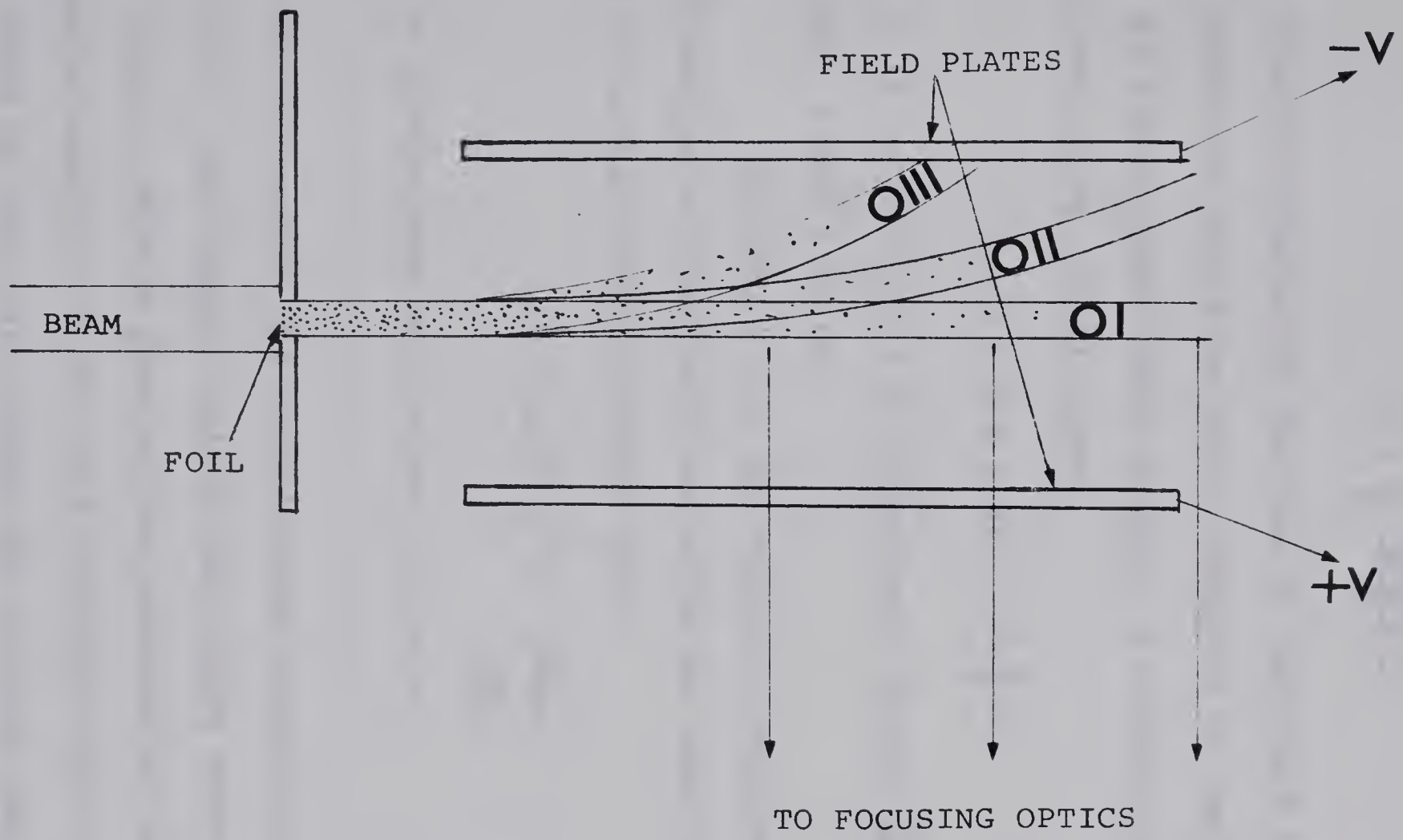

FIG. 4.2 ARRANGEMENT FOR THE CHARGE DEFLECTION EXPERIMENTS

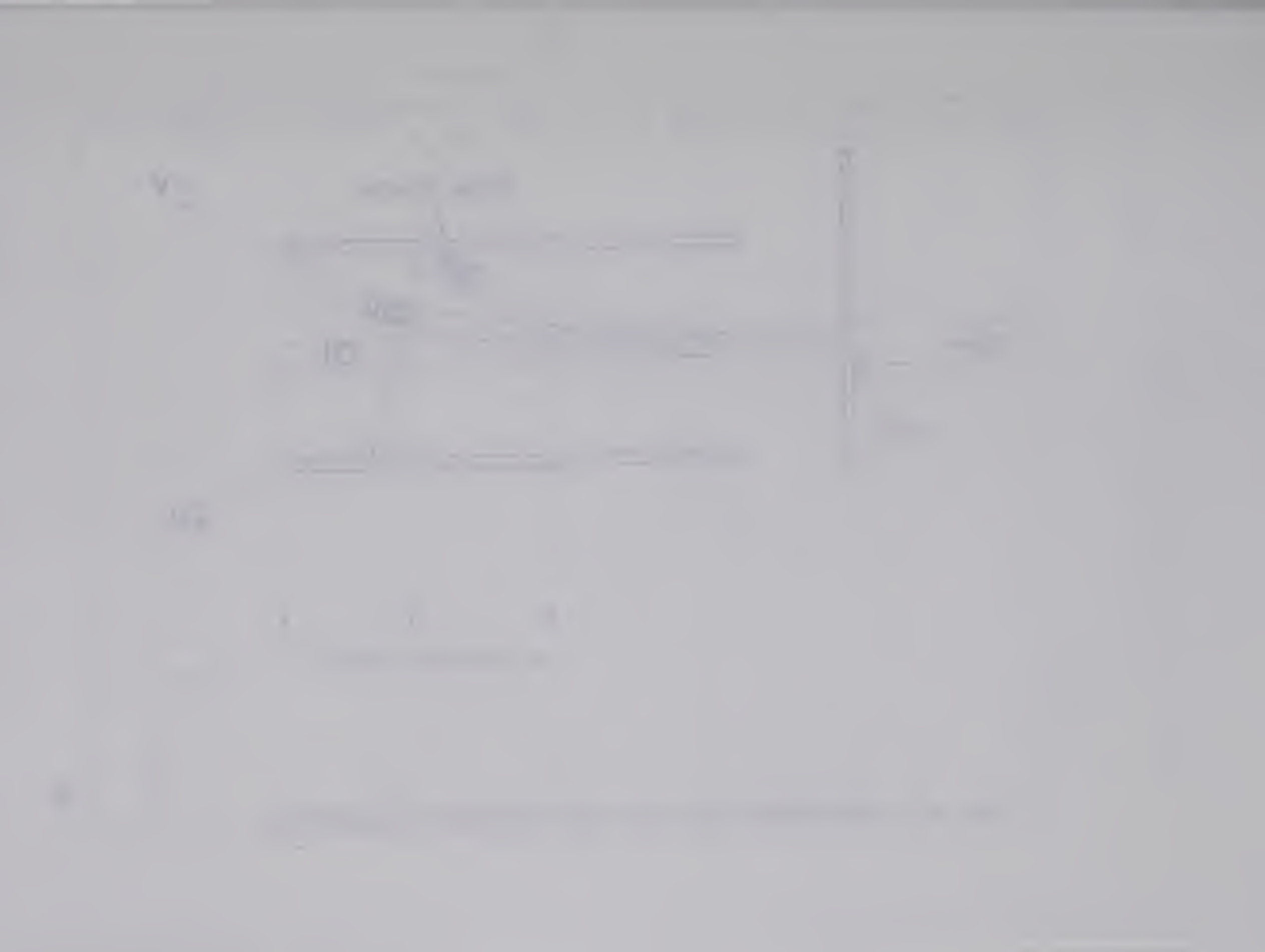

tion of the field is given by

$$Y = \frac{1}{4} \frac{q \mathcal{E} \ell^2}{E} \qquad (4.1)$$

where q is the charge of the ion, $\mathcal{E}$ the field intensity ℓ the distance that ions have travelled in the field and E is the incident beam energy. A conversion of the units used in Eq. (4.1) gives

$$Y = 2.5 \times 10^{-4} \frac{q \mathcal{E} \ell^2}{E} \qquad (4.2)$$

where q is in the units of electronic charge, $\mathcal{E}$ in kv/cm E in MeV, ℓ and Y in cm.

Writing $\dot{Y}$ for the velocity acquired along the direction of the field and using the same units as in Eq.(4.2) we can readily obtain that

$$\dot{Y} = 6.95 \times 10^{5} \frac{q \mathcal{E} \ell}{\sqrt{ME}} \qquad (4.3)$$

where M is the mass of the ion in a.m.u.

Table IV.1 presents the calculations according to Eq. (4.2) and (4.3). The Doppler shifts per charge state expected for a line at 4000 Å from an ion produced by an incident 0^+ beam of energy 0.5 MeV, and 40 KV/cm field intensity are listed on the last column (An incident beam of 0_2^+ ions at 1 MeV dissociates at the foil giving 2 0^+ ions at 0.5 MeV for each incident molecule).

TABLE IV.1 DOPPLER SHIFTS DUE TO A TRANSVERSE ELECTROSTATIC FIELD (40 KV/cm)

Distance ℓ (cm)	Displacement (10^{-2}cm)	Velocity (10^{6}cm/sec)	Doppler Shift at 4000 Å $\Delta\lambda$ (Å)
0.5	0.5	4.92	0.66
1	2.0	9.83	1.31
1.5	4.5	14.85	1.97
2	8.0	18.66	2.62
2.5	12.5	23.57	3.28
3.0	18.0	29.44	3.93

The appropriate position for observation is determined by the amount of Doppler shift which is required, and by the rate of decay of the line intensity. In order to be able to see as many lines as possible, it is best to observe the radiation as close to the foil as will produce a wavelength shift that is enough to distinguish one charge state from another. In ordinary experimental conditions, the center of the spectral line can be easily determined to an accuracy of ± 0.5 Å. Hence about 2 Å shift per charge state is necessary for a confident assignment. It is to be noted that the field direction can be reversed and a shift in the other direction obtained. Thus about 1 Å shift per charge state in each direction will provide enough information for the charge identification. In the case of a blend of lines of different charge states a total

of 4 Å shift per charge state would be required because of the relatively low resolution of the spectrometer when used with slit widths of 100 microns or more, as is normally the case in beam-foil studies.

A charge deflection chamber was built and tested in this project. The operation was not completely satisfactory as a relatively poor vacuum limited the maximum field to about 10 KV/cm. Observations were made at 2.5 cm from the foil and hence only strong, long lived lines could be detected. Fig. (4.3) shows two OII lines which are both shifted by 2 Å. Fig. (4.4) presents an OIII line shifted by 3.8 Å. Fig. (4.5) indicates a blend of OII and OIII or OIV lines. The main peak is shifted by 2 Å while the subpeak is shifted from the lower-wavelength-side of the main peak to the higher-wavelength-side. A definite assignment of the subpeak would require a larger wavelength shift. However, the intensity variation with energy of this blend suggests that it is a mixture of OII and OIII.

The charge deflection method has the advantage that it is actually a direct measurement of the charge of the ion, hence no comparison with known identifications is necessary. But there is the drawback that observations are made comparatively far from the foil so that only strong and long lived lines will be detected. In the vacuum ultraviolet region, the lifetimes for oxygen states are mostly shorter than 1 nsec, so that it would be difficult to apply the charge deflection method.

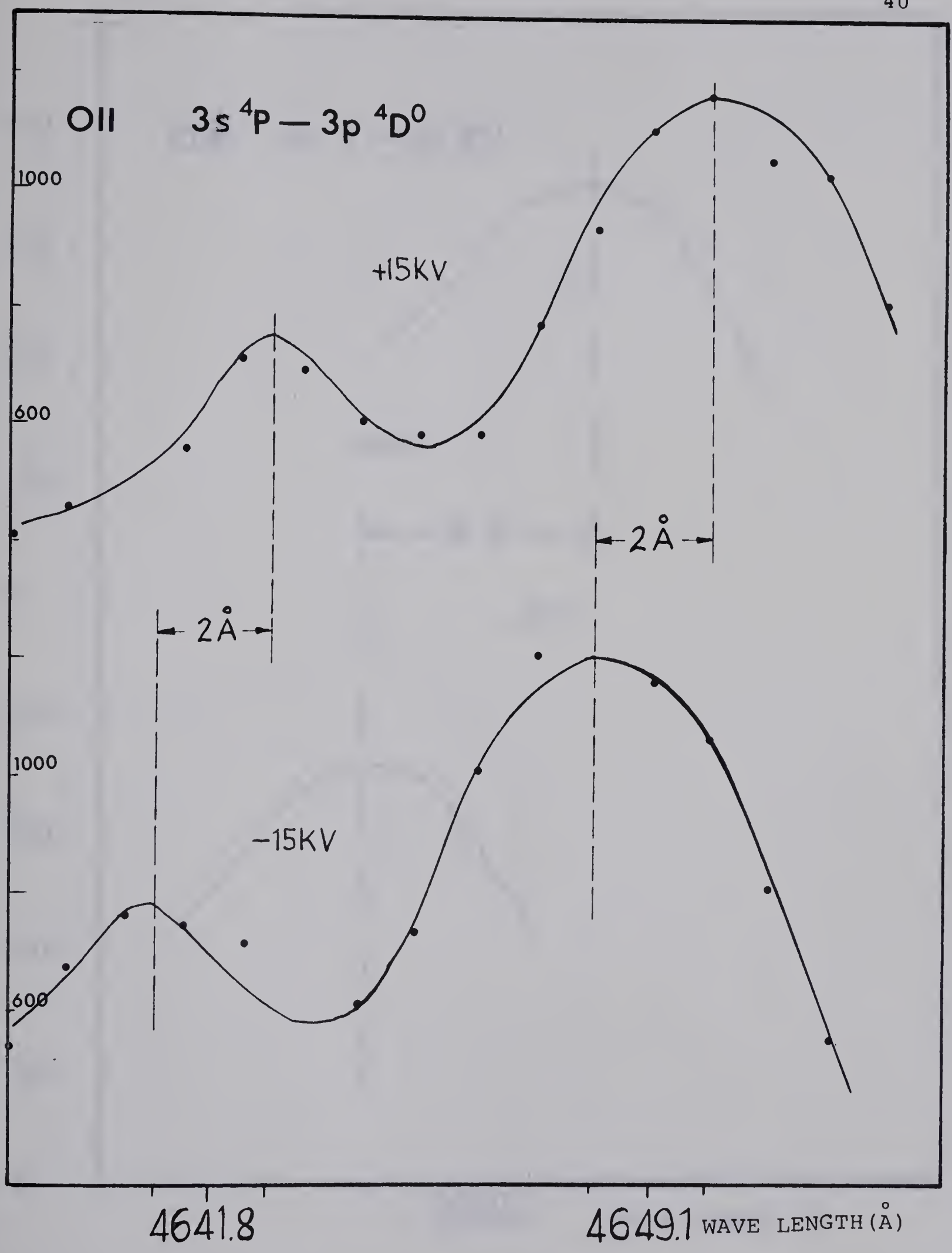

FIG. 4.3 DOPPLER SHIFTS FOR OII LINES

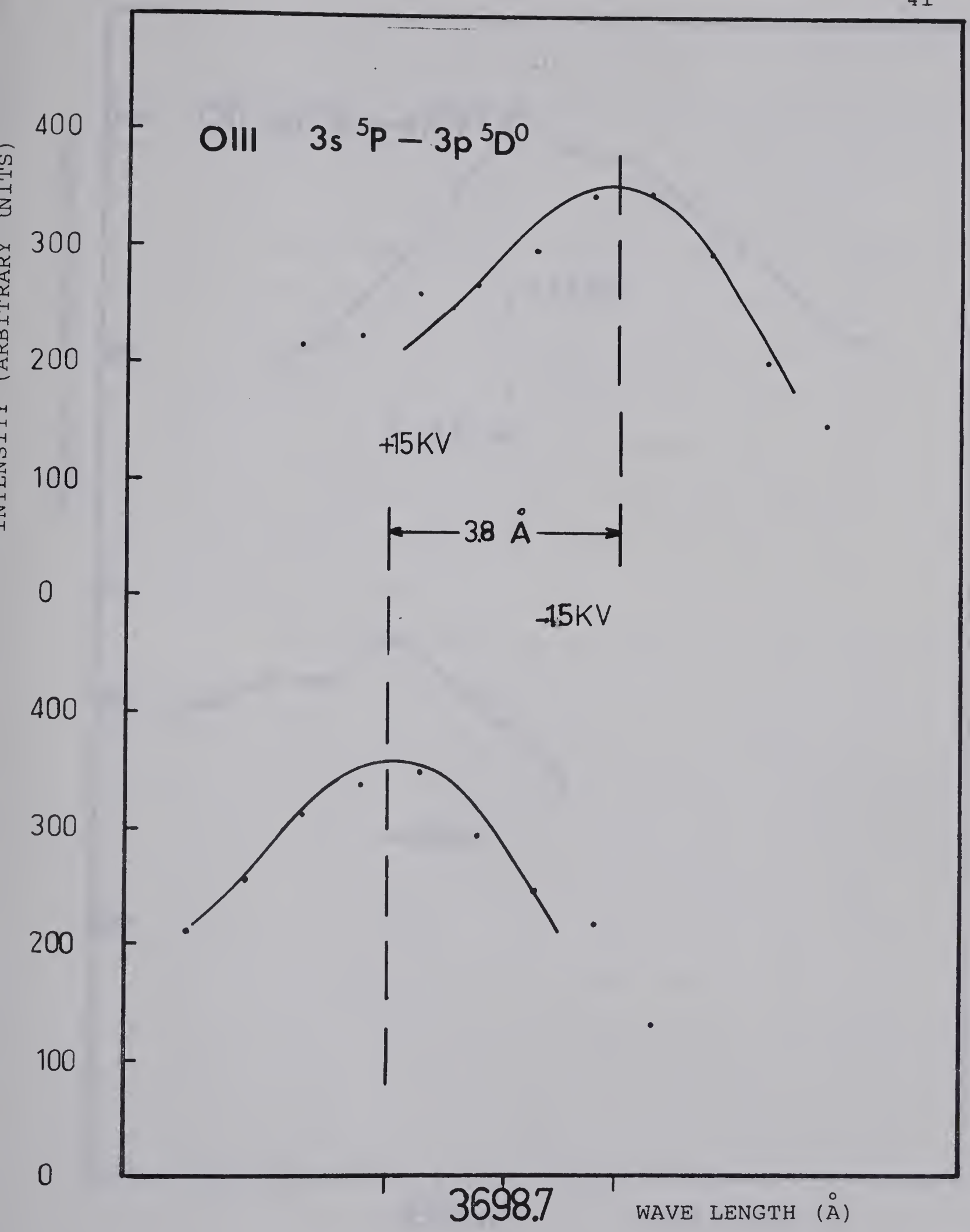

FIG. 4.4 DOPPLER SHIFT FOR OIII LINE AT 3699 Å

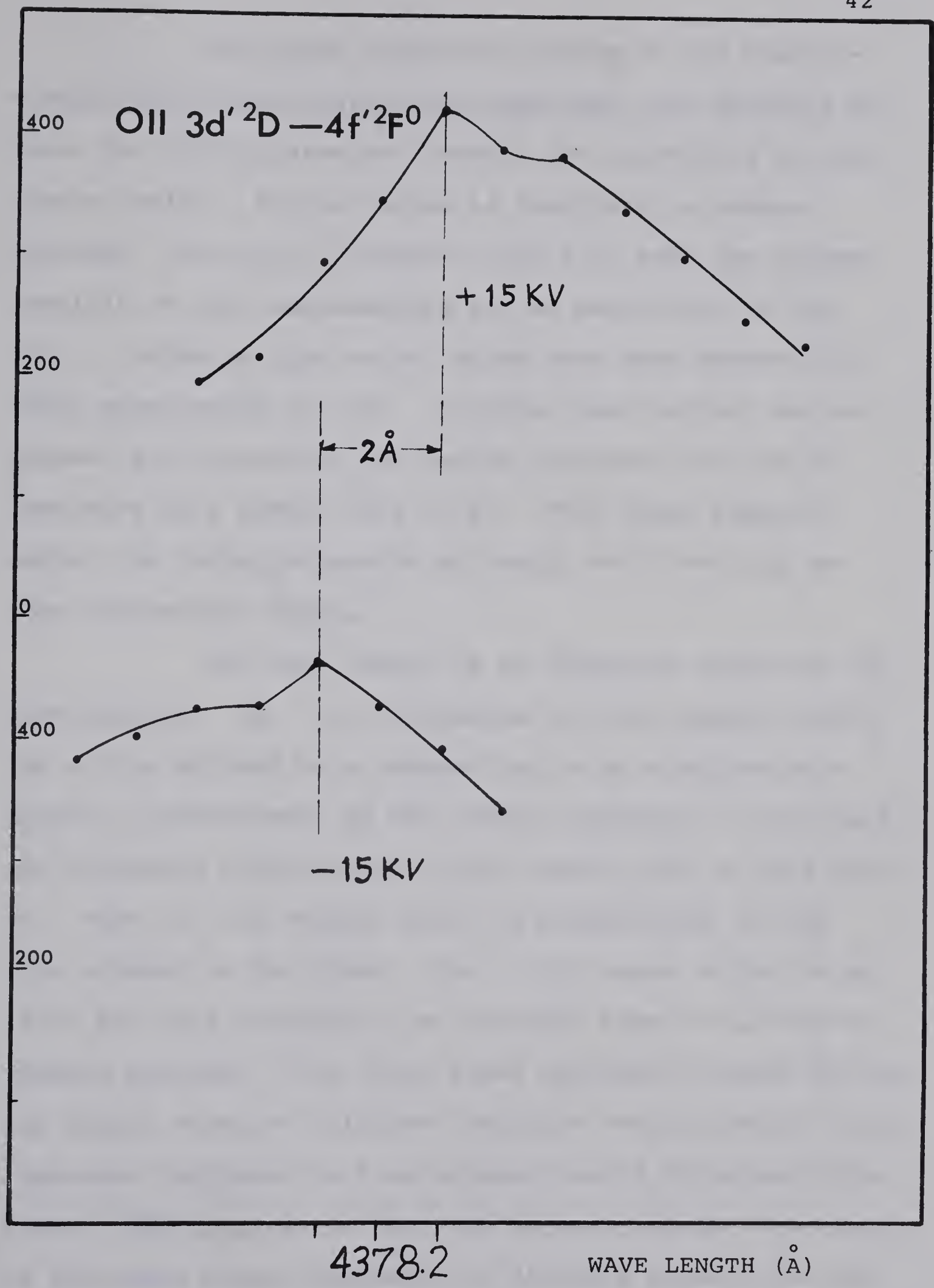

FIG. 4.5 DOPPLER SHIFT FOR A BLEND LINE

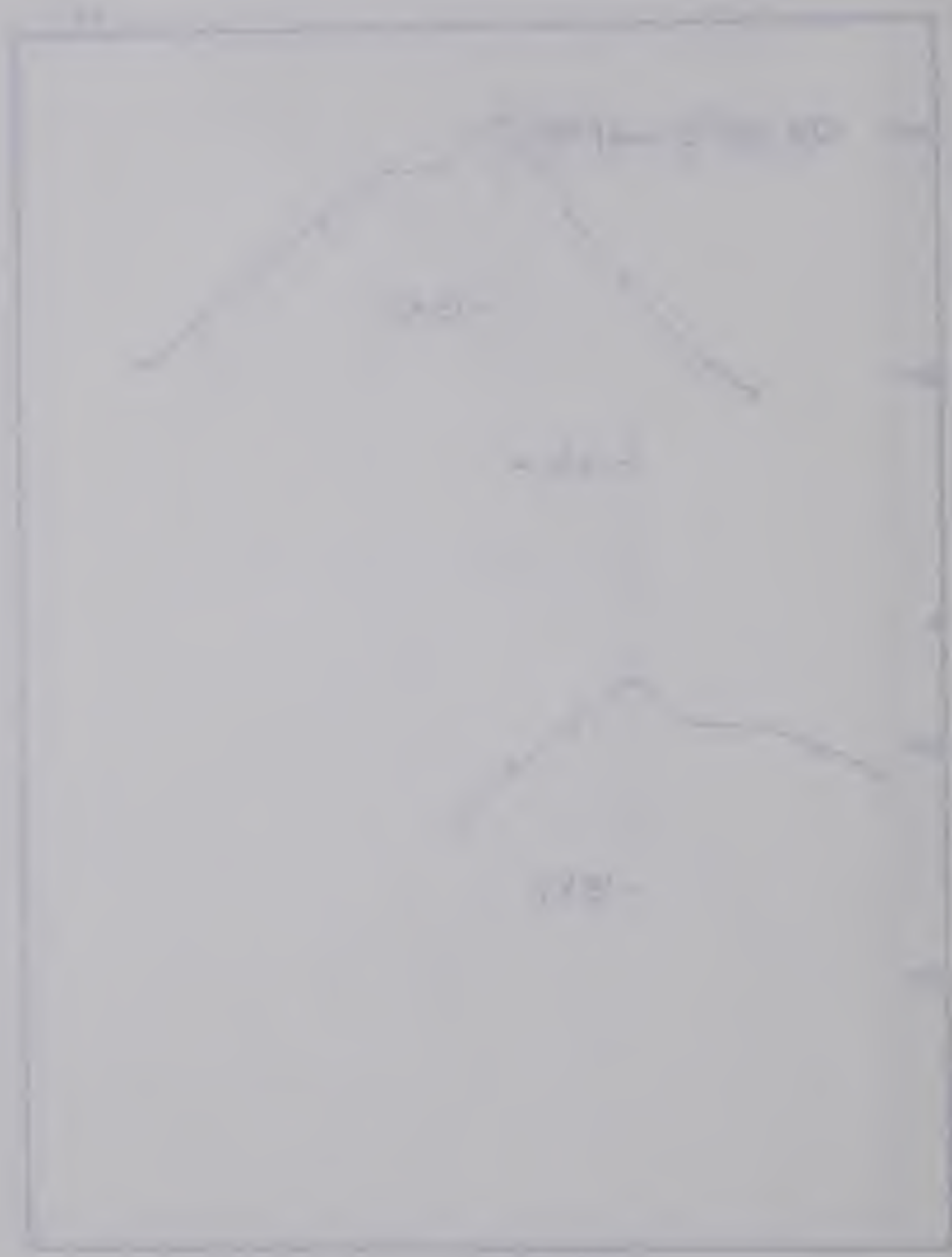

The major technical problem in the electrostatic field charge deflection experiment was sparking between the field plates and between the electrodes and the chamber walls. A good vacuum is important to reduce sparking. The field intensity should be made the highest possible so that measurements can be made close to the foil. Fields as high as 80 KV/cm have been reported in other experiments (Ca 70). A higher beam current and an optimal foil thickness can easily increase the line intensities by a factor of 5 to 10. With these improvements, the technique should be useful well into the vacuum ultraviolet region.

The beam energy is an important factor in the measurements. Eq. (4.3) indicates that the Doppler shift for a line emitted by a charged ion in an electrostatic field is proportional to the length travelled in the field and inversely proportional to the square root of beam energy. That is, the Doppler shift is proportional to the time elapsed in the field. Fig. (4.6) shows a plot of Eq. (4.3) for ions produced by an incident beam of O_2^+ ions at various energies. The solid lines represent Doppler shifts per charge state at different energies and the broken lines represent the decay in line intensities of different lifetimes. The abscissa is the time in nsec and the intercepts of the solid lines represent the distance between the foil and the edge of the field plates, which is 0.5 cm in this case.

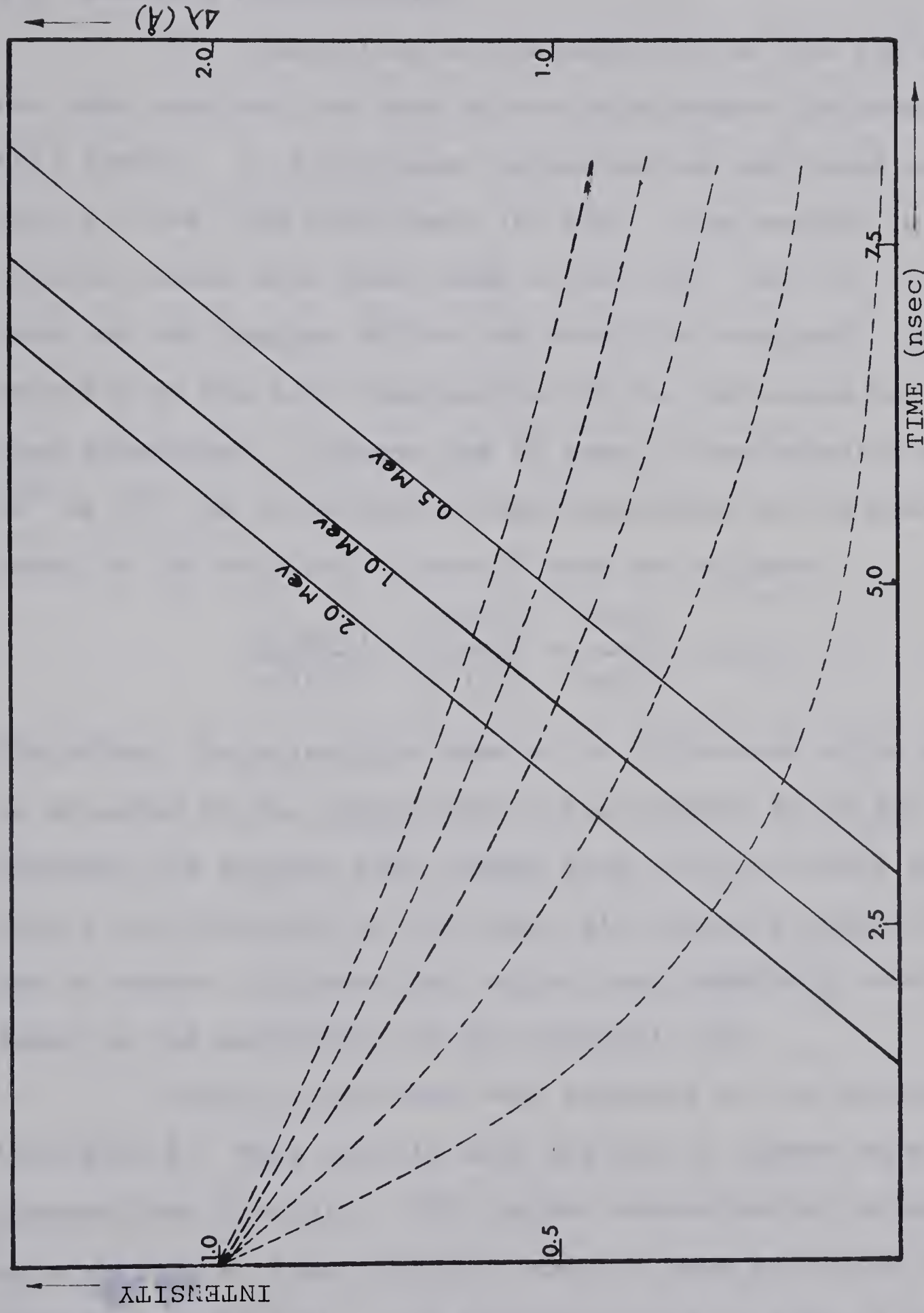

FIG. 4.6 DOPPLER SHIFTS AT POSITIONS ALONG THE ELECTRIC FIELD AT DIFFERENT ENERGIES

4.3 Possible Contamination.

The possibility of contamination of the ion beam has been examined for each of the experiments discussed in this thesis. No significant contamination was found except for the 1968 experiment (Pi 69a). The spectra in the visible region have been taken at both 90° and 30° to the beam and the Doppler shifts for each line examined. The velocity of the ions responsible for the radiation was thus determined. Suppose the O_2^+ beam is contaminated with CO^+ or N_2^+, the velocities of the impurities can be compared to the velocity of the O_2^+ beam as follows:

$$\frac{v^2(CO^+)}{v^2(O_2^+)} = \frac{v^2(N_2^+)}{v^2(O_2^+)} = \frac{m(O_2^+)}{m(N_2^+)} = 1.14$$

Therefore, the velocities have a 7 % difference which can be detected by the comparison of the spectra at 90° and 30°. Although the spectra have proved that no significant impurities are contained in the beam, all possible transitions due to carbon, nitrogen and oxygen ions have been considered in the assignment of any spectral line.

Carbon lines have been detected in the region 1000-2000 Å. They are all weak and due to carbon atoms ejected from the foil. This carbon contamination becomes more serious at lower energies and for beam particles of higher mass (Be 70a). The Doppler shifts of some of the carbon lines have been observed with an argon beam at 1 MeV.

The shifts detected at 30° are generally less than 2 Å, indicating directly the low speed of the emitting ions.

Hydrogen lines at 4861 and 1216 Å have also been detected. The line at 1216 Å is very strong and has a decay curve characterised by times of 0.17 and 1.51 nsec, assuming the speed is the same as the oxygen ions. The decay of Lyman-α has been studied carefully by Chupp et al.(Ch 68) and resulted in decay times of 1.61 and 18.0 nsec. This suggests that the hydrogen contamination is mainly ejected from the foil. Four facts have been observed for the hydrogen lines:

1. The decay in intensity as a function of distance from the foil is also present up-stream of the foil and follows the same pattern.
2. The radiation at 1216 Å can be detected from the beam without the foil.
3. The radiation is present with beams of oxygen, argon and nitrogen (De 70).
4. The intensities are strong and favor lower energy.

In summary, it is concluded that the beam is essentially free from contamination, but that ejected carbon atoms may be significant at lower energies and hydrogen lines seem to be present with various energies and beam particles. Nevertheless, these contaminations do

not interfere with the lifetime measurements. On the contrary, they provide interesting problems, further investigations of which may result in important contributions to beam-foil spectroscopy in the future.

4.4 Line Assignment and Observed New Lines

One of the major difficulties met in beam-foil spectroscopy is the accurate determination of the wavelength of the spectral lines. The line width is generally broad due to the Doppler effect because of the high speed of the radiating source and finite acceptance angle of the instrument. In principle this broadening can be eliminated by refocusing the spectrometer (St 70) or used to increase the line intensity (St 71). The line width may be as high as 10 Å, depending upon the wavelength of the line. The cause of the Doppler broadening can be illustrated by Fig. 4.7.

Let $\Delta\Phi$ be the angle subtended by the focusing optics or the grating in the McPherson monochromator, then the instrument accepts a spectral line with a full line width given by

$$\Delta\lambda = \lambda_o \beta \Delta\Phi \qquad (4.5)$$

The speed of the emitters is in general about 1% of the speed of light and the acceptance angle of the instrument is about 0.1 radian. Hence for a line at 5000 Å, the broadening due to the Doppler effect is about 5 Å. This, plus wide slits of 200-500 μ, make accurate wavelength determination difficult. Therefore the assignment

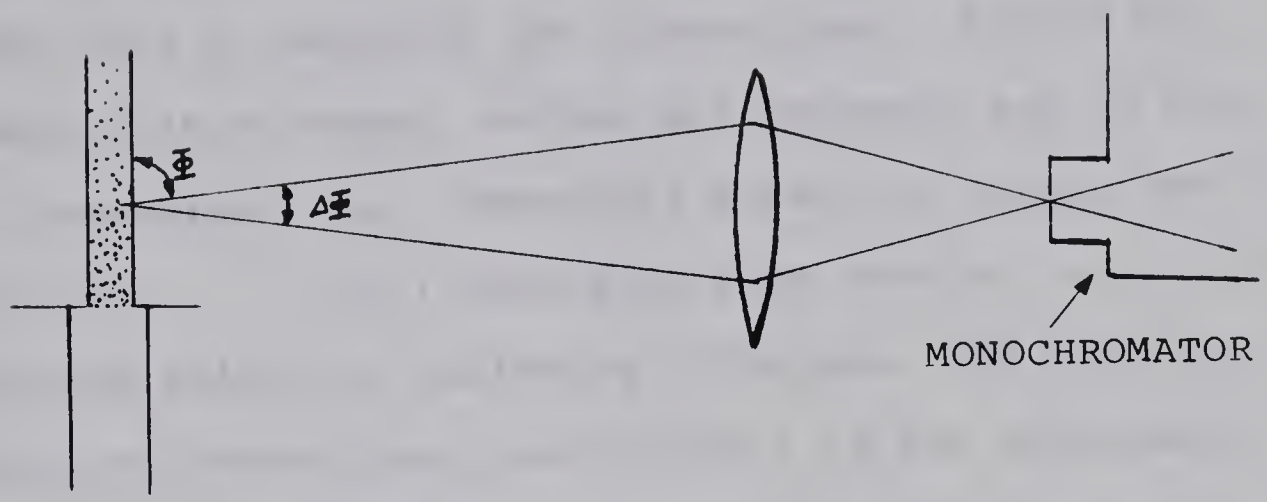

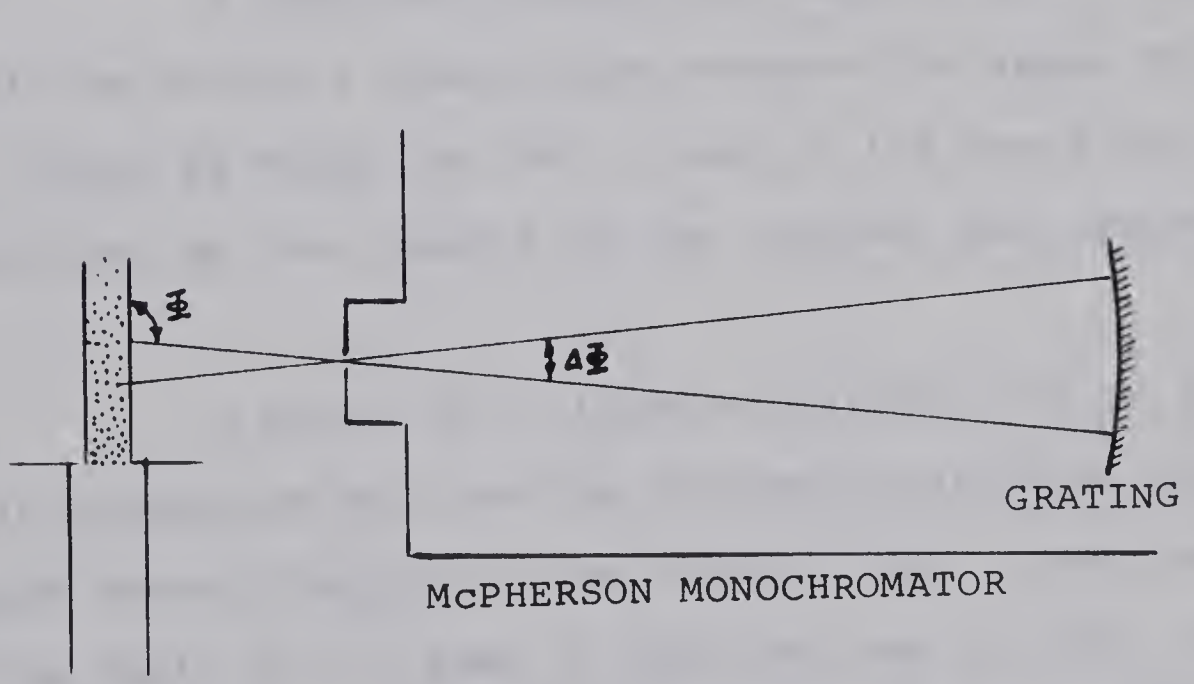

FIG. 4.7 ILLUSTRATION OF THE CAUSE OF DOPPLER BROADENING

of the transition responsible for the spectral line is not always a simple matter.

In the assignments of observed lines, the charge identification results, the published tables by Moore (Mo 50, Mo 59), Striganov et al (St 68), and Kelly (Ke 68) have been used to identify the transitions. Notice has been taken that nitrogen, carbon and hydrogen may be present as contaminations. Beam-foil papers on oxygen (Ma 70, Sm 71, Le 68, ... etc.) have also been used as references. The reported values on radiative lifetimes, and sometimes the relative intensities, are valuable in the assignments.

A computer program has been devised to predict all the possible transitions between the known energy levels listed by Moore (Mo 49). Many of the new lines can be identified by the results of the program (see Appendix II).

A total of 17 lines are identified by the computer program as well as the intensity-variation method of charge identification as new oxygen lines. They are listed in Table IV.2. Most of them are due to OIII, except the lines at 1501 and 4434 Å (due to OII) and the lines at 1165 and 1605 Å (due to OIV). The lines at 1197, 1317 and 4533 Å may be blends of transitions due to OII and OIII. It is interesting to note that many of these 17 lines involve inner shell excitation, e.g.,

$$2s^2 2p(^2P^\circ)3s\ ^3P^\circ - 2s2p^2(^4P)3s\ ^3P$$

TABLE IV.2

OBSERVED NEW OXYGEN LINES

Wave-length (Å) Obs.[a]	Calc.	Charge Id.	Ion	Possible Assignment Transition
1165[w]	1164.5	OIV	OIII	$2s2p3d_1'\,^2F°-2s2p4f_1'\,^2G$
1174[w]	1172.5-74.6	OIII	OIII	$2s^22p(^2P°)3p\,^3D-2s^22p(^2P°)4d\,^3D°$
1197[s]	1197.5-02.6	OII?,III	OIII	$2s^22p(^2P°)3p\,^3D-2s^22p(^2P°)4d\,^3F°$
1209[m]	1205.6-09.9	OIII	OIII	$2s^22p(^2P°)3s\,^3P°-2s2p^2(^4P)3s\,^3P$
1240[s]	1237.7-41.1	OIII	OIII	$2s^22p(^2P°)3p\,^3D-2s2p^2(^4P)3p\,^3D°$
1267[s]	1266.2	OIII	OIII	$2s^22p(^2P°)3p\,^1S-2s^22p(^2P°)5s\,^1P°$
1311[w]	1308.6-13.0	OIII	OIII	$2s^22p(^2P°)3d\,^3P°-2s2p^2(^4P)3d\,^3D$
1317[m]	1315.6-20.4	OII,III	OII	$2s^22p^2(^3P)3s\,^4P-2s^22p^2(^3P)5p\,^4P°$
			OIII	$2s\,2p^2(^4P)\,^3P°-2s2p^2(^2D)3d'\,^3D$
			OIII	$2s^22p(^2P°)3d\,^3F°-2s2p^2(^4P)3d\,^3P$
1358.5[w]	1358.3-59.4	OIII	OIII	$2s^22p(^2P°)4d\,^3D°-2s2p^2(^2D)3d'\,^3F$
1389[w]	1388.8-90.6	OIII	OIII	$2s^22p(^2P°)3d\,^3P°-2s2p^2(^4P)3d\,^3F$
1501[m]	1501.1-04.1	OII	OII	$2s2p^4\,^2D-2s^22p^2(^1D)3p\,^2P°$
			OII	$2s^22p^2(^3P)3p^2D°-2s^22p^2(^1D)5s'\,^2D$
1605[w]	1604.6-04.9	OIV	OIV	$2s^24f\,^2F-2s^2\,6g\,^2G°$ (Br 70)
1727[m]		OIII		?
2510[w]	2503.7-20.3	OIII?	OIII	$2s2p^2(^4P)3d\,^5P-2s2p^2(^4P)\,4p\,^5D°$
4434[m]	4437.2	OII	OII	$2s2p^2(^3P)4s\,^4P-2s2p^2(^3P)5p\,^4D°$
4516[w]	4514.1-19.2	OII	OII	$2s^22p^2(^3P)4s\,^4P-2s2p^2(^3P)5p\,^4P°$
4533[w]	4530.6-35.5	OII,III	OII	$2s2p^2(^3P)4s\,^4P-2s2p^2(^3P)5p\,^4D°$

a Intensity of the line, s=strong, m=medium, w=weak.

CHAPTER V

ANALYSIS OF RADIATIVE LIFETIMES

5.1 Beam Velocity

To relate the radiative lifetime of an upper level of a transition to the intensity decay of the spectral line, the velocity of the ion responsible for the transition has to be known. The beam velocity can be calculated from the estimated energy loss in traversing the carbon foil and the incident beam energy. If the actual beam energy is given in MeV and the mass of the beam ions in a.m.u., the beam velocity, v, in cm/sec would then be

$$v = 1.389 \times 10^9 \sqrt{E/M} \qquad (5.1)$$

Another approach is to measure the Doppler shifts at angles different from 90° to the ion beam and the velocity is then calculated according to the equation

$$\lambda_\circ - \lambda = \lambda_\circ(\beta\cos\theta + \tfrac{1}{2}\beta^2 + ...) \qquad (5.2)$$

where β is the ratio of the beam velocity to the velocity of light and θ is the angle of observation. In the present experiments, the beam velocities have been measured at various energies by observing at both 10° and 30° to the beam. The results are plotted in Fig. 5.1. Each point on the graph is the average velocity at the energy based on

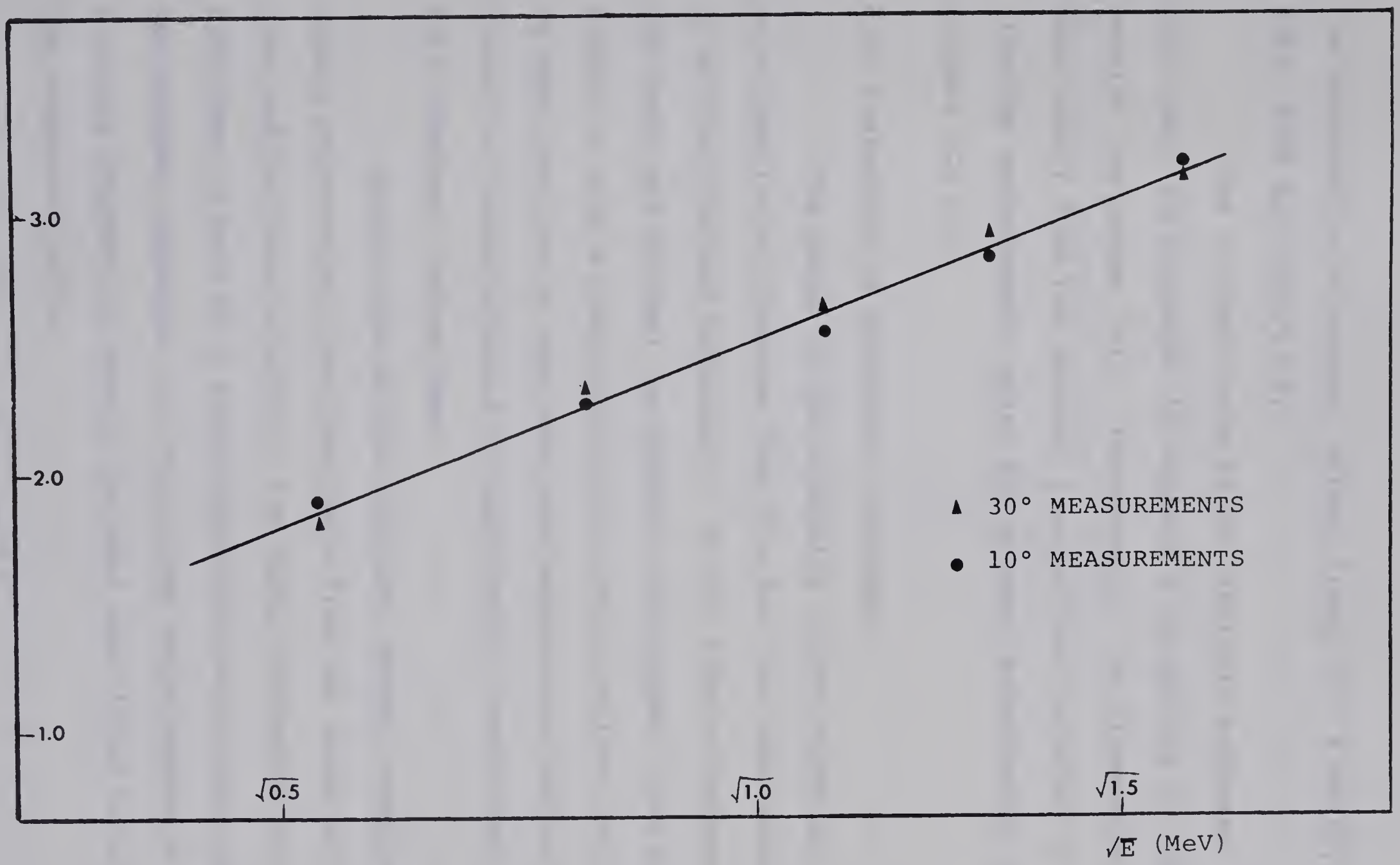

FIG. 5.1 BEAM VELOCITY MEASUREMENTS

the observation of several strong lines (OII 4346/49, 4367, 4378 and 4415/17 Å).

The incident beam is not strictly monoenergetic and, furthermore, it suffers a straggling in traversing the carbon foil. Fortunately, the dispersion in beam energy does not present a significant problem in lifetime measurements under the present experimental conditions (Cu 70).

5.2 Evaluation of Radiative Lifetimes

The decay of the intensity of the spectral line as a function of distance from the foil has been measured by photon-counting techniques. At the time of measurement the decay was plotted on semilog graph paper. The plot served to give a rough idea of the decay pattern, to judge at what position to make the next measurement and to indicate any abrupt changes in experimental conditions, e.g., foil breakage, vacuum loss.

Estimations of the lifetime, using singly or double exponentials, are then made from the slope of the plot and the beam velocity. The final evaluation of the lifetimes is made by a least-squares-curve-fitting computer program (Appendix I). For curves which appear to be a single exponential decay, the data are fitted to a single component curve,

$$S_1 = Ae^{-t/\tau} \qquad \ldots\ (5.3)$$

For curves which appear to be a multi-exponential decay, the data are fitted to a double-component curve,

$$S_2 = Ae^{-t/\tau_1} + Be^{-t/\tau_2} \quad \ldots\ (5.4)$$

An accuracy parameter, which is defined by

$$Ap = \frac{\sum_{i=1}^{N} (\Delta C_i)^2 / C_i}{(N \sum_{i=1}^{N} C_i)^{\frac{1}{2}}} \quad \ldots\ (5.5)$$

with C_i the number of counts at data point i, ΔC_i the difference between the computed and the observed number of counts and N the number of data points, is also calculated by the computer program and is an indication of the goodness of the fit. This parameter is simply a sum-of-squares parameter modified to take account of the fact that more intense lines tend to give more accurate lifetimes (Pi 70).

The linearity of the semilog plot of a decay does not guarantee that it is a single exponential decay. Fig. 5.2 illustrates that the summation of two exponential decays, with the lifetime for curve b twice that for curve a, may appear to be a single exponential decay. Therefore, for each line with a linear semilog plot, the possibility of blending and cascade repopulation of the upper level must be investigated. Observed examples are the OII 4189, 4592, 4660 Å and OIII 3350, 3385 Å lines.

Cascading is a major problem met in the analysis of the radiative lifetimes. It can be shown that, for a

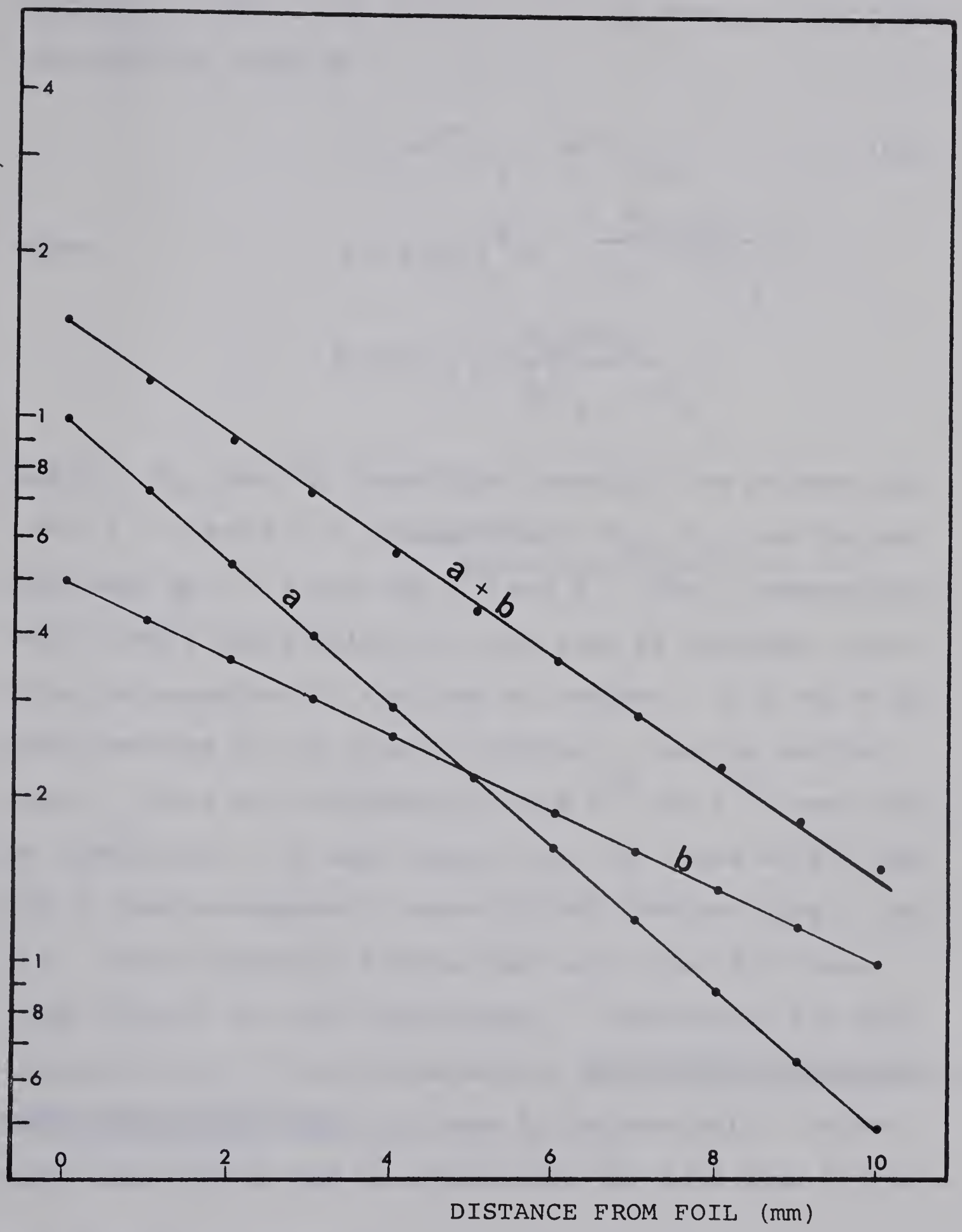

FIG. 5.2 THE SUMMATION OF TWO EXPONENTIALS

cascading scheme given by Fig. 5.3, the decay of the light intensity is given by

$$I = Ae^{-t/\tau_i} + Be^{-t/\tau_k} \qquad \ldots\ (5.6)$$

where

$$A = KA_{ij}\left(N_{io} - \frac{A_{ki}\,N_{ko}}{1/\tau_i - 1/\tau_k}\right)$$

$$B = KA_{ij}\left(\frac{A_{ki}\,N_{ko}}{1/\tau_i - 1/\tau_k}\right)$$

and A_{ij}, A_{ki} are the transition probabilities between the level $i \rightarrow j$ and $k \rightarrow i$, respectively; N_{io}, N_{ko} are the populations at $t = 0$ for the i^{th} and k^{th} level, respectively. Both A and B are positive for the case of blending, while B can be negative for the case of cascade. If A and B are both positive in the case of cascade τ_i must be smaller than τ_k, thus the lifetimes for the i^{th} and k^{th} level can be indentified. In some cases, e.g. the lines at 510 and 526 Å, double-component curve-fitting does not give a good fit. Three-component fitting has been tried for these lines without too much improvement. Considering the statistical error of the measurements, curve-fitting with more than three components does not seem to be meaningful, unless very large counts can be accumulated for each data point.

5.3 Error Estimation

Statistically, the mean square deviation of the signals obtained in the photon-counting technique is given

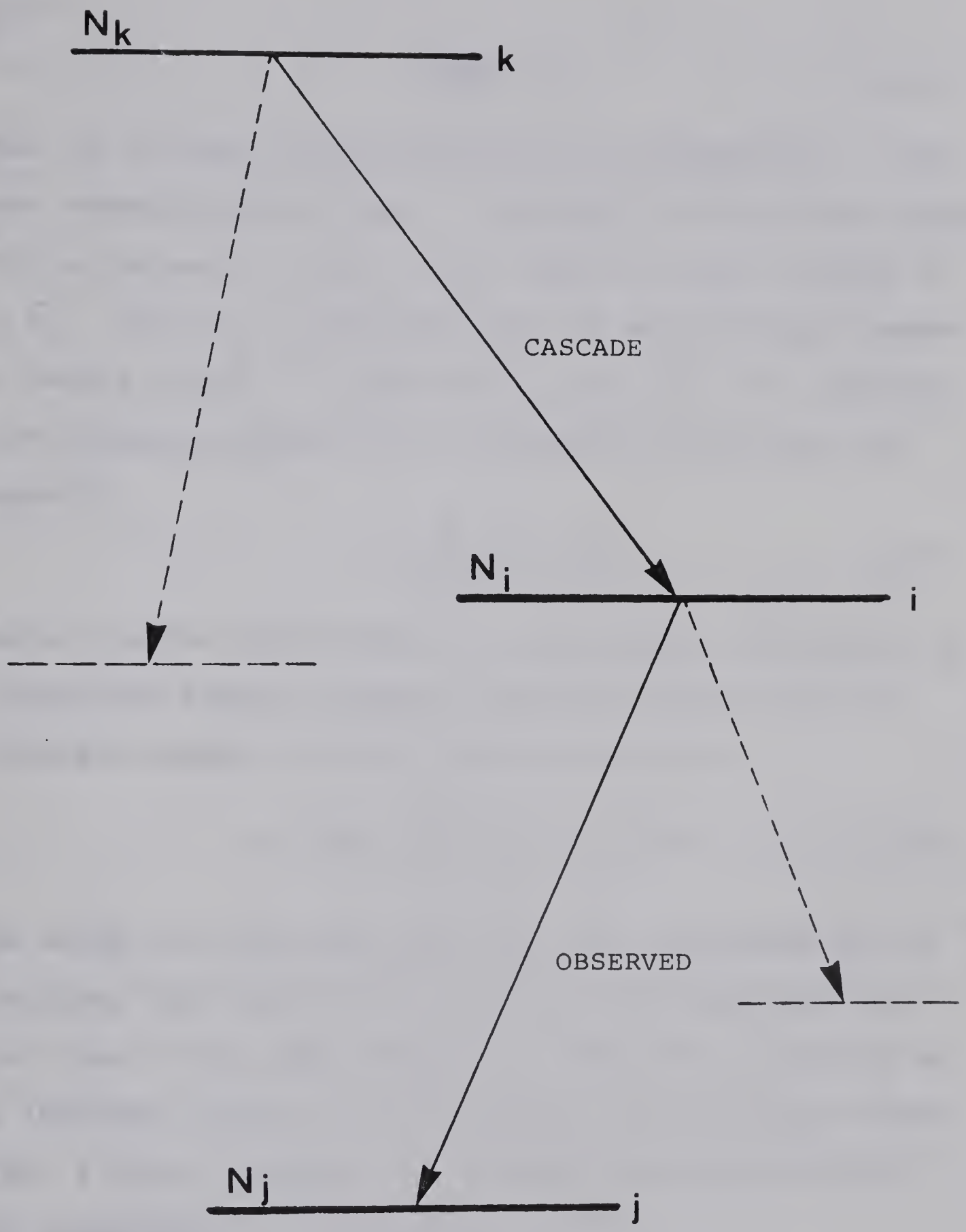

FIG. 5.3 DIAGRAM FOR A CASCADE TRANSITION

by

$$\overline{(\Delta n)^2} = \bar{n} \qquad \ldots\ (5.7)$$

That is, the mean square deviation is proportional to the most probable photon count. Therefore, in the least-squares fitting process, to each $(\Delta S_i)^2$ must be given a weight of $1/\overline{S_i}$. Here ΔS_i = deviation from the most probable number of counts at the i^{th} observation point, $\overline{S_i}$. The computer least-squares program is thus designed to minimize the quantity

$$D = \sum_{i=1}^{N} (\Delta S_i)^2/\overline{S_i} \qquad \ldots\ (5.8)$$

where N is the total number of data points. Dividing D by N gives the average weighted least deviation, which in principle yields 1 for an ideal decay curve

$$\alpha = D/N = \sum_{i=1}^{N} ((\Delta S_i)^2/\overline{S_i})/N = 1 \qquad \ldots\ (5.9)$$

The value of α for each decay has been calculated and it indicates the relative reliability of the observed data for lines of the same intensity. Since line intensity is an important factor in the accuracy of the observed life-time, a better parameter to indicate the uncertainty of the measurement is β defined by (Pi 70)

$$\beta = \alpha/(\text{mean intensity})^{1/2}$$

$$= \sum_{i=1}^{N} \frac{(\Delta S_i)^2}{S_i} \Big/ \left(N \sum_{i=1}^{N} \overline{S_i}\right)^{1/2} \qquad \ldots\ (5.10)$$

The percentage error due to the statistical fluctuations of photon emission for a single exponential decay is then

about 20β (Pi 70). For most of the cases, cascading or blending are involved and the estimation of the error becomes more difficult. The value of β for each decay curve is also computed; thus the relative accuracy can be compared. A larger value for β indicates a lower accuracy for the observed lifetime. Other factors such as beam velocity uncertainty, foil aging (Bi 68b) and the noise to be subtracted from the observed signal have to be added to obtain the total error. The contribution of these three factors was estimated to be about 3%.

Considering the errors mentioned above, total uncertainties for single exponential decay curves with medium or strong intensity are about ± 10%, the same as is obtained by comparing the lifetime values reported by other workers (Pi 70). The uncertainties for multi-exponential decay curves should depend on the relative intensity of the components. The weaker component would be strongly effected by the fluctuations of the stronger component so that the accuracy of the lifetime value obtained for the weaker component must be worse than that for the stronger one. In these cases, the lifetime values are probably uncertain to about ± 20% or worse.

In summary, for single exponential curves it is possible to calculate the uncertainty arising from the statistical fluctuations of photon emission, and to combine this with the contributions arising from the various experimental factors mentioned above. The resulting error

estimate of ± 10% agrees well with the variation found between data obtained at different laboratories for single exponential decay curves. In practice, however, most decay curves must be fitted to a function of the form

$$I = A.\exp(-t/\tau_i) + B.\exp(-t/\tau_k) + ...$$

for which the statistical fluctuations normally preclude the justification of more than the first two terms. For such double-exponential decay curves, the contribution to the uncertainty of the lifetime τ_i arising from the statistical fluctuations will exceed that forecast by the factor β which assumes a single exponential decay curve, but will approach this forecast value as the ratio B/A approaches zero.

CHAPTER VI

RESULTS

6.1 The Spectrum

The spectra were recorded in three regions (2000 - 5000 Å, 1000 - 2000 Å and 370 - 1000 Å) at different energies, using three different photon detectors. The uncertainties in wavelength were estimated to be ± 2 Å for the region above 2000 Å and ± 1 Å below 2000 Å. The half widths of the lines observed were about 4 - 5 Å. A total of 112 lines were identified as due to oxygen and their distributions among the charge states and regions of observation are summarized in Table VI.1:

TABLE VI.1 NUMBER OF LINES OBSERVED FOR OXYGEN

Region	OI	OII	OIII	OIV	OV	Total
2000-5000 Å	0	34	16	0	0	50
1000-2000 Å	2	3	18	4	1	28
370-1000 Å	5	8	10	7	4	34
Total	7	45	44	11	5	112

Fig. 6.1 gives the partial spectrum of oxygen at 0.5 MeV/atom taken with the arrangement 3 described in Chapter III. The lines at 1129, 1188, 1279, 1296 and 1330 Å are due to carbon ions ejected from the foil. The line at 1216 Å is due to hydrogen and is strong at all energies employed. It

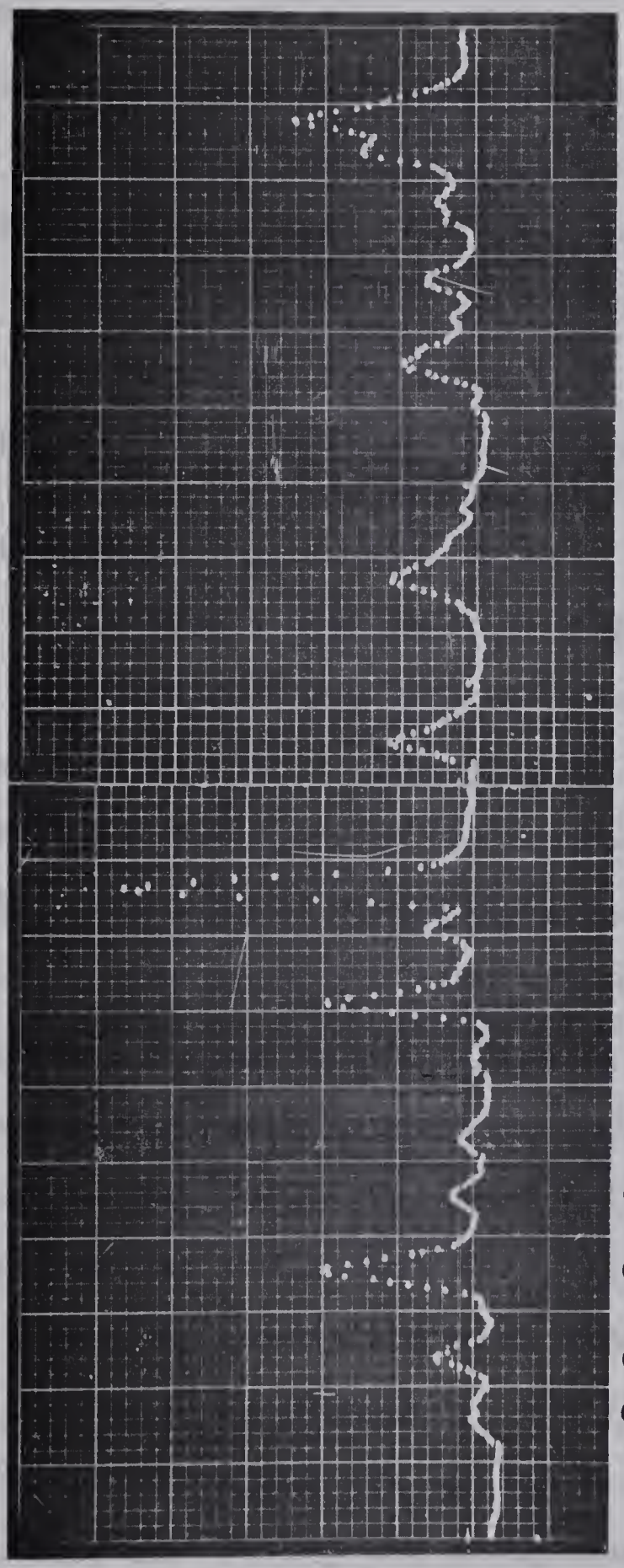

FIG. 6.1 PARTIAL SPECTRUM OF OXYGEN AT 0.5 MeV/ATOM

is mainly due to hydrogen ejected from the foil as discussed in section 4.3. The lines at 1197, 1209, 1240, 1267, 1273, 1311 and 1317 Å are new lines identified as due to OIII.

Fig. 6.2 presents partial spectra of oxygen at two different energies. The intensity variations with energy are dramatic for the line at 1153 Å which is identified as due to OI and the line at 1165 Å which is due to OIV. Some of the intensity-variation plots are given in Fig. 4.1.

6.2 Lifetimes

Lifetimes for about 90 lines were measured with values which ranged from 0.1 to several x 10 nsec. The decay curves show that cascading or blending is present for most of the lines. Fig. 6.3-6 represent typical decays and their decompositions. The measurements of Fig. 6.5 were made at 1.4 MeV hence the time scale is different from that for which the beam energy was 1 MeV for the rest of the decays. Fig. 6.6 illustrates a line decomposed into three components and also a line which is difficult to analyze. The final lifetime values are obtained by a computer least-squares fitting program. The results, including comparison with other works and theoretical values wherever available, are listed in Table VI.2. The theoretical values are strictly speaking only upper limits as they are simply the reciprocals of the sums of the transition probabilities calculated for transitions from the level in question, so that unless all possible transitions have been included, the theoretical "lifetime" will

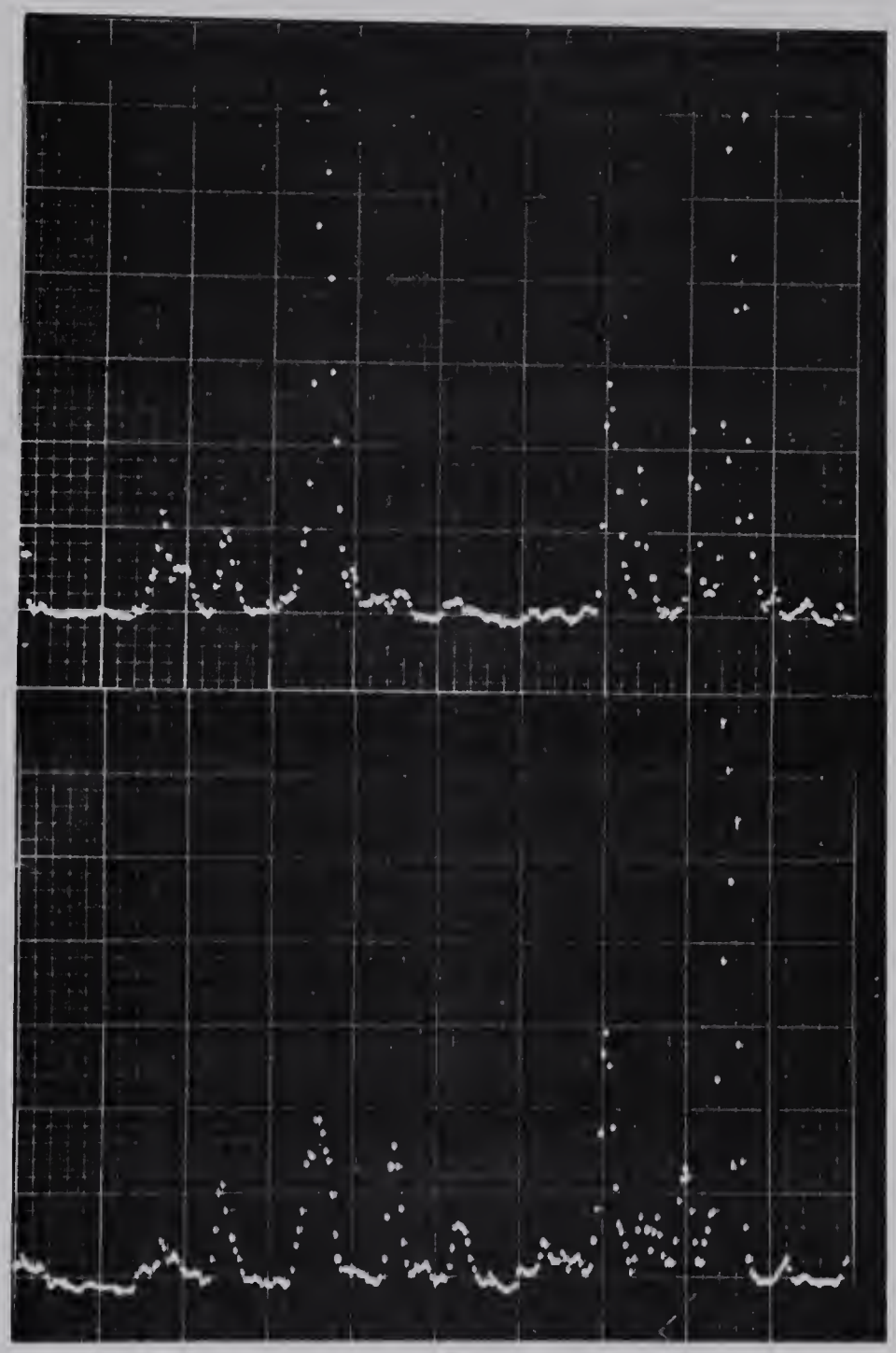

FIG. 6.2 PARTIAL SPECTRA OF OXYGEN AT 0.35 AND 0.7 MeV/ATOM

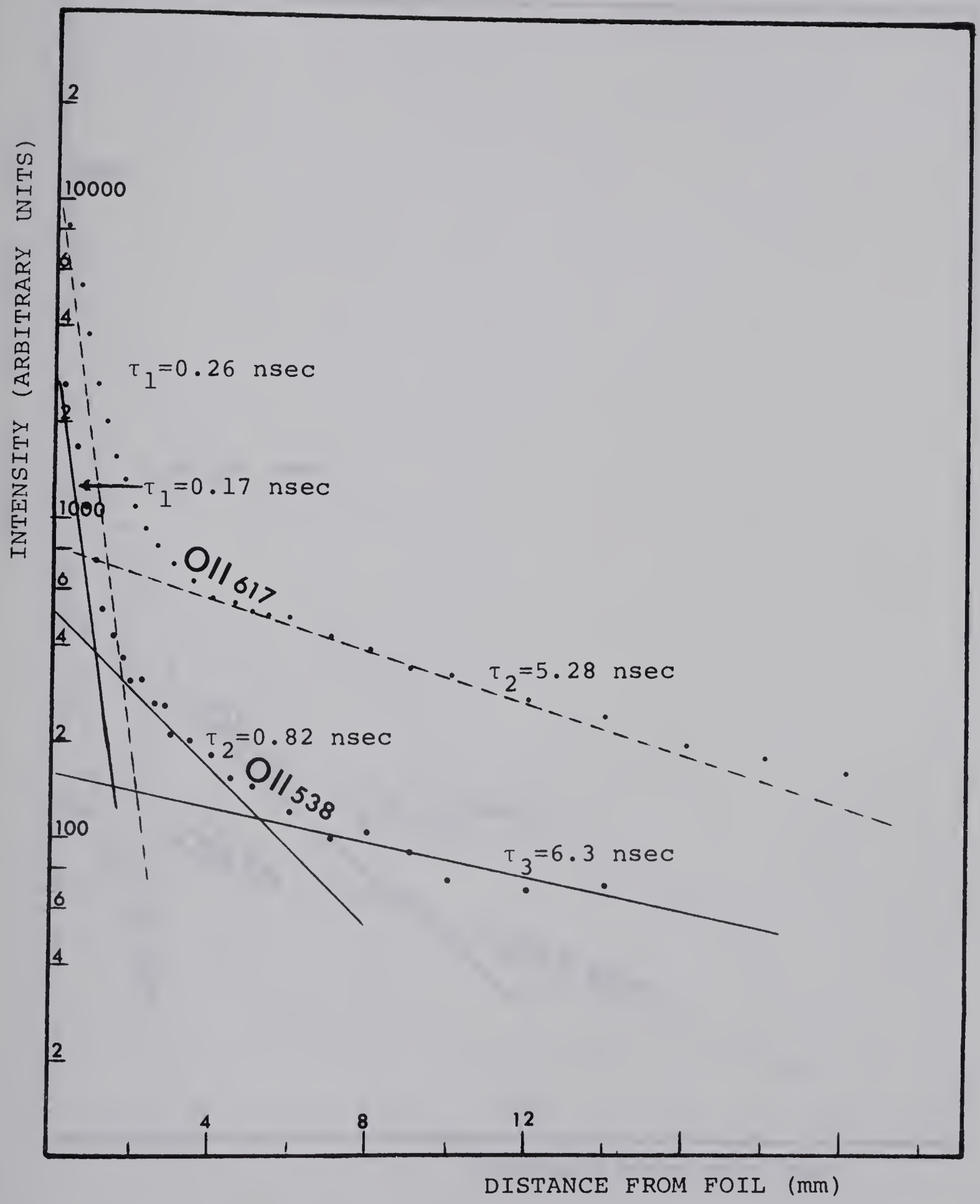

FIG. 6.3 THE INTENSITY DECAY OF OII 538 Å AND 617 Å

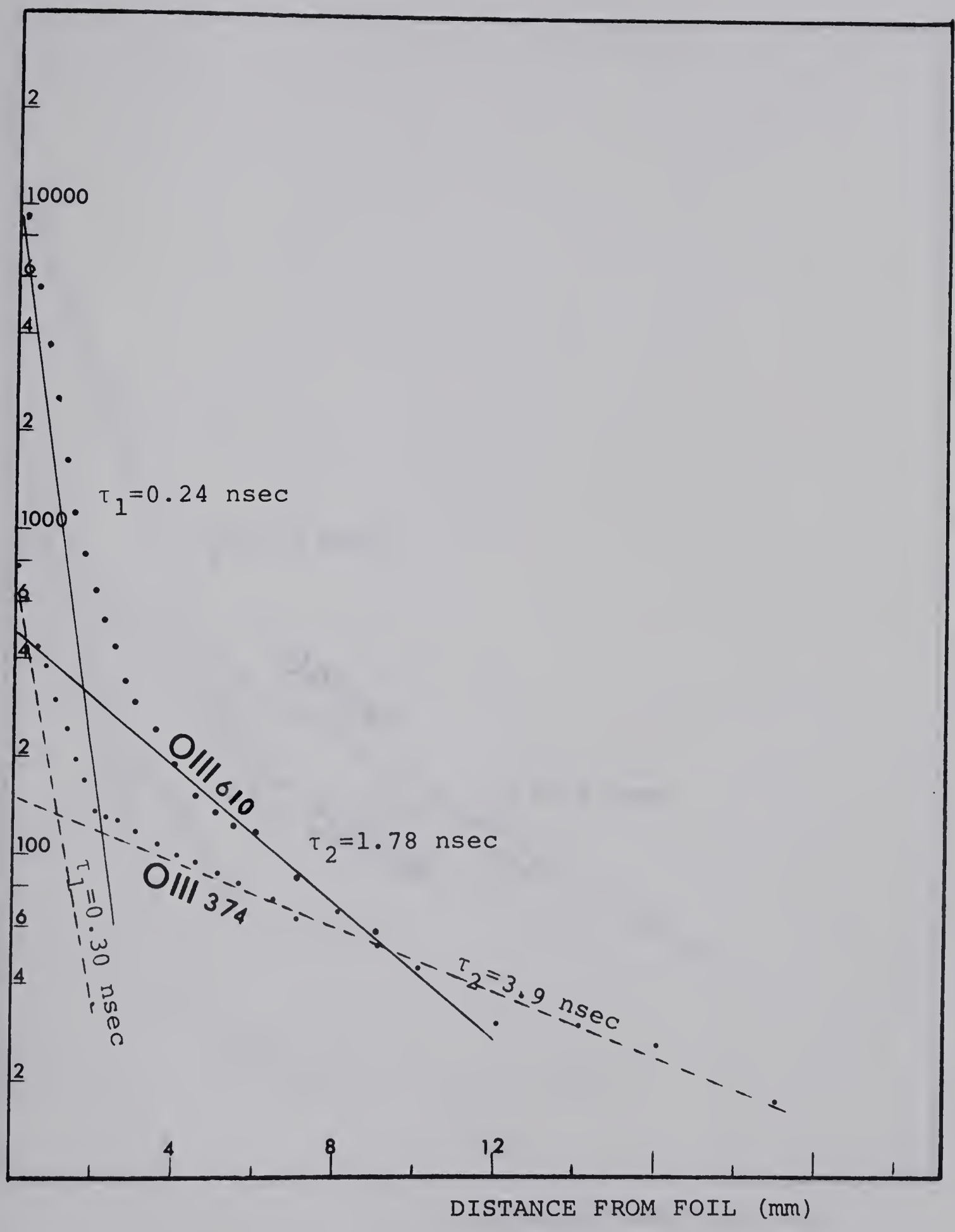

FIG. 6.4 THE INTENSITY DECAY OF OIII 374 Å AND 610 Å (PROBABLY OIV, SEE TEXT)

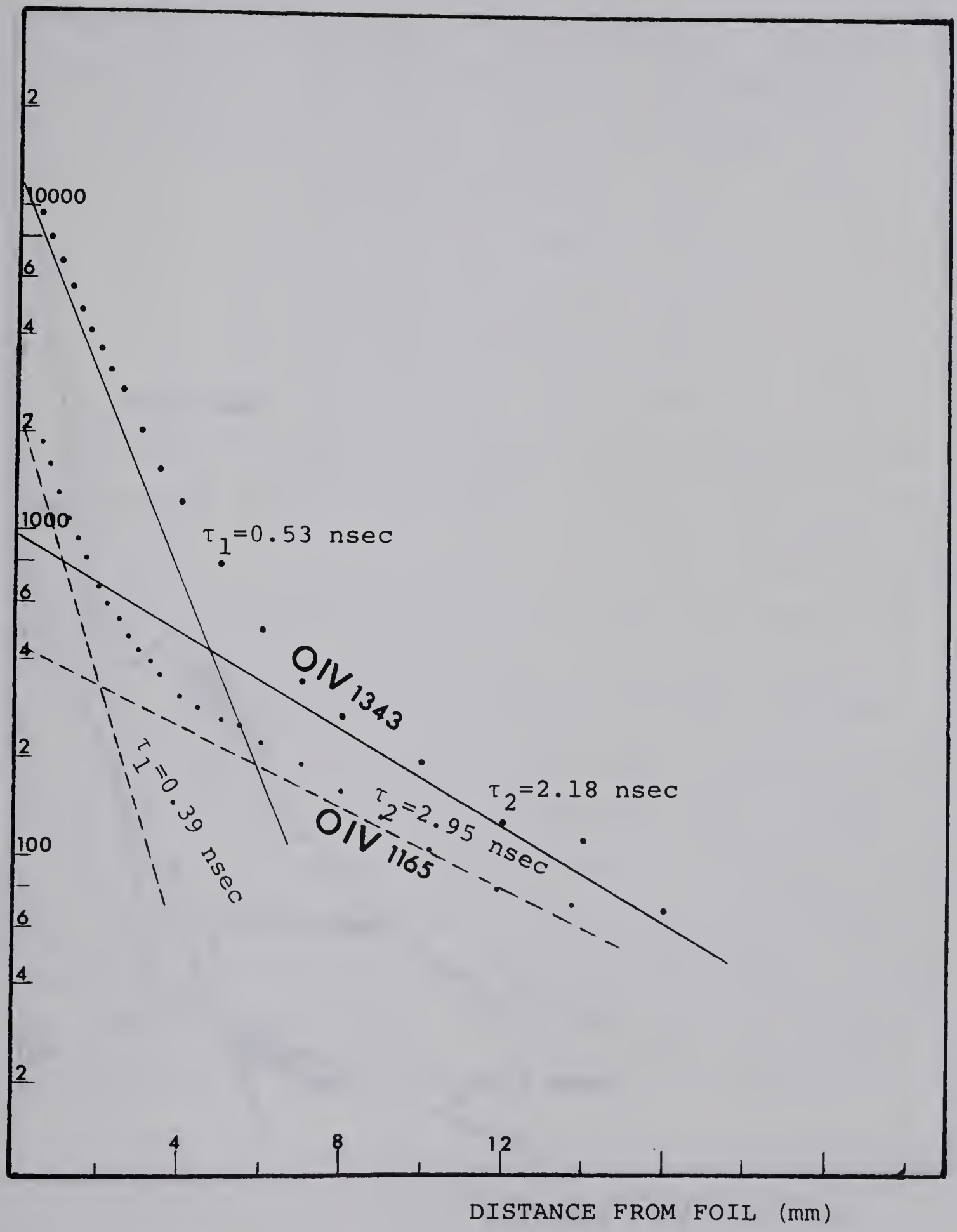

FIG. 6.5 THE INTENSITY DECAY OF OIV 1165 Å AND 1343 Å

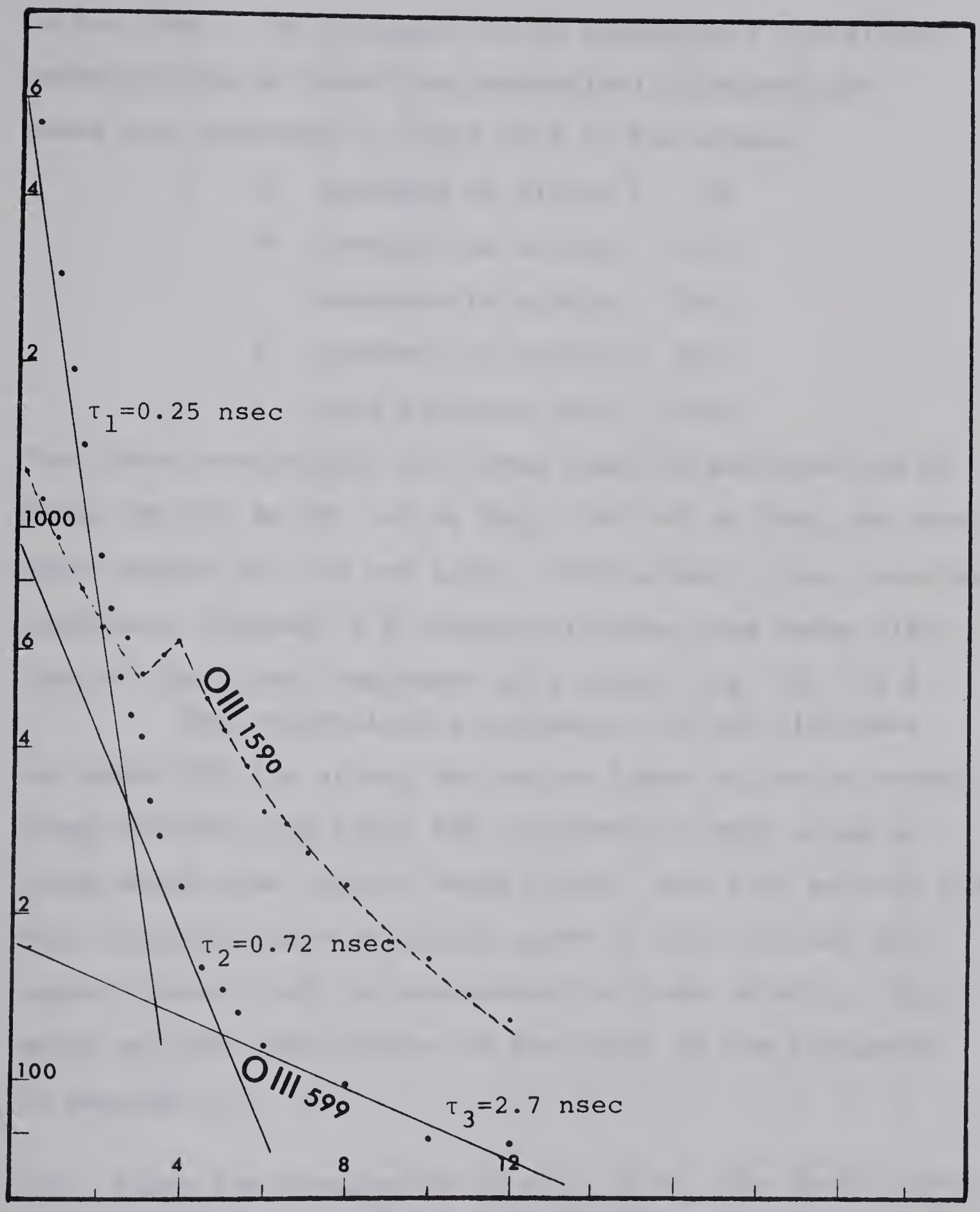

FIG. 6.6 THE INTENSITY DECAY OF OIII 599 Å AND 1590 Å

be too long. The accuracy of the theoretical transition probabilities on which the theoretical lifetimes are based are indicated in Table VI.2 by the scheme:

A	accurate to within ±	3%
B	accurate to within ±	10%
C	accurate to within ±	25%
D	accurate to within ±	50%
E	less accurate than ±	50%

The listed wavelengths are taken from the publications by Moore (Mo 50, Mo 59) and by Kelly (Ke 68) or from the computer output for the new lines. The column τ_2 may sometimes represent, instead of a cascade lifetime, the decay lifetime of the second component of a blend, e.g. OII 538 Å.

The uncertainties estimated for the lifetimes are about 10% for strong and medium lines following normal decay patterns and about 20% or worse for weak lines or lines which have strange decay curves (see also section 5.3). This includes the statistical error of the data and systematic errors such as uncertainty in beam velocity, foil-aging and the subtraction of the noise as was discussed in section 5.3.

N.B. Since the preparation of Fig. (6.4), the decay curve obtained at 610 Å has been re-assigned to OIV.

TABLE VI.2

RADIATIVE LIFETIMES IN OI-OV

Wave-Length (Å) Obs.	Listed	Transition	This Work τ_1 (nsec)	τ_2	R(0)[r]	Other Values[q] (nsec)	Theory[j] (nsec)
OI							
1153	1152.2	$2p^4\,{}^1D\text{-}3s'\,{}^1D^\circ$	1.78±0.2	5.77±1.0?	0.09	1.9±0.2[f,d], 1.77±0.14[g] 1.9±0.3[b]	2.22E
1304	1302.2-06.0	$2p^4\,{}^3P\text{-}3s\ {}^3S^\circ$	1.41±0.3	7.12±1.0?	0.16	1.75±0.2[f], 1.82±0.05[d] 1.79±0.17[g], 1.70±0.3[b]	2.63D
OII							
485	483.8 -84.0	$2p^3\,{}^2D\text{-}3d\ {}^2P$	0.37±0.5	3.08±0.05	0.21		0.84D_
	485.1 -85.5	$2p^3\,{}^2D^\circ\text{-}3d\ {}^2F$					0.40D_
538	537.8 -38.3	$2p^3\,{}^2D^\circ\text{-}2p^4\,{}^2P$	0.17±0.02			0.12±0.03[f]	
	539.1 -39.9	$2p^3\,{}^4S^\circ\text{-}3s\ {}^4P$		0.82±0.2		0.9±0.3[f]	1.16E
581	580.4 -81.0	$2p^3\,{}^2P^\circ\text{-}2p^4\,{}^2P$	0.12±0.02	0.83±0.2	0.05		
617	616.9 -17.0	$2p^3\,{}^2D^\circ\text{-}3s\ {}^2P$	0.26±.03	5.28±1.0	0.07		0.37E
1317	1315.3-19.9	$3s\ {}^4P\text{-}5p\ {}^4P^\circ$	1.78±0.2	11.3±2.0	0.20	1.3±0.2[f]	
1501	1501.1-04.1	$2p^4\,{}^2D\text{-}3p\ {}^2P^\circ$	5.0 ±0.5				

Wave-Length (Å) Obs.	Listed	Transition	This Work τ_1 (nsec)	τ_2 (nsec)	R(0)[r]	Other Values[q] (nsec)	Theory[j] (nsec)
OII							
1654	1650.7-57.9	3s ^{4}P-4p ^{4}D°	0.21±0.04	1.58±0.5	0.25	0.93±0.15[f]	
2445	2444.3-45.6	3s ^{2}P-3p' ^{2}D°	3.72±0.4				
3726	3727.3	3s ^{4}P-3p ^{4}S°	4.80±1.0	2.09±0.5	0.97	(5.4[p]),(5.8[p])	5.6C
3973	3973.3	3s ^{2}P-3p ^{2}P°	6.01±0.6			7.1[p]	6.8C
4072	4072.2	3p ^{4}D°-3d ^{4}F	7.76±0.8?			5.29[m],(4.18[m]),5.6[p]	5.1C
4075	4075.9	3p ^{4}D°-3d ^{4}F	8.61±0.9?			5.6[p]	
4087	4085.1	3p ^{4}D°-3d ^{4}F	8.82±0.9?				
4096	4092.9-94.2	3p ^{4}D°-3d ^{4}F	9.64±1.0?			4.2[p]	5.1C
4119	4119.2-20.6	3p ^{4}P°-3d ^{4}D	4.46±0.5			3[p],(2.6[p]),(3[p])	4.5C
4140	4140.7	3p ^{4}P°-3d ^{4}P	1.82±0.4	7.20±1.5	0.45		0.25C
4151	4153.3	3p ^{4}P°-3d ^{4}P	1.97±0.4	9.28±2.0	0.33	4.2[p]	0.25C
4185	4185.5	3p' ^{2}F°-3d' ^{2}G	8.47±0.9?			9.5[p]	4.0C
4189	4189.8	3p' ^{2}F°-3d' ^{2}G	5.59±1.1?	64.8±13.0	0.58	5.05[m],6.1[p]	4.0C
4253	4253.7-54.0	3d' ^{2}G -4f' ^{2}H°	6.19±0.6			4.35[m],6.9[o],5.5[p]	3.8C

Wave-Length (Å) Obs.	Listed	Transition	This Work (nsec) τ_1	τ_2	R(0)[r]	Other Values[q] (nsec)	Theory[j] (nsec)
OII							
4276	4275.5	3d ^{4}D -4f ^{4}F°	4.22±0.4			4.0[p]	4.7C
4313	4313.4-15.8	3d ^{2}F -4f ^{4}F°	2.98±0.6				4.7C
4345	4345.6	3s ^{4}P -3p ^{4}P°	7.05±0.7				9.5C
4349	4349.4	3s ^{4}P -3p ^{4}P°	7.69±0.8			7.7[m],(8.54[m]),7.7[p],(8.5[p])	9.5C
4366	4366.9	3s ^{4}P -3p ^{4}P°	11.3±2.0	2.23±0.5			9.5C
4379	4378.0-78.4	3d' ^{2}D -4f' ^{2}F°	2.16±0.4	11.3±3.0	0.41	4.0[p]	
4415	4414.9-17.0	3s ^{2}P -3p ^{2}D°	9.92±1.0			11.85[m],11[p]	8.8C
4434	4437.2	4s ^{4}P -5p ^{4}P?	1.78±0.4	16.3±3.0	0.47		
4447	4448.2	3p' ^{2}F°-3d' ^{2}F	0.90±0.2	7.81±1.5	0.54	(0.64[n])	0.36D
4452	4452.4	3s ^{2}P -3p ^{2}D°	8.83±0.9				8.8C
4467		?	6.74±1.0	2.30±0.5	0.94		
4475		?	2.72±0.5	19.3±4.5	0.35		
4533		?	2.71±0.3				
4592	4591.0	3s' ^{2}D -3p' ^{2}F°	10.1±2.0	4.60±0.9	0.87	12.8[m],8.7[o],14[p]	9.0C

Wave-length (Å) Obs.	Listed	Transition	This Work (nsec) τ_1	τ_2	R(0)[r]	Other Values[q] (nsec)	Theory[j] (nsec)
OII							
4610	4610.4-13.7	3d ^{2}D-4f ^{2}F°	6.30±1.5			4.4[p]	5.5C
4639	4638.9-41.8	3s ^{4}P-3p ^{4}D°	29.8±5.0?			12.[p]	9.8C
4649	4649.1-50.8	3s ^{4}P-3p ^{4}D°	21.94±4.0?	4.18±0.8?	2.01	10.[p]	9.8C
4660	4661.6	3s ^{4}P-3p ^{4}D°	11.9±2.0?			19.[p]	9.8C
4676	4676.2	3s ^{4}P-3p ^{4}D°	14.5±3.0?				9.8C
4701	4699.2	3p'^{2}D°-3d'^{2}F	0.81±0.1				0.36D-
		3p ^{2}D°-3d ^{2}F					0.38D-
OIII							
374	373.8-374.4	2p ^{3}P-3s ^{3}P°	0.30±0.03	3.89±0.5	0.17		0.26E
508	507.4-508.2	2p ^{3}P-2p^3 ^{3}S°	0.10±0.01	0.85±0.1	0.10	0.105±0.012[c]	0.067E;0.071[i]
526	525.8	2p ^{1}D-2p^3 ^{1}P°	0.15±0.03	0.32±0.08	0.18	0.134±0.013[c]	0.083E;0.098[i]
599	597.8	2p ^{1}S-2p^3 ^{1}P°	0.25±0.03	0.72±0.15	0.06		0.083E;0.098[i]
	599.6	2p ^{1}D-2p ^{1}D°					0.147E;0.181[i]

Wave-length (Å) Obs.	Listed	Transition	This Work (nsec) τ_1	τ_2	R(0)[r]	Other Values[q] (nsec)	Theory[j] (nsec)
OIII							
1138	1138.5	$2p^3\ ^1P^o-2p^4\ ^1D$	0.43±0.04			0.45±0.05[f], (0.45±0.04[f])	
1174	1170.6-75.5	$3p\ ^3D-4d\ ^3D^o$	0.72±0.07			1.1±0.1	
1197	1197.5-02.6	$3p\ ^3D-4d\ ^3F^o$	2.37±0.25	5.77±1.5	0.21		
1209	1205.9-09.9	$3s\ ^3P^o-3s\ ^3P$	0.25±0.03	2.66±0.6	0.46		
1240	1237.7-41.1	$3p\ ^3D-3p\ ^3D^o$	0.86±0.09	7.27±1.5	0.22		
1267	1266.2	$3p'\ ^1S-5s\ ^1P^o$?	0.32±0.03	2.46±0.5	0.56		
1311	1308.6-13.0	$3d\ ^3P^o-3d\ ^3D$	1.09±0.1	5.81±1.0	0.28		
1359	1358.3-59.4	$4d\ ^3D^o-3d'\ ^3F$	0.57±0.06	2.81±0.6	0.16		
1389	1388.8-92.8	$3d\ ^3P^o-3d\ ^3F$	2.11±0.2				
1590	1590.1	$3d\ ^3D-4s\ ^3P^o$	0.55±0.06	2.82±0.5	0.06	0.44±0.06[f]	
1727		?	0.34±0.03	2.17±0.4	0.29	0.83±0.1[f]	
1768	1767.8-68.2	$3d\ ^3F^o-4f\ G[^9/_2]$ $3d\ ^3F^o-4f\ G[^7/_2]$	0.83±0.2	13.8±4.0	0.14	1.2±0.1[f], (1.4±0.1[f])	
1780	1779.2±84.9	$3d\ ^3F-4f\ G[^7/_2]$ $3d\ ^3F-4f\ G[^5/_2]$	1.38± 0.3				
1787	1784.9-89.7	$3d\ ^3F-4f\ G[^7/_2]$ $3d\ ^3F-4f\ G[^5/_2]$	1.61±0.4				

Wave-length (Å) Obs.	Listed	Transition	This Work τ_1 (nsec)	τ_2	R(0)[r]	Other Values[q] (nsec)	Theory[j] (nsec)
OIII							
2455	2455.0	3s ^{1}P°-3p ^{1}S	1.78±0.2			2.2[p]	2.5C
2510	2509.4-10.7	3d ^{5}P-4p ^{5}D°	3.60±0.4			3.6[p],(3.4[p],3.7[p],3.3[p])	
2983	2983.8	3s ^{1}P°-3p ^{1}D	3.93±0.4			3.37[m],3.25[n],4.6[o],2.9[p]	4.5C
3045	3043.0-47.4	3s ^{3}P°-3p ^{3}P	2.52±0.4	0.06±.02	17.0	3.35[m],(3.71[m]),3.36[n], (2.20[n]),3.[p],(2.8,3.7,2.1)[p]	4.9C
3260	3260.98	3p ^{3}D-3d ^{3}F°	4.97±1.0	2.13±0.4	1.00	(5.04[m]),4.81[n],(5.13[n]) 5.7[p],(7.0[p])	4.8C
3350	3350.7-51.0	3s ^{5}P-3p ^{5}P°	10.2±1.0			22.8[n],7.2[p],(7.0[p])	6.7C
3385	3382.7-85.0	3p ^{5}P°-3d ^{5}D	15.2±2.0			(2.12,1.44,2.84)[m],25.2[n] 8.6[p],(7.0[p])	4.8C
3450	3450.9	3p ^{5}D°-3d ^{5}F	7.60±0.7			9.0[n],6.4[o],6.6[p]	6.0C
3455	3455.1	3p ^{5}D°-3d ^{5}F	6.29±0.6			7.61[n]	6.0C
3700	3698.7-03.4	3s ^{5}P-3p ^{5}D°	7.65±1.1	3.01±0.6	1.97	10.4[p],(10.6[p])	9.2C
3736	3734.8	3s ^{5}P-3p ^{5}D°	5.40±0.8	3.31±0.7	0.67		9.2C
3754	3754.7	3s ^{3}P°-3p ^{3}D	5.00±0.7	1.66±0.4	1.36	7.8[p]	9.3C
3759	3759.9	3s ^{3}P°-3p ^{3}D	7.09±1.0	2.25±0.4	0.99	8.6[p]	9.3C
3773	3774.0	3s ^{3}P°-3p ^{3}D	6.50±0.7			4.67[n],5.9[p]	9.3C
3791	3791.3	3s ^{3}P°-3p ^{3}D	6.99±1.4	1.68±0.4	2.35	7.6[p]	9.3C

Wave-Length (Å) Obs.	Listed	Transition	This Work (nsec) τ_1	τ_2	R(0)[r]	Other Values[q] (nsec)	Theory[j] (nsec)
OIII							
4516	4514.0	4d ^{3}D°-3d ^{3}F	1.48±0.3	33.3±7.0	0.33	(11.3[n]),(10.3[n])	
OIV							
554	553.3-55.3	2p ^{2}P°-2p^2 ^{2}P	0.21±.04	1.63±0.3	0.10	0.17±.04[f]	0.121E,0.139[i] 0.135[h]
610	608.4-609.8	2p ^{2}P°-2p^2 ^{2}S	0.24±.02	1.78±0.3	0.03	0.27±.03[f]	0.185E,0.265[i] 0.261[h]
1165	1164.3-64.5	3d ^{2}F°-4f ^{2}G[(k)]	0.39±.04	2.95±0.6	0.21	0.65±.08[f]	
1339	1338.6	2p^2 ^{2}P-2p^3 ^{2}D°	0.62±.06	1.19±0.3	0.05	0.67±.07[f],0.9[l]	
1343	1338.6-43.5	2p^2 ^{2}P-2p^3 ^{2}D°	0.53±.05	2.18±0.5	0.05	0.65±.07[f]	
1605	1604.6-04.9	4f ^{2}F-6g ^{2}G°[(k)]	1.18±0.2	4.37±0.9	0.31	1.42±0.1[f]	
OV							
1370	1371.3	2p ^{1}P°-2p^2 ^{1}D	2.93±0.2			3.2±0.2[f,l],3.0 0.1[a]	1.49D,2.29[e]

a Reference [Bi 69]

b Reference [Ga 68]

c Reference [He 68]

d Reference [La 70]

e Reference [Li 69]

f Reference [Ma 71]

g Reference [Sm 71]

h Reference [We 69a]

i Reference [We 69b]

j Reference [Wi 66] unless otherwise cited

k Reference [Br 70]

l Reference [Ce 70]

m Reference [Dr 69]

n Reference [Le 69]

0 Reference [Pi 69b]

p Reference [Dr 71]

q Brackets indicate lifetime observed at different wavelength

r Initial replenishment ratio $R(o) = (1 - \tau_1/\tau_2)/(1 + A/B)$, where A and B are the initial intensities of the two components. Smaller values of R(0) indicate that the radiative lifetime measurement is less perturbed by cascade repopulation of the radiating level, $R(0) < 0.1$ indicating that the error introduced by cascading is probably less than 10%.

? Uncertain in the lifetime value

CHAPTER VII

DISCUSSION

7.1 The OI Terms

3s' $^1D^o$: The decay of this level has been measured by many workers (Ma 71, La 70, Sm 71, Ga 68). The results are in good agreement. The average of the values listed in Table VI.2 gives 1.85 ± 0.2 nsec which is noticeably shorter than the theoretical value, 2.22 nsec. The value given for τ_2, 5.77 ± 1.0 nsec, may not represent the true cascade lifetime because the decay was followed only to about 10 nsec after the excitation. Three possible cascades are listed by Wiese et al. (Wi 66) in the infrared region with lifetime 38 nsec from 3p' ^1F, 21 nsec from 3p' ^1D, and 46 nsec from 3p' ^1p. Smith et al. (Sm 71) reported an experimental cascade lifetime of 10 ± 2 nsec.

3s $^3S^o$: The observed lifetime, 1.42 ± 0.2 nsec, appears to be rather low. The results obtained by other workers agree very well and average to 1.77 ± 0.2 nsec. Allowed cascades to this level are from the 3p ^3p level with a calculated lifetime 35.7 nsec and from the 4p ^3p level with negligible estimated transition probabilities. The cascade lifetime given for this level may not be correct for the same reason as for the multiplet 3s' $^1D^o$. The a-value (Eq. 5.9) for this line was 2.0, indicating some source of

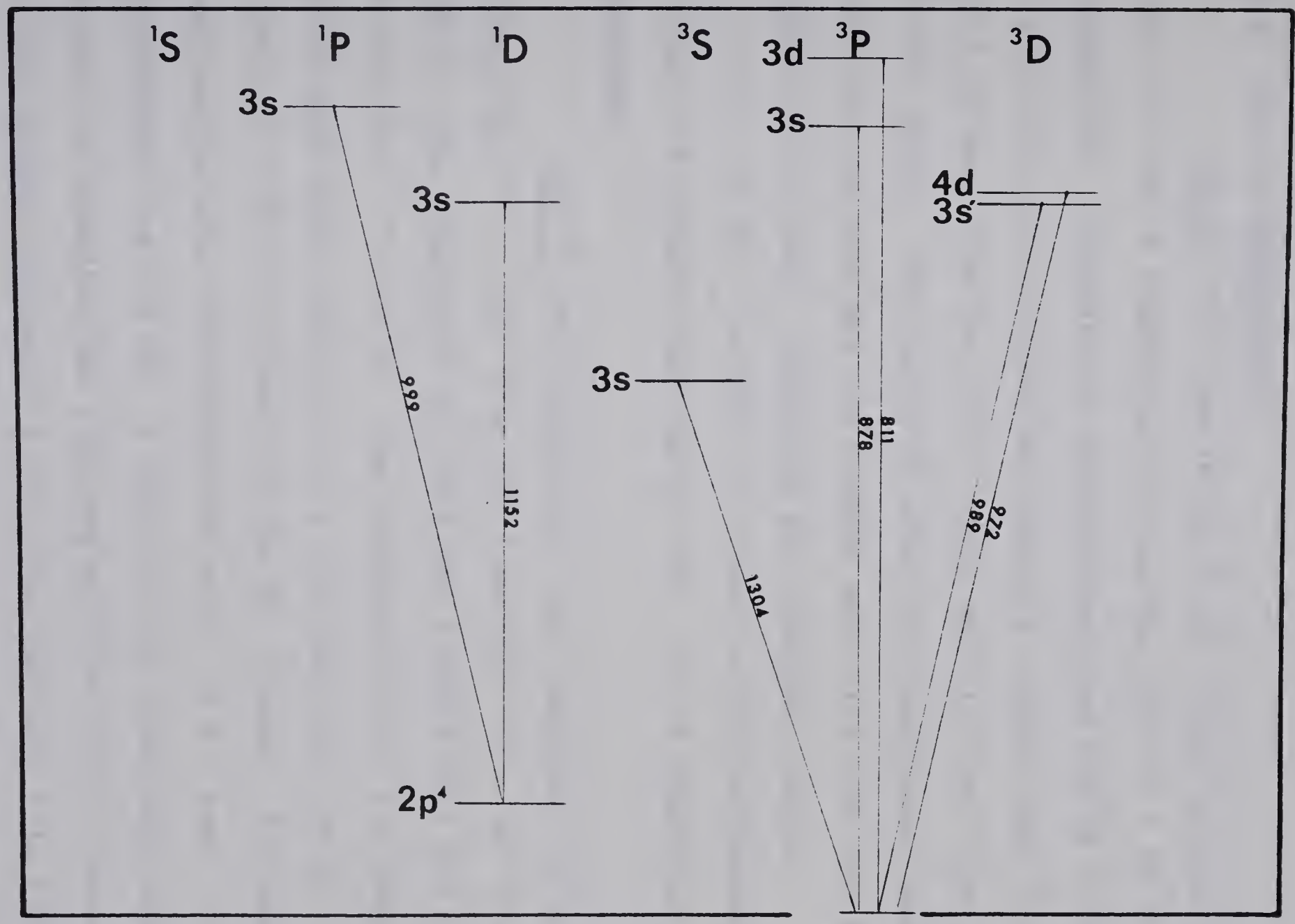

FIG. 7.1 PARTIAL ENERGY LEVEL DIAGRAM FOR OI SHOWING ALL LINES DETECTED IN THESE EXPERIMENTS (N.B. DUE TO PRACTICAL PROBLEMS, LIFETIMES WERE NOT MEASURED FOR THE LINES BELOW 1000 Å)

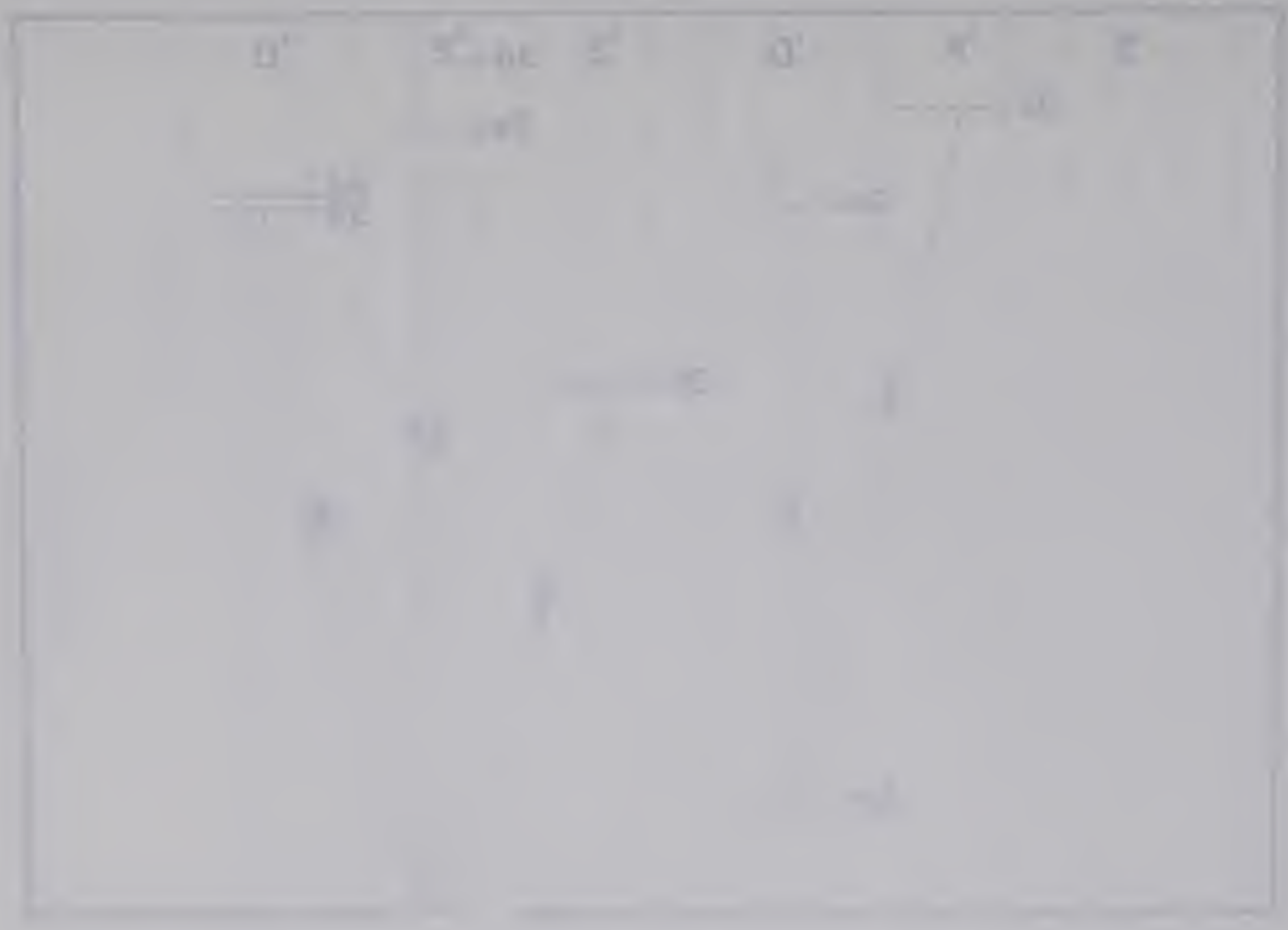

error in addition to statistical fluctuations. The uncertainty in τ for this line has therefore been set at ±20%.

7.2 The OII Terms

3d ^{2}F: The line at 485 Å can either be from the $2p^3\ ^2D^\circ$ - $3d\ ^2F$ transition or from the $2p^3\ ^2D^\circ$ - $3d\ ^2P$ transition. Theoretical calculations give the $3d\ ^2F$ level a mean life of 0.40 nsec and possible cascade mean lives of 4.32 nsec from the $4f\ ^2G^\circ$ level and 11.8 nsec from the $5f\ ^2G^\circ$ level. For the $3d\ ^2P$ level the theoretical mean life is 0.84 nsec and the cascade mean life from the $4f\ ^2D^\circ$ level is 5.5 nsec. Comparing the observed results, $\tau_1 = 0.37 \pm 0.05, \tau_2 = 3.08 \pm 0.5$ nsec, with the theoretical values, it appears that the $2p^3\ ^2D^\circ$ - $3d\ ^2F$ transition is dominant.

$2p^4\ ^2P$: Two transitions were observed for the level: $2p^3\ ^2D^\circ$ - $2p^4\ ^2P$ at 538 Å and $2p^3\ ^2P^\circ$ - $2p^4\ ^2P$ at 581 Å. The transition at 538 Å was a blend with the transition $2p^3\ ^4S^\circ$ - $3s\ ^4P$. The decomposition of the decay curve gave mean lives of 0.17 ± 0.02 nsec for the $2p^4\ ^2P$ level and 0.82 ± 0.2 nsec for the $3s\ ^4P$ level, following subtraction of a third component with $\tau_3 = 6.3$ nsec. The measurement for the $2p^4\ ^2P$ level at 581 Å was more accurate because no blending was involved and the initial intensity of the second component of the decay was only 1/15 that of the first component. The lifetimes obtained from the analysis of the two decay curves, 0.12 ± 0.1 nsec and 0.17 ±0.2 nsec agree excellently with the value reported by Martinson et al. (Ma 71), 0.12 ± 0.03 nsec.

3s ^{4}P: The decay was observed at 538 Å, a blend with the $2p^3\ ^2D^\circ$-$2p^4\ ^2P$ transition as discussed for the $2p^4\ ^2P$ level. Cascades to this level were observed at 1317 Å from the 5p $^4P^\circ$ level, 1654 Å from the 4p $^4D^\circ$ level, 4345-66 Å from the 3p $^4P^\circ$ level, 4639-76 Å from the 3p $^4D^\circ$ level and 3726 Å from the 3p $^4S^\circ$ level. The lifetimes for these cascades were 1.78, 0.21, 7.7, 10, and 4.8 nsec, respectively. A three-component curve fitting for the decay of the line at 538 Å gave a third component of τ_3=6.3±1.5 nsec, which might represent the mixed cascades lifetime to the 3s ^4P level.

3s ^{2}P: The observed lifetimes were 0.26±0.3 nsec for the decay and 5.28±1.0 nsec for the cascade. The calculated values are 0.37 nsec for the decay and 34.8 nsec for the cascade from the 3p $^2S^\circ$ level, 8.84 nsec from the 3p $^2D^\circ$ level, 6.8 nsec from the 3p $^2P^\circ$ level and a negligible contribution from the 3p $^4S^\circ$ level. It is possible that the $2p^3\ ^2D^\circ$-3s ^2P transition was blended with the OIV $2p^2\ ^2D$-$2p^3\ ^2P^\circ$ transition at 617 Å for which Martinson et al. obtained a value of 0.27±0.3 nsec.

5p $^4P^\circ$: The measurement at 4434 Å gave τ_1=1.78±0.4 and τ_2=16.3±3.0 nsec. The decay of the line at 1317 Å was followed to 20 nsec after the excitation, giving lifetimes τ_1=1.78±0.2 and τ_2=11.3±2.0 nsec. It is possible that the OIII 3d $^3F^\circ$-3d ^3P transitions between 1315.8 and

1317.7 Å and OIII 3p ^{3}P° - 3d ^{3}D transitions between 1315.8 and 1320.4 Å may have been involved in the decay.

3p ^{2}P°: This level was observed both at 1501 Å for the transition 2p^4 ^{2}D - 3p ^{2}P° and at 3973 Å for the transition 3s ^{2}P - 3p ^{2}P°. It is to be noted that the measurements of the decay for the two lines were made with different arrangements (different photon detector, monochromator and scanning mechanism) yet the lifetime results, 5.0 ± 0.5 and 6.0 ± 0.6 nsec agree within experimental error. Druetta et al. (Dr 71) obtained 7.1 nsec for the line at 3973 Å. A theoretical lifetime for this level is 6.8 nsec.

4p ^{4}D°: The decay curve for this level is very noisy. One component of the decay, which has a lifetime of 0.21 ± 0.04 nsec, is possibly significant but the second component, τ_2 = 1.58 ± 0.5 nsec, is doubtful. Martinson et al. (Ma 71) reported 0.93 ± 0.15 nsec for the decay.

3p' ^{2}D°: The transition observed was 3s ^{2}P - 3p' ^{2}D° at 2445 Å for which Striganov et al. (St 68) listed transition wavelengths of 2444.26 and 2445.55 Å. The repopulation from the 3d' ^{2}F level was observed at 4701 Å with an experimental lifetime of 0.81 ± 0.1 nsec. Two exponential curve fitting was not attempted because of lack of intensity. The single component fitting gave 3.72 ± 0.4 nsec for the decay.

3p $^4S°$: The decay curve for the transition 3s ^4P - 3p $^4S°$ at 3726 Å was multi-exponential. The analysis gave 4.80 ± 1.0 nsec for the decay and 2.09 ± 0.5 nsec for the cascade. Possible cascades to the upper level are 3d ^4P with a theoretical lifetime 0.25 nsec, 3d ^4D with 4.5 nsec and 3d ^2F with 0.4 nsec. The lifetime for the 3d ^4D level was measured at 4119 Å and resulted in 4.46 ± 0.5 nsec, in good agreement with the theoretical estimation. The calculated lifetime for the 3p $^4S°$ level is 5.6 nsec.

3d ^4F: The transitions 3p $^4D°$ - 3d ^4F were observed at 4072, 4075, 4087 and 4096 Å. The lifetimes obtained: 7.76 ± 0.8, 8.61 ± 0.9, 8.82 ± 0.9 and 9.64 ± 1.0 nsec, respectively, are high in comparison with the values obtained by other workers (Dr 69, Dr 71) and the theoretical estimation. The decays of these lines were not followed long enough for significant decomposition. Druetta et al. (Dr 71) reported a second component lifetime of 20 nsec for this level. The 3d ^4F - 4f $^4G°$ transitions might have been blended in the measurements of the decays at 4087 and 4096 Å.

3d ^4P: The transition 3p $^4P°$ - 3d ^4D has a theoretical lifetime of 4.5 nsec which agrees excellently with the observed value, 4.46 ± 0.5 nsec. Repopulation from the 4f $^4F°$ level has a calculated lifetime of 5.5 nsec. This cascade was actually observed at 4276 Å with τ = 4.22 ± 0.4 nsec. Blending with the transition 3p $^4P°$ - 3d ^4P at 4121.48 Å may have been involved. The transition

at 4121.48 Å has a calculated lifetime of 5.46 nsec. The cascading and blending in this case would effect the measurements of the lifetime only slightly because the lifetimes are essentially the same.

3d ^{4}P: The measurements of the decay of the lines at 4140 Å and 4151 Å gave 1.82 ± 0.4 and 1.97 ± 0.4 nsec for the decay of this level. The value obtained by Druetta et al. (Dr 71), 4.23 nsec, may be too high. The theoretical estimation is 0.25 nsec. Two observed cascade values are 7.20 ± 1.5 and 9.28 ± 2.0 nsec (for 4140 and 4151 Å respectively) whereas Druetta et al. reported 10 nsec.

3d′ ^{2}G: The transitions 3p′ ^{2}F° - 3d′ ^{2}G were observed at 4185 and 4189 Å. The measurements at 4189 Å were more accurate because the cascade correction was applied. The result, 5.59 ± 1.1 nsec, agrees with the values measured by Druetta et al. (Dr 69, Dr 71). The cascade from the 4f′ ^{2}H° level was observed as a strong line with a lifetime equal to 6.19 ± 0.6 nsec. The measurements for the decay lifetime for 4189 Å may thus be more indicative of the cascade lifetime.

4f′ ^{2}H°:This level is responsible for the repopulation of the 3d′ ^{2}G level. Two possible transitions, 4253.74 and 4253.78 a, are listed for the 3d′ ^{2}G - 4f′ ^{2}H° multiplet by Striganov et al. (St 68). No allowed transition to the upper level was found by the computer program. The observed lifetime for this level is 6.19 nsec,

and Druetta et al. (Dr 69, Dr 71) obtained 4.35 and 5.48 nsec, all noticeably higher than the theoretical value, 3.8 nsec.

4f $^4F°$: The decay of this level was observed for two transitions: 3d ^4D - 4f $^4F°$ at 4276 Å and 3d ^2F - 4f $^4F°$ at 4313 Å. The latter transition was weak and the measurements may not be as accurate as for the former transition. The decay of the line at 4276 Å indicated a lifetime of 4.22 ± 0.4 nsec for the 4f $^4F°$ level and Druetta et al. (Dr 71) reported 3.96 nsec.

3p $^4P°$: The transitions 3s ^4P - 3p $^4P°$ were observed at 4345, 4349, and 4366 Å. The measurements for the first two lines gave 7.05 ± 0.7 and 7.69 ± 0.8 nsec for the decay of the level, agreeing excellently with the value obtained by Druetta et al. (Dr 69, Dr 71), 7.7 nsec. But cascades from 3d ^4P, 3d ^4D, 3d ^2F and 3d ^2P are possible of which the 3p $^4P°$ - 3d ^4D transition predominates, and was observed at 4119 Å with a lifetime of 4.46 ± 0.5 nsec. The cascade from the 3d ^4P was also important and observed at 4140 and 4151 Å. The experimental lifetimes may be somewhat low because no cascade correction was applied. The observation at 4366 Å was a blend with the transition 3p $^2D°$ - 3d ^2D at 4369.28 Å which has a theoretical lifetime of 0.93 nsec. In theory, at least three-component curve fitting must be used to analyze the decay of this curve.

4f' ^{2}F°: Both the decay and the cascade lifetimes obtained were much shorter than those reported by Druetta et al. (Dr 71), 4.0 and 25 nsec, respectively. No theoretical lifetime is available.

3p ^{2}D°: The transitions 3s ^{2}P-3p ^{2}D° at 4415, 4452 Å were measured and gave 9.92±1.0 and 8.83±0.9 nsec, in good agreement with values measured by other workers (Dr 69, Dr 71) and theoretical estimation. Cascades are possible from the 3d ^{4}D, 3d ^{2}F, 3d ^{2}P and 3d ^{2}D level which was observed at 4701 Å as a weak and short lived line, hence the cascading effect may be negligible.

3d' ^{2}F: The transition 3p' ^{2}F°-3d' ^{2}F was observed at 4447 Å and was a blend with the OIII 3p ^{5}S°-3d ^{5}P transition at 4447.82 Å with a theoretical lifetime of 7.5 nsec. The 3d' ^{2}F level has a calculated lifetime of 0.38 nsec and can be populated by the 2f' ^{2}G° level with a cascade lifetime of 4.5 nsec. Analysis of the decay gave τ_1=0.90±0.2 and τ_2=7.81±1.5 nsec, in fairly good agreement with the theoretical estimations.

3p' ^{2}F°: The transition 3s' ^{2}D-3p' ^{2}F° was observed at 4592 Å. The average of the two most reliable measurements gave 10.13±2.0 nsec for the decay and

4.60 ± 0.9 nsec for the cascade. Cascading from the 3d' ^{2}G level was observed at 4189 Å and the measured lifetime was 5.59 nsec. Reference (Dr 71) reported 14 nsec for the decay and 4 nsec for the cascade.

4f ^{2}F°: The decay of the 4f ^{2}F° level was observed at 4610 Å as a weak line. The measured lifetime, 6.30 ± 1.5 nsec, agrees with the theoretical value, 5.5 nsec. Druetta et al. measured 4.4 nsec for the decay and 25 nsec for the second component.

3p ^{4}D°: This level was heavily repopulated by upper levels. The transitions

3p ^{4}D°- 3d ^{4}F in the range 4072.16 - 4106.03 Å,

3p ^{4}D°- 3d ^{4}P in the range 3864.13 - 3926.58 Å,

3p ^{4}D°- 3d ^{4}D in the range 3842.82 - 3883.15 Å,

and 3p ^{4}D°- 3d ^{2}F in the range 3851.47 - 3875.82 Å

are allowed. The first transition was measured with a lifetime of 7.76 ± 0.8 nsec. The rest were not individually observed but the sum of all these cascades certainly affected the measurements of the 3p ^{4}D° level. The upper levels of these cascading transitions were again populated by higher levels as shown in the energy level diagram (Fig. 7.2). The results given in Table VI.2 are doubtful because of the complicated cascading problems. Druetta et al. (Dr 71) had the same problem; they reported 12, 10 and 19 nsec for the measurements at 4640, 4650 and 4660 Å.

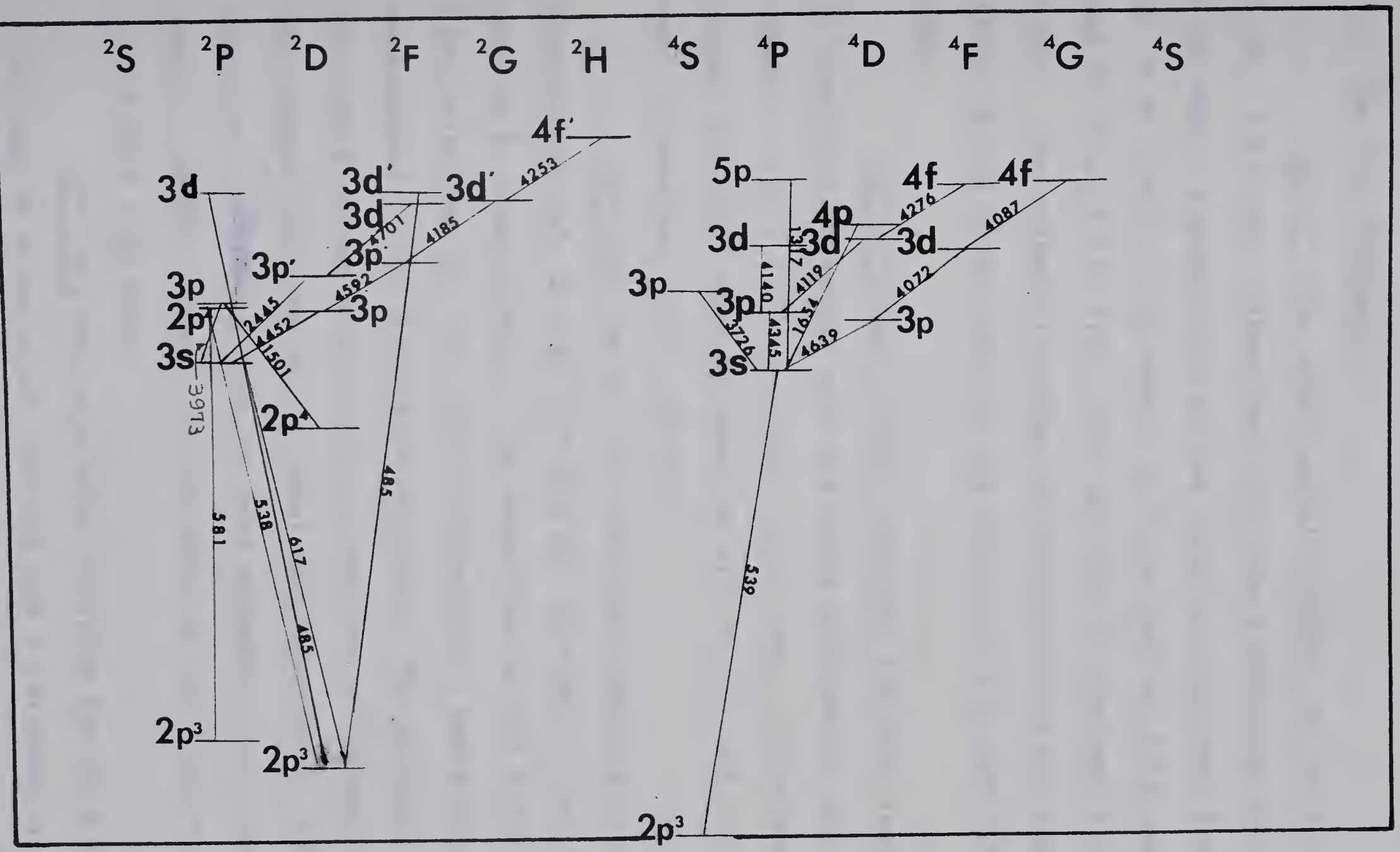

FIG. 7.2 PARTIAL ENERGY LEVEL DIAGRAM FOR OII

7.3 The OIII Terms

3s $^3P^\circ$: The experimental lifetime for this level, 0.30 ± 0.03 nsec, agrees well with the calculated value, 0.26 nsec. Repopulation of the level was observed from 3s ^3P at 1209 Å (0.25 nsec), 3p ^3P at 3045 Å (2.52 nsec) and 3p ^3D at 3754, 3759, 3773 and 3791 Å (averaged 6.4 nsec). The cascade lifetime, as obtained from the analysis of the decay curve of the line at 374 Å, was 3.89 ± 0.5 nsec.

$2p^3$ $^3S^\circ$: The lifetime obtained for this level is in excellent agreement with the value obtained by Heroux (He 68), 0.10 ± 0.01 vs 0.105 ± 0.012 nsec. Calculated values are 0.067 nsec by Wiese et al. (Wi 66) and 0.071 nsec by Westhaus et al. (We 69b)

$2p^3$ $^1P^\circ$: The $2p^3$ $^1P^\circ$ level was observed via the transitions $2p^2$ ^1D - $2p^3$ $^1P^\circ$ and $2p^2$ ^1S - $2p^3$ $^1P^\circ$ at 526 and 599 Å, respectively. The transition at 599 Å was a blend with the $2p^2$ ^1D - $2p^3$ $^1D^\circ$ transition, hence the measurement at 526 Å was more reliable. The lifetime result again agrees with the value obtained by Heroux (He 68). The cascade from the $2p^4$ ^1D level was observed at 1138 Å with τ_2 = 0.43 ± 0.04 nsec, in good agreement with the result from the analysis of the decay of the line at 526 Å, τ_2 = 0.38 ± 0.08 nsec.

$2P^3$ $^1D^\circ$: The calculated lifetime for this level is 0.147 nsec by Wiese et al. (Wi 66) and 0.181 nsec by Westhaus et al. (We 69b). The decay was observed at 599 Å

which was blended with the transition $2p^2\ ^1S - 2p^3\ ^1P°$ and resulted in 0.25 ± 0.03 nsec. Three-component curve fitting was applied to the decay and the lifetime for the third component was 6.8 ± 1.6 nsec.

$2p^4\ ^1D$: The transition $2p^3\ ^1P° - 2p^4\ ^1D$ at 1138 Å was essentially single exponential and was responsible for the repopulation of the $2p^3\ ^1P°$ level as discussed before. The observed lifetime for this level agrees with the value obtained by Martinson et al. (Ma 71) as well as with the value from the analysis of the decay of the $2p^3\ ^1P°$ level.

$4d\ ^3D°$: The computer program predicted six possible transitions for the multiplet, $3p\ ^3D - 4d\ ^3D°$ at 1170.6 - 1175.5 Å. The line observed at 1174 Å was weak and resulted in 0.72 ± 0.07 nsec for the decay. Cascade from $3d'\ ^3F$ was observed at 1359 Å with τ_1 = 0.57 0.06 and τ_2 = 2.81 ± 0.3 nsec.

$4d\ ^3F°$: The transition $3p\ ^3D - 4d\ ^3F°$ is again identified by the computer program. The measurements were made at 1197 Å and resulted in 2.37 ± 0.25 nsec for the decay and 5.77 ± 1.5 nsec for the cascade. The initial intensity ratio for the two components is about 2:1. Martinson et al. (Ma 71) observed a line at 1195 Å, which they classified as originating from OI-II, with a lifetime 1.8 ± 0.2 nsec.

3s ^{3}P: Five possible transitions were predicted for the multiplet 3s ^{3}P° - 3s ^{3}P in the wavelength range 1205.9 - 1209.9 Å. Possible cascades are from the 3p ^{3}D° with a theoretical lifetime of 10.6 nsec which is too high as will be discussed in the next paragraph, and from the 3p ^{3}P° level with a theoretical lifetime of 6.8 nsec. The decay curve for the line at 1209 Å indicated two components of about the same initial intensity with lifetimes 0.25 ± 0.03 and 2.66 ± 0.6 nsec, respectively.

3p ^{3}D°: Five transitions are allowed within the multiplet 3p ^{3}D - 3p ^{3}D° in the wavelength range 1237.6 - 1241.1 Å. The theoretical lifetime can be extracted from transition probabilities given in the table by Wiese et al. (Wi 66), but it will be too high because important transitions such as the one being discussed now are not included. Cascades to the upper level are allowed from the 3d ^{3}F level with a calculated lifetime of 6.3 nsec and from the 3d ^{3}D level with a calculated lifetime of 4.9 nsec. The transitions from the 3d ^{3}F level were actually observed by Lewis et al. (Le 69) at 3727.4 and 3729.1 Å. The reported values are 11.3 and 10.3 nsec. However the observations at 1389 Å and 1311 Å gave 2.11 nsec for the 3d ^{3}F level and 1.09 nsec for the 3d ^{3}D level.

5s ^{1}P°: The assignment of this level is not certain. The computer program predicted a transition within the multiplet 3p'^{1}S - 5s ^{1}P° at 1266.2 Å. The

measured lifetimes are τ_1=0.32±0.03 and τ_2=2.46±0.5 nsec. Martinson et al. observed a line at 1268 Å and identified as OI-II with τ=1.5±0.1 nsec.

3d ^{3}D: Six allowed transitions are predicted for the multiplet 3d ^{3}P°-3d ^{3}D within the wavelength range 1308.6-1313.0 Å. The measured lifetimes are 1.09±0.1 and 5.81±0.1 nsec. The theoretical value extracted from the transitions 3p ^{3}D°-3d ^{3}D and 3p ^{3}P°-3d ^{3}D is 4.9 nsec.

3d' ^{3}F: The transition 4d ^{3}D°-3d' ^{3}F was observed at 1359 Å. The two components gave 0.57±0.06 and 2.82±0.5 nsec for the lifetimes with an initial intensity ratio of about 4:1. Two transitions at 1358.3 and 1359.4 Å are allowed according to the computer program. The transition 4d ^{3}P°-3d' ^{3}D at 1361.1 Å may have been blended with 1359 Å in this measurement.

3d ^{3}F: Three transitions are allowed within the multiplet 3d ^{3}P°-3d ^{3}F, in the wavelength range 1388.8-1392.8 Å. No apparent cascading was indicated by the decay of the level and the lifetime obtained was 2.11±0.2 nsec.

4s ^{3}P°: The decay of the line at 1590 Å gave 0.55±0.06 nsec for the lifetime of this level, and 2.82±0.6 nsec for the cascade. Martinson et al. (Ma 71) obtained 0.44±0.06 nsec for the decay lifetime.

4f ^{3}G: The decays of the lines at 1768, 1780, and 1788 Å are very noisy and follow the same pattern. The possible transitions for these three lines are listed in Table VI.2. The line at 1768 Å was much stronger than the other two lines and the decomposition of the decay gave 0.83 ± 0.2 nsec for the decay. A single-component curve fitting resulted in 1.45 ± 0.3 nsec. The other two lines were weak and only single component curve fitting was attempted resulting in 1.38 ± 0.3 and 1.61 ± 0.4 nsec. Martinson et al. (Ma 71) also observed the line at 1768 Å and reported 1.2 ± 0.1 nsec for the lifetime.

3p ^{1}S: The transition 3s ^{1}P° - 3p ^{1}S was observed at 2445 Å. The line was weak and gave essentially a single exponential decay. The experimental lifetime was 1.78 ± 0.2 nsec, in agreement with Druetta et al.'s value (Dr 71). The theoretical estimate is 2.5 nsec. Cascade from the 3d ^{3}P level is allowed but its effect on the measurements may be neglible as the transition probability is small.

4p ^{5}D°: Measurements were made at 2510 Å, a new line identified by the computer program. Druetta et al. (Dr 71) observed the same multiplet at 2288, 2497, 2509 and 2515 Å and reported values of 3.3, 3.7, 3.6 and 3.4 nsec. The result of the present observation was 3.60 ± 0.4 nsec.

3p ^{1}D: The decay of this level follows a single exponential. Possible cascades from the 3d ^{1}D°, 3d ^{1}F°, and 3d ^{1}P° levels were not seen in the spectrum. Druetta et al. (Dr 69, Dr 71) and Lewis et al. (Le 69) have also studied the multiplet and their reported values agree with the present observation.

3p ^{3}P: The observation was made at 3045 Å. The decay gave 2.25 ± 0.4 nsec for the decay and 0.06 nsec for the cascade. Cascades from the 3d ^{3}D° and 3d ^{3}P° levels are allowed, the former has transition wavelengths at about 305 Å and the latter at about 313 Å. The theoretical lifetimes for these two cascading levels are 0.06 and 0.1 nsec, respectively. Druetta and Poulizac (Dr 69) measured the lifetimes for the 3d ^{3}P° and 3d ^{3}D° levels as 2.43 and 2.86 nsec, respectively. In their measurements, cascades from the 3d ^{3}P° - 4p ^{3}S transition (theoretical τ = 5.8 nsec) and the 3d ^{3}D° - 4p ^{3}D (theoretical τ not available) might be strong. The 3p ^{3}P level has been studied by Druetta et al. (Dr 69, Dr 71) and Lewis et al. (Le 69) and the results are in fairly good agreement.

3d ^{3}F°: The experimental lifetimes for the two components are 4.97 ± 1.0 and 2.13 ± 0.4 nsec, respectively. The theoretical value for this level is 4.8 nsec, in excellent agreement with the present results and other worker's values (Dr 69, Le 69, Dr 71). Cascading from the 4p ^{1}P level is possible but may be neglected in comparison with the cascades from the 4p ^{3}D level, lying between

2372.21 and 2388.20 Å which are listed as fairly strong lines by Striganov et al. (St 68).

3p ^{5}P°: The strongest line in the multiplet 3s ^{5}P - 3p ^{5}P° is 3350.99 Å. The observation was made at 3350 Å and resulted in 10.2 ± 2.0 nsec for the lifetime. Cascading from the 3d ^{5}D level was seen at 3385 Å with an experimental lifetime of 15.2 ± 0.2 nsec. The theoretical lifetime for the 3p ^{5}P° level is shorter than the observed value, indicating a strong cascading effect. Cascades from the 3d ^{5}P° level are also present although no line was strong enough for lifetime measurements.

3d ^{5}D: The transition 3p ^{5}P° - 3d ^{5}D has a calculated lifetime of 4.8 nsec and the measured value is 15.2 ± 2.0 nsec. Cascades from the 4p ^{5}D° level (2475.73 - 2492.2 Å) and the 4p ^{5}P° level (2421.2 - 2454.21 Å) are listed by Striganov et al. (St 68). The computer program also predicted allowed transitions in the far infrafed at about 2.9 μ, in the visible region at 3260-3280 Å and in the ultraviolet region at about 1920 Å. Lifetime values reported by other workers are completely different, reference (Dr 69) gave 2.12, 1.44 and 2.84 nsec for the observation at 3063, 3075 and 3088 Å, reference (Le 69) gave 25.2 nsec for the observation at 3382.94 Å and reference (Dr 71) gave 8.6 and 7.0 nsec for the observation at 3385 and 3088 Å. These widely different values may be caused by the strong cascade effects, since different experimental conditions can result in different cascade contributions to the final decay curve.

3d ^{5}F: Two lines were observed for this level: 3450 and 3455 Å, corresponding to the 3p ^{5}D° - 3d ^{5}F transitions. The measured lifetimes agree with the calculated value and the values obtained by Lewis et al. (Le 69) and Druetta et al. (Dr 71), although possible cascadings from the 4p ^{5}D° (2285.07 - 2288.36 Å) are listed by Striganov et al. (St 68).

3p ^{5}D°: Two lines were observed with τ_1 = 7.65 ± 1.1, τ_2 = 3.01 ± 0.6 nsec for the line at 3700 Å and τ_1 = 5.40 ± 0.8, τ_2 = 3.31 ± 0.7 nsec for the line at 3736 Å. The latter was a blend with the OII 3p' ^{2}P° - 4s' ^{2}D transition at 3735.94 Å which has a theoretical lifetime of 4.1 nsec. The cascade from the 3d ^{5}F level was observed at 3450 Å with τ_2 = 7.6 nsec. Druetta et al. (Dr 71) measured 10.6 and 10.4 nsec for the decay and 5 nsec for the cascade.

3p ^{3}D: Measurements were made at 4 wavelengths with the following results:

3754 Å τ_1 = 5.00 ± 0.7, τ_2 = 1.66 ± 0.4 nsec,

3759 Å τ_1 = 7.09 ± 1.0, τ_2 = 2.25 ± 0.4 nsec,

3773 Å τ_1 = 6.50 ± 0.7 nsec,

3791 Å τ_1 = 6.99 ± 1.4, τ_2 = 1.68 ± 1.4 nsec.

At least two cascades were involved in the observations. The 3p ^{3}D - 3d ^{3}F° transition was observed at 3260 Å with τ = 4.97 ± 1.0 nsec and the 3d ^{3}F° level may in turn be populated by the 4p ^{3}D level. Another cascade is from the 3d ^{3}D° level with a theoretical lifetime of 0.06 nsec.

Therefore, at least three-component curve fitting is needed for a correct result. Three component fitting has been attempted for these lines but only in the case 3759 Å was the fit significantly improved, giving the three lifetimes 10.87, 2.56 and 0.77 nsec. It may be significant that this result, 10.87 nsec, is in better agreement with the theoretical value than are any of the other values.

3d ^{3}F: The line at 4516 Å was identified by the computer program as arising from the transition $2s^2\ 2p(^2P^\circ)$ $4d\ ^3D^\circ$ - $2s\ 2p^2\ (^4P)\ 3d\ ^3F$, one of the two two-electron transitions observed for OIII. The experimental lifetimes are $\tau_1 = 1.48 \pm 0.3$ and $\tau_2 = 33.3 \pm 7.0$ nsec.

7.4 The OIV Terms

$2p^2\ ^2P$: Experimental lifetimes for this level are 0.21 ± 0.04 nsec for the decay and 1.63 ± 0.3 nsec for the cascade. Martinson et al. observed a decay lifetime of 0.17 ± 0.04 nsec. Theoretical lifetimes obtained from Wiese et al. (Wi 66), Westhaus et al. (We 69b) and Weiss (We 69a) are 0.121, 0.139 and 0.135 nsec, respectively. Cascades to this level were observed from $2p^3\ ^2D^\circ$ at 1339 and 1343 Å and from $2p^3\ ^2P^\circ$ at 922 Å which had their own cascade problems. The $2p^3\ ^2D^\circ$ level has an averaged experimental lifetime of 0.62 nsec and the $2p^3\ ^2P^\circ$ level has 0.26 nsec (Table VI.2, Ma 71). The experimental lifetime for the $2p^2\ ^2P$ level may be too high because of the complicated cascades, especially as the cascade from

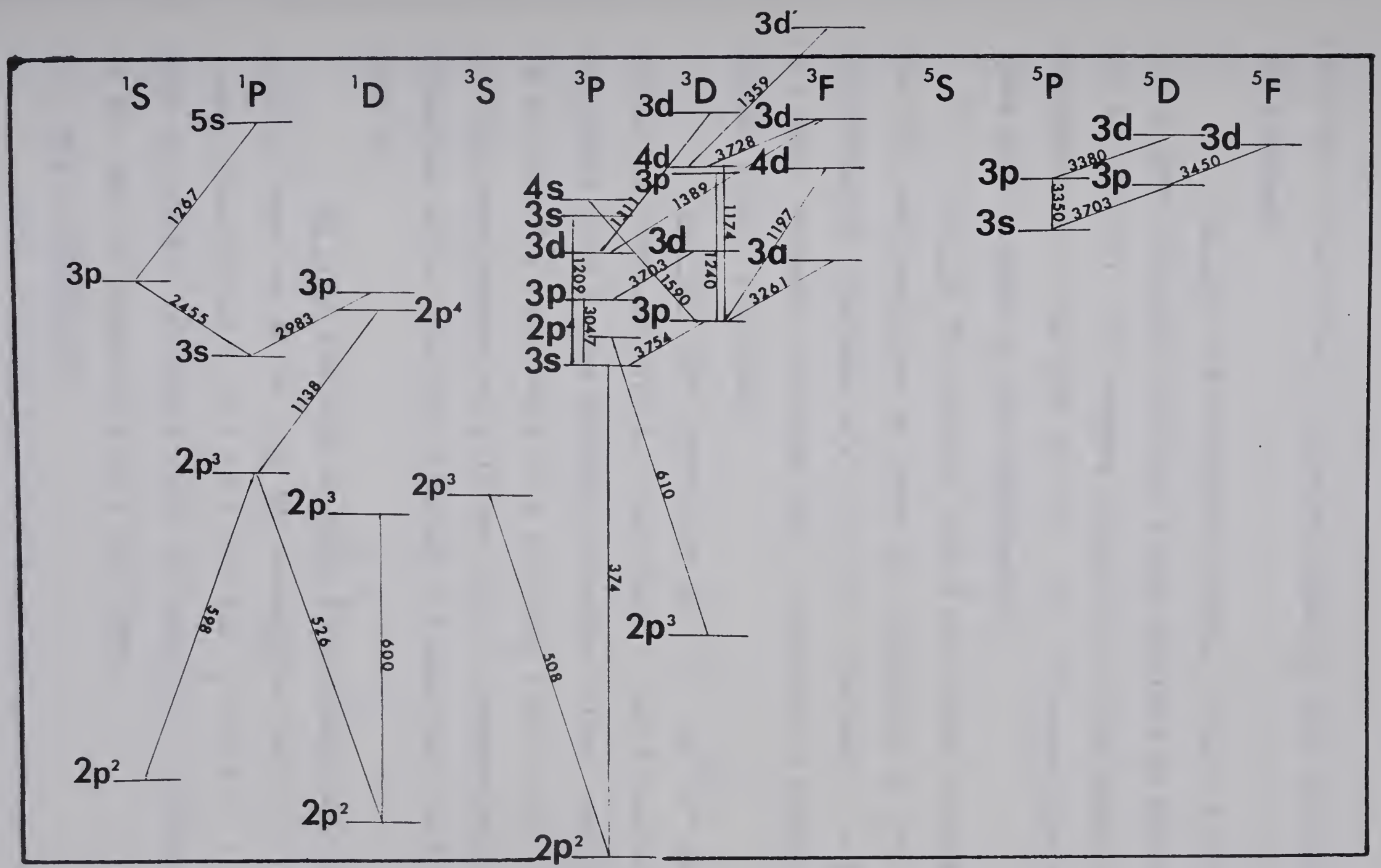

FIG. 7.3 PARTIAL ENERGY LEVEL DIAGRAM FOR OIII

the $2p^3\ ^2P$ level has a lifetime close to that of the level of interest.

$2p^2\ ^2S$: The measured lifetime, 0.24 ± 0.02 nsec, is in good agreement with the value obtained by Martinson et al. (Ma 71). No cascade transition to the upper level was observed. The OIII $2p^3\ ^3D^\circ$ - $2p^4\ ^3P$ transition may have been blended in the measurements.

$4f\ ^2G$: The line at 1165 Å was found in reference (Br 70) and identified as from the transition $3d\ ^2F^\circ$ - $4f\ ^2G$. The observed lifetimes are τ_1 = 0.39 ± 0.04 and τ_2 = 2.95 ± 0.6 nsec, whereas reference (Ma 71) reported a higher value, 0.65 ± 0.08 nsec.

$2p^3\ ^2D^\circ$: The transition $2p^2\ ^2P$ - $2p^3\ ^2D^\circ$ was observed at 1339 and 1343 Å. The line at 1343 Å was stronger and might give a more accurate lifetime value. Martinson et al. (Ma 71) reported 0.67 ± 0.07 and 0.65 ± 0.07 nsec for the measurements at 1339 and 1343 Å, respectively. Ceyzeriat et al. (Ce 70) obtained 0.9 nsec for the line at 1339 Å.

$6g\ ^2G^\circ$: The line at 1605 Å was identified as arising from the $4f\ ^2F$ - $6g\ ^2G^\circ$ transition (Br 70). It was a weak line giving τ_1 = 1.18 ± 0.2 and τ_2 = 4.37 ± 0.9 nsec with an initial intensity ratio of about 7:5. Martinson at al. (Ma 71) reported 1.42 ± 0.10 nsec.

7.5 The OV Terms

Five transitions were observed for OV: $2s^2\ ^1S$ - $2p\ ^1P^\circ$ at 630 Å, $3d\ ^3D$ - $4f\ ^3F^\circ$ at 681 Å, $3d\ ^1D$ - $4f\ ^1F^\circ$ at

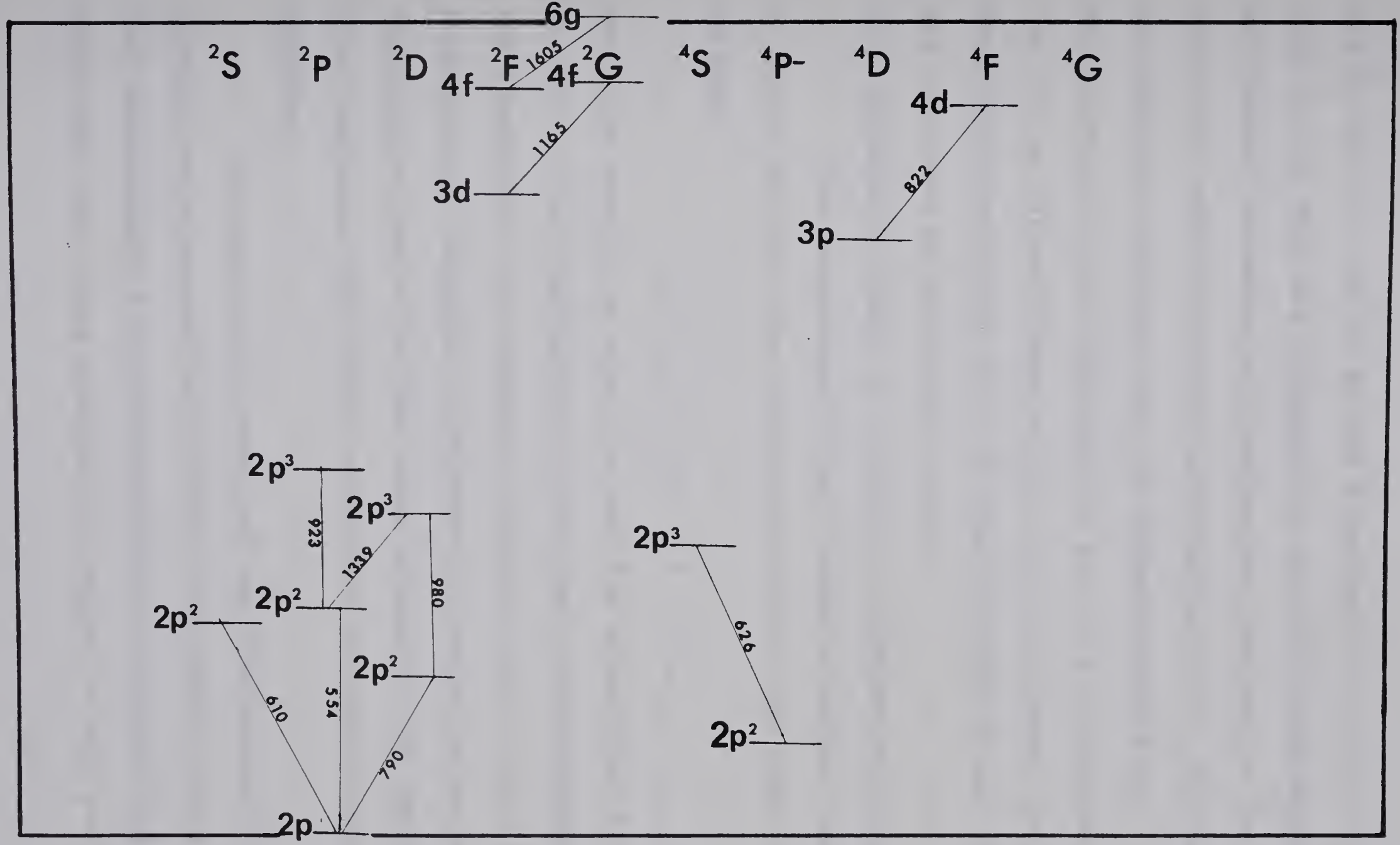

FIG. 7.4 PARTIAL ENERGY LEVEL DIAGRAM FOR OIV

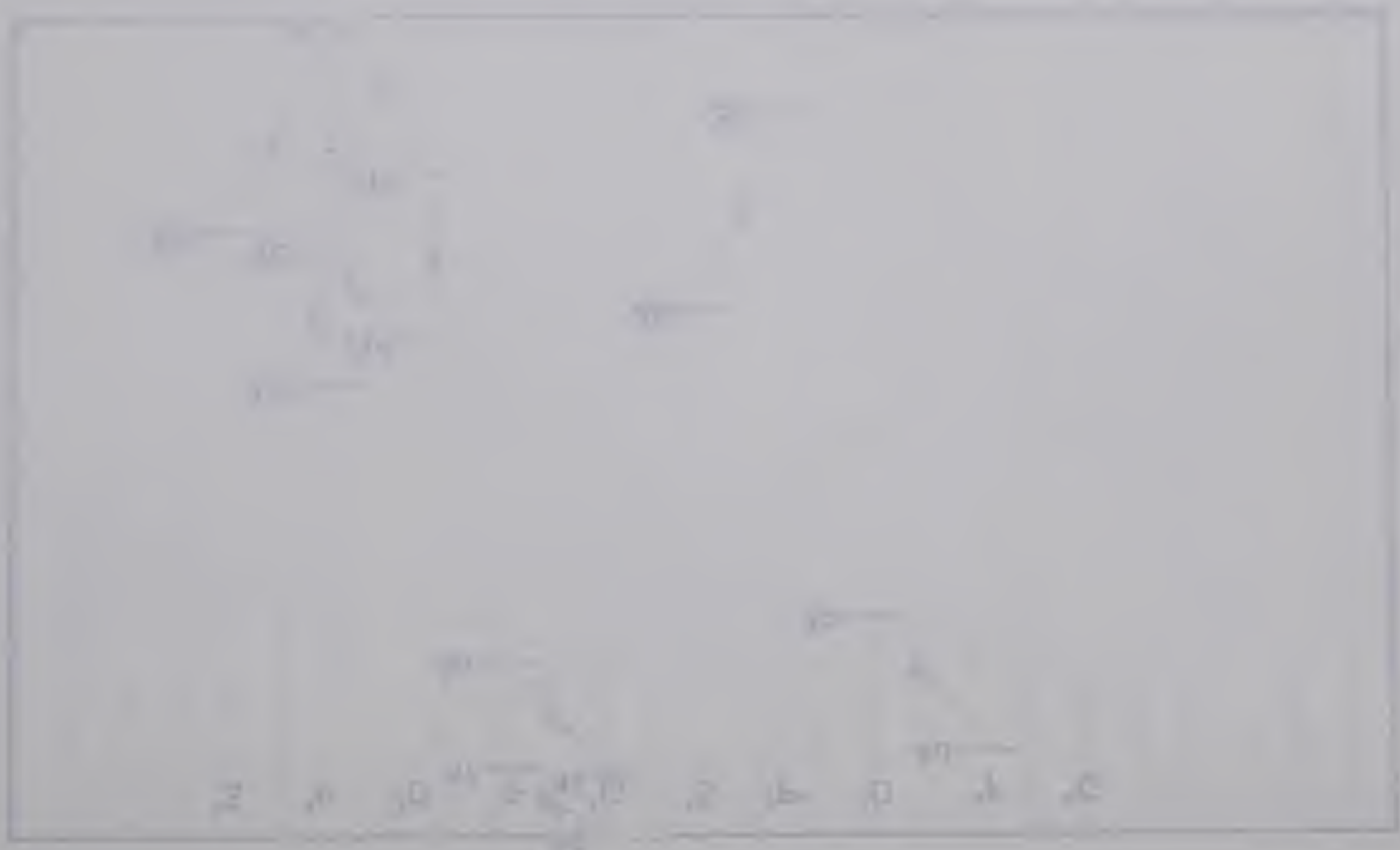

728 Å, 2p $^3P°$ - $2p^2$ ^3P at 760 Å and 2p $^1P°$ - $2p^2$ ^1D at 1370 Å, but only the lifetime for the $2p^2$ ^1D was measured. No apparent cascading or blending was involved in the transition and the observed lifetime was 2.93 ± 0.2 nsec, in excellent agreement with the values reported by Martinson et al. and Ceyzeriat et al., 3.2 ± 0.2 nsec, (Ma 71, Ce 70) and Bickel et al., 3.0 ± 0.1 nsec, (Bi 69). Theoretical estimates are 1.49 nsec by Wiese et al. (Wi 66) and 2.29 nsec by Linderberg (Li 69).

7.6 Systematic Trends of f-values in Isoelectronic Sequences

The dependence of the f-value on nuclear charge, Z, can be derived from perturbation theory and reads (Wi 68, We 69a)

$$f = f_o + f_1 Z^{-1} + f_2 Z^{-2} + : \quad .... \quad (7.1)$$

The first term f_o is equal to zero for transitions with $\Delta n = 0$. It is interesting to plot the f-value against Z^{-1} and investigate the systematic trend of the f-value in an isoelectronic sequence. The beam-foil technique is particularly suitable for this study because of the capability of producing many atomic species in an isoelectronic sequence.

No experimental study of the Z-dependence of the f-value was attempted; but f-values obtained by other beam-foil measurements for many sequences are compiled and compared with the values observed for oxygen in this project.

Theoretical values are also taken either from Wiese et al.'s tabulation (Wi 66) or from Weiss's SOC (superposition of configurations) calculations (We 69a).

The plot of the f-value against Z^{-1} provides useful information concerning the oscillator strength as well as the electronic configuration. Fig. 7.5(A) represents a case in which the values obtained from the theory based on the single configuration independent particle model do not agree with experimental values. The configuration interaction is important in this case and the SOC calculation is required to obtain more accurate results. Fig. 7.5(B) shows the trend of the $2s^2\ 2p\ ^2P^o$ - $2s\ 2p^2\ ^2S$ transition. Experimental values agree very well with Weiss calculations (We 69a) and Wiese et al.'s tabulation (Wi 66), although the latter are not plotted on the graph. Fig. 7.6 gives some more examples of the variation of the f-value with nuclear charge in BI and NI sequences.

The experimental values always fit fairly well to a smooth curve although the data are obtained by different laboratories, indicating a good reliability of the beam-foil measurements. The theoretical values are, for the most cases, accurate; but when the configuration interaction is severe, more elaborate treatment is necessary to bring the theoretical values closer to the experimental ones.

It is worth noting that additional f-values may be obtained by extrapolation or interpolation from the

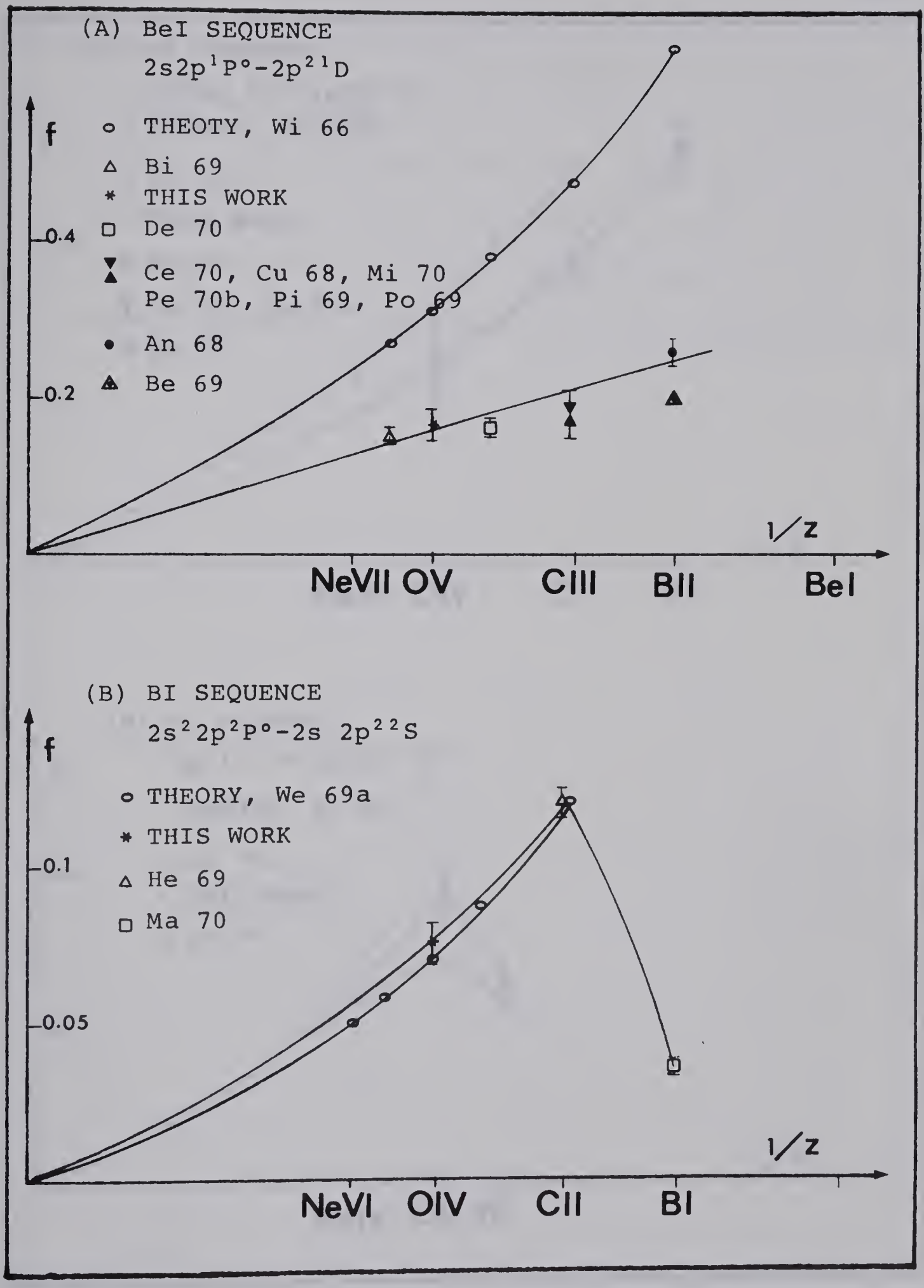

FIG. 7.5 VARIATION OF f-VALUE WITH Z^{-1} IN ISOELECTRONIC SEQUENCES (I)

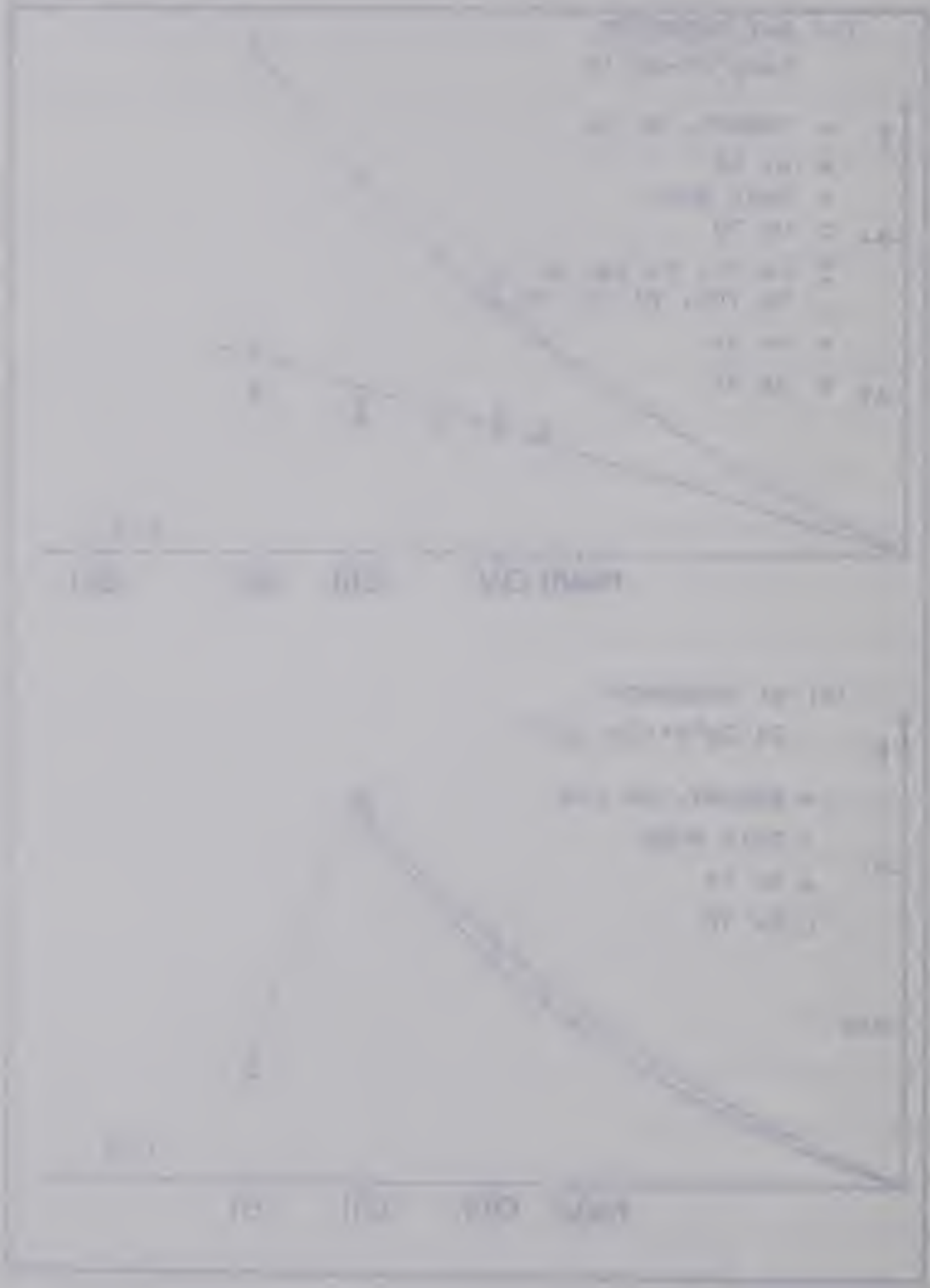

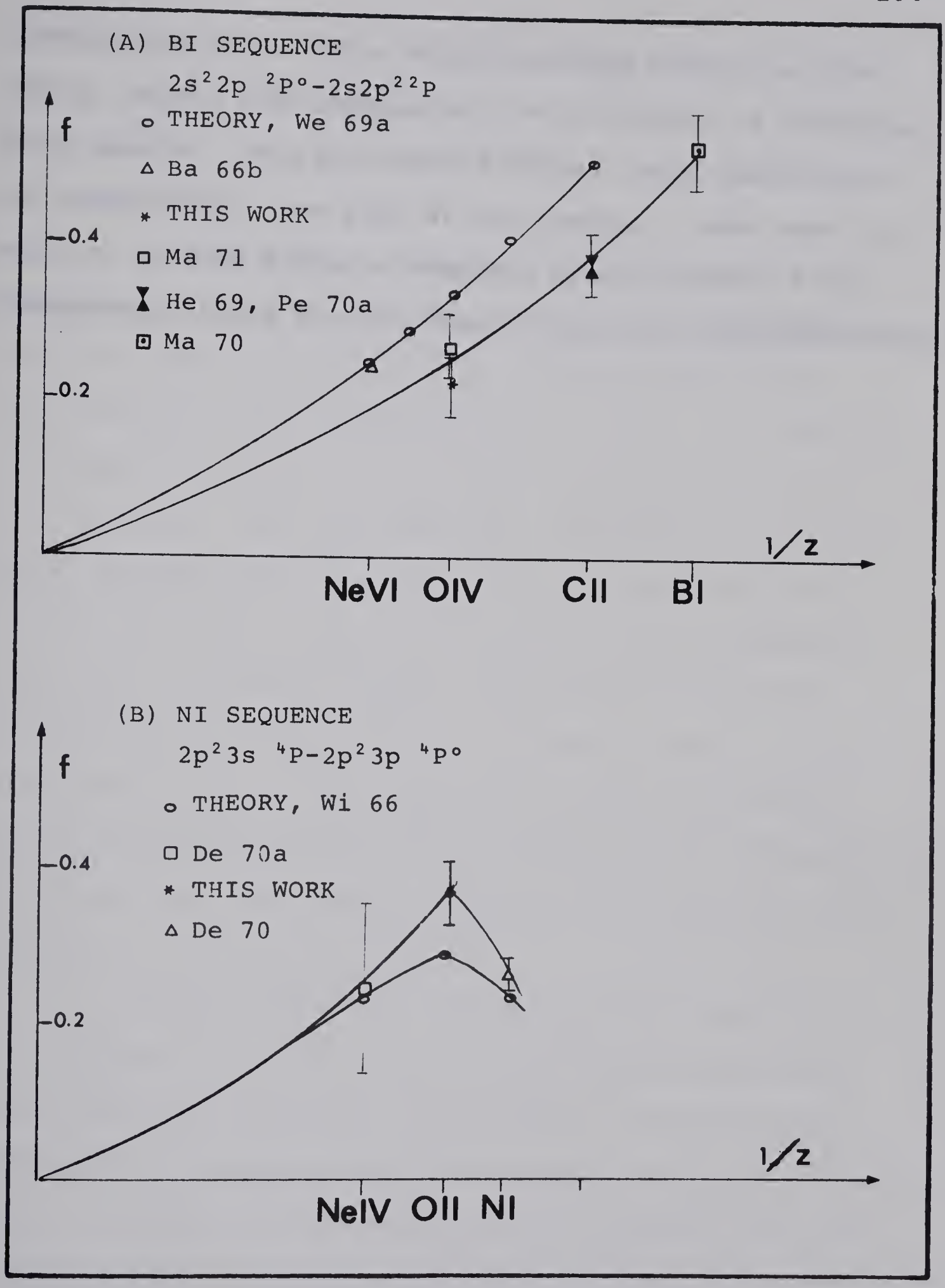

FIG. 7.6 VARIATION OF f-VALUE WITH Z^{-1} IN ISOELECTRONIC SEQUENCES (II)

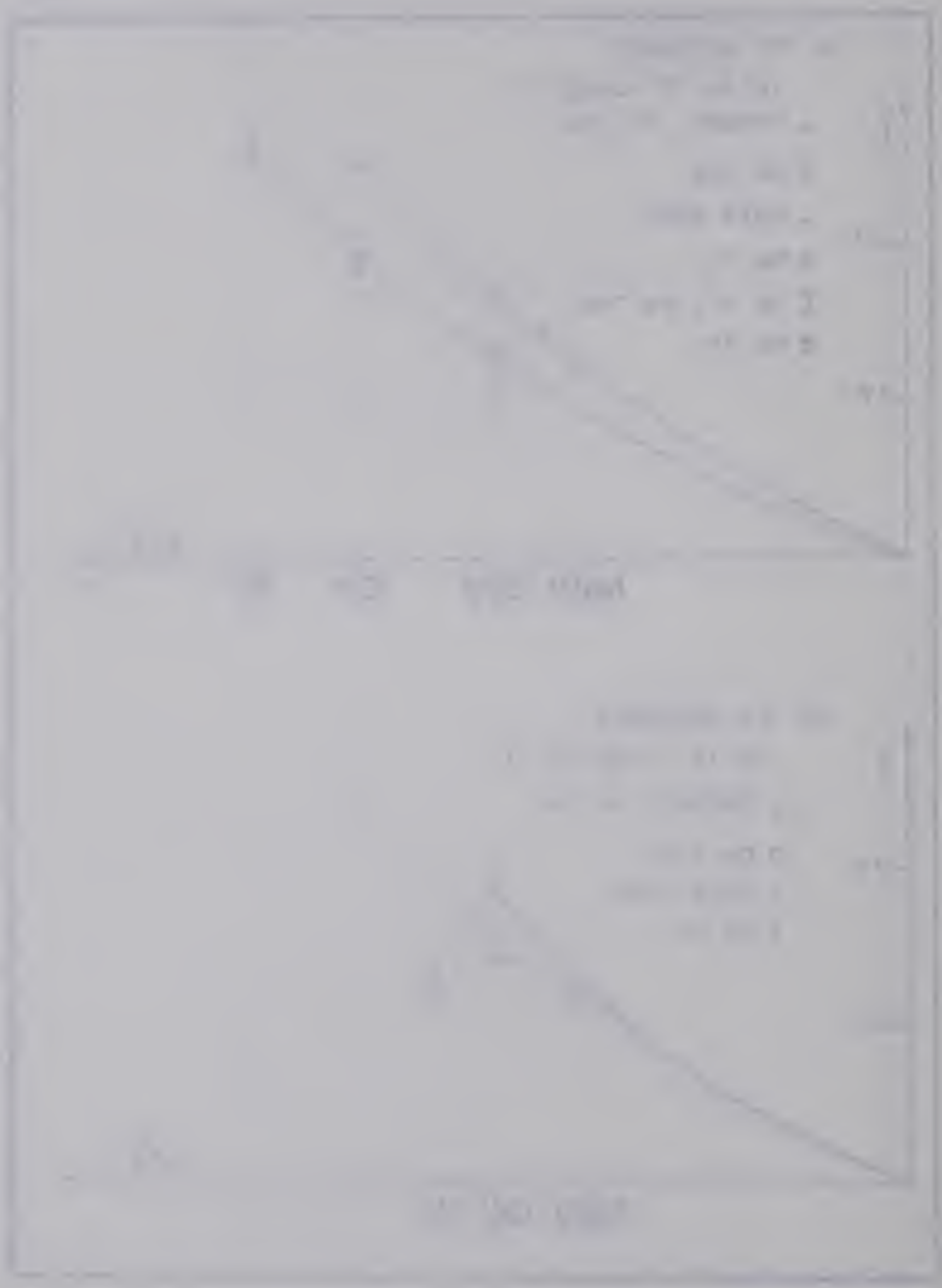

Z-dependence plot. This is particularly useful for the highly ionized ions because of the difficulty in producing these species. The available f-values, both theoretical and experimental, are rare at the present. Much work remains to be done before a complete establishment of the Z-dependence trend for the known transitions will be possible.

CHAPTER VIII

SUMMARY

The beam-foil technique has been employed to measure the radiative lifetimes of excited oxygen levels. Over 100 lines were observed in the wavelength range 370 - 5000 Å. The ionization stages of the ions detected ranged from OI to OV, with OII and OIII being the most populous. The lifetimes were measured at 0.6 - 1.4 MeV O_2^+ incident beam energies. The analysis was based on the beam velocity measured directly from the beam by observing the Doppler shifts. Lifetimes as short as 0.1 nsec were measured with an accuracy of about ± 10%. The decomposition of the decay into two, or sometimes three, components for the lines which appeared to be multi-exponential was made with a computer least-square fitting program.

Charge identifications were mostly made by the intensity variation method. The charge deflection method was also employed in the visible region and confirmed the assignments for many strong lines.

About ten carbon lines in CI through CIII were detected. That the carbon ions were ejected from the foil was verified by a direct measurement of the ion velocity, which was small in comparison to the ions

accelerated by the machine. Seventeen lines were identified as new oxygen lines which had not been observed previously in more conventional light sources, mostly being due to OIII.

The results are generally in good agreement with other workers' values. Disagreements happen only when severe cascading or blending is involved, where the assignment becomes uncertain and the degree of cascade is different for each experiment. The reliability of the lifetime value for each multiplet is discussed and compared to other measurements. The possibilities of cascading and blending for each line are also investigated.

Some of the lifetimes have been transformed into oscillator strengths. The systematic trends of f-values in isoelectronic sequences have been studied wherever the f-values in the sequence are available from other beam-foil measurements. Some theoretical values are also included for comparison.

More than twenty laboratories are now engaged in beam-foil work and at least forty elements have been used for the research (Ba 70). The technique has been proved to be a powerful approach for lifetime measurements, yet the lifetime data are still far from complete. Many investigations about the beam-foil technique remain to be done. Some of the interesting problems which can be studied are:

a) foil structure and excitation mechanism.

The process of the excitation and the effects

of the foil thickness and foil material on the excitation have rarely been studied. Investigation of this problem may lead to important conclusions for the beam-foil interaction.

b) ejected carbon and hydrogen ions. The ejected ions have been observed by several laboratories but no systematic study has been attempted. Observations of the spatial and velocity distributions of the ejected ions may clarify the cause and process of the ejection.

c) foil-aging or beam intensity effects on lifetime values. The problem of foil aging was first reported by Bickel (Bi 68b), and the effect of the beam intensity on the lifetime by Oona and Bickel (Oo 70). The causes of these effects are not well understood and other factors such as foil material, foil thickness and incident beam energy may have some effect and need to be investigated.

d) weak intensity and broad lines. These problems make measurements inaccurate and identification difficult. Furthermore, the lifetime data is limited only to strong multiplets. The development of an optical system that would reduce Doppler broadening and collect more photons, or the development of a more sensitive photon detector, say with higher quantum efficiency and lower dark noise, would improve the capability of the technique greatly.

e) identifications of new lines. Assignments for new lines are usually not certain. Experiments

leading to line identifications, such as charge deflection and Zeeman effect experiments would be very useful and important, particularly for highly-ionized ions for which the conventional studies are so incomplete. Improved theoretical calculations of the unclassified energy levels will be necessary in future beam-foil research.

f) the second order Doppler shift. The second order Doppler shift can be verified, at least qualitatively, by measuring the wavelength shifts in a direction perpendicular to the beam for different energies. The alignment of the optics may not be exactly perpendicular, hence the first order shifts will still be seen. However, the first order shift is linear with respect to the beam velocity. Thus appreciable deviations of the shift from linearity would provide measurements of the second order shift. The H_α line at 6563 Å should have second order shifts of 1.8, 3.5 and 7.0 Å for 0.5, 1.0 and 2.0 MeV H_2^+ beams, respectively, which could be easily detected.

REFERENCES

An 68 T. Andersen, K. A. Jessen and G. Sorensen, Phys. Letters 28A (1968) 459

Ba 64 S. Bashkin, L. Heroux and J. Show, Phys. Letters 13 (1964) 229

Ba 65 S. Bashkin, Science 148 (1965) 1047

Ba 66a S. Bashkin U. Fink. P. R. Malmberg, A. B. Meinel and S. G. Tilford, J. Opt. Soc. Am. 56 (1966) 1064

Ba 66b S. Bashkin, R. K. Wangsness and L. Heroux, Phys. Rev. 151 (1966) 87

Ba 70 S. Bashkin, Nucl. Inst. Meth. 90 (1970) 3

Be 69 I. Bergstrom, J. Bromander, R. Buchta, L. Lundin and I. Martinson, Phys. Letters 28A (1969) 721

Be 70a H. G. Berry, I. Martinson and J. Bromander, Phys. Letters 31A (1970) 521

Be 70b H. G. Berry, W. S. Bickel, I Martinson R. J. Weymann and R. E. Williams, Astrophys. Letters 5 (1970) 81

Bi 66 W. S. Bickel and A. S. Goodman, Phys. Rev. 148 (1966) 1

Bi 67a W. S. Bickel, Appl. Opt. 6 (1967) 1309

Bi 67b W. S. Bickel and S. Bashkin, Phys. Rev. 162 (1967) 12

Bi 68a W. S. Bickel, J. Opt. Soc. Am. 58 (1968) 213

Bi 68b W. S. Bickel, in Beam-Foil Spectroscopy, edited by S. Bashkin (Gordon and Breach, New York, 1968), Vol. I, p. 233

Bi 69 W. S. Bickel, H. G. Berry, I. Martinson, R. M. Schectman and S. Bashkin, Phys. Letters 29A (1969) 4

Br 62 L. Brewer, Rev. Sci. Inst. 33 (1962) 1450

Br 63 L. Brewer, R. A. Berg and G. M. Rosenblatt, J. Chem. Phys. 38 (1963) 1381

Br 70 K. B. Bromander, Arkiv för Fysik Bd 40 nr 23 (1070) 257

Ca 70 G. W. Carriveau and S. Bashkin, Nucl. Inst. Meth. 90 (1970) 203

Ce 70 P. Ceyzeriat, A. Denis, J. Desesquelles, M. Druetta and M. C. Poulizac, Nucl. Inst. Meth. 91 (1970) 103

Ch 68 E. L. Chupp, L. W. Dotchin and D. J. Pegg, Phys. Rev. 175 (1068) 44

Cu 68 B. Curnutte, W. S. Bickel, R. Girardeau and S. Bashkin Phys. Letters 27A (1968) 680

Cu 70 L. J. Curtis, H. G. Berry and J. Bromander, Physica Scripta 2 (1970) 216

De 69a A. Denis, J. Desesquelles and M. Dufay, J. Opt. Soc. Am. 59 (1969) 976

De 69b A. Denis, C. R. Acad. Sc. Paris 268 (1969) 383

De 70 J. Desesquelles, Ph. D. Thesis, Lyon Univ., (1970)

De 70a A. Denis, P. Ceyzeriat and M. Dufay,
J. Opt. Soc. Am. 60 (1970) 1186

Di 63a R. W. Dichburn, Light
(Blackie & Son, London, 1963) 711

Di 63b R. W. Ditchburn, Light
(Blackie & Son, London, 1963) 686

Dr 69 M. Druetta and M. C. Poulizac,
Phys. Letters 29A (1969) 651

Dr 70 M. Druetta, M. C. Poulizac and J. Desesquelles,
J. Opt. Soc. Am. 60 (1970) 1463

Dr 71 M. Druetta, M. C. Poulizac and M. Dufay,
J. Opt. Soc. Am. 61 (1971) 515

Du 70 M. Dufay, Nucl. Inst. Meth.90 (1970) 15

Ev 55a R. D. Evans, The Atomic Nucleus
(McGraw-Hill Book Company, 1955) 786

Ev 55b R. D. Evans, The Atomic Nucleus
(McGraw-Hill Book Company, 1955) 750

Fi 68 U. Fink, G. N. McIntire and S. Bashkin,
J. Opt. Soc. Am. 58 (1968) 465

Fi 68a U. Fink, J. Opt. Soc. Am. 58 (1968) 937

Fi 68b U. Fink, Appl. Opt. 7 (1968) 2373

F0 64 E. W. Foster, Reports on Progress in Phys.
27 (1964) 469

Ga 68 M. Gaillard and J. E. Hesser,
Astrophys. J. 152 (1968) 685

He 68 L. Heroux, in Beam-Foil Spectroscopy, edited by
S. Bashkin (Gordon and Breach, New York, 1968),
Vol. I, p. 205

He 69 L. Heroux, Phys. Rev. 180 (1969) 1

Ka 63 L. Kay, Phys. Letters 5 (1963) 36

Ka 65 L. Kay, Proc. Phys. Soc. 85 (1965) 163

Ka 67 K. Karstensen and J. Schramm,
J. Opt. Soc. Am. 57 (1967) 654

Ke 68 R. L. Kelly, Atomic Emission Lines Below 2000 Angstroms, NRL Report 6648 (U. S. Govt. Printing Office, Washington, D. C., 1968)

Ki 66 J. Z. Klose, Phys. Rev. 141 (1966) 181

La 66 G. M. Lawrence and B. D. Savage,
Phys. Rev. 141 (1966) 67

La 70 G. M. Lawrence, Phys. Rev. A2(2) (1970) 397

Le 67 M. R. Lewis, T. Marshall, E. H. Carnevale, F. S. Zimnoch and G. W. Wares, Phys. Rev. 164 (1967) 94

Le 69 M. R. Lewis, F. S. Zimnoch and G. W. Wares,
Phys. Rev. 178 (1969) 49

Li 69 J. Linderberg, Phys. Letters 29A (1969) 467

Ma 29 L. R. Maxwell, Phys. Rev. 34 (1929) 199

Ma 31 L. R. Maxwell, Phys. Rev. 38 (1938) 1664

Ma 65 P. R. Malmberg, S. Bashkin and S. G. Tilford,
Phys. Rev. Letters 15 (1965) 98

Ma 70 I. Martinson, W. S. Bickel and A. Ölme.
J. Opt. Soc. Am. 60 (1970) 1213

Ma 71 I. Martinson, H. G. Berry, W. S. Bickel and H. Oona,
J. Opt. Soc. Am. 61 (1971) 519

Mi 70 D. L. Mickey, Nucl. Inst. Meth. 90 (1970) 77

Mo 49 C. E. Moore, Atomic Energy Levels, Vol. I, NBS Circular 467 (U. S. Govt. Printing Office, Washington, D. C., 1949)

Mo 50 C. E. Moore, An Ultraviolet Multiplet Table, NBS Circular 488 (U. S. Govt. Printing Office, Washington, D. C., 1950)

Mo 59 C. E. Moore, A Multiplet Table of Astrophysical Interest, NBS Technical Note 36 (U. S. Govt. Printing Office, Washington, D. C., 1959)

Ni 68 L. L. Nichols and W. E. Wilson, Appl. Opt. 7 (1968) 167

Oo 70 H. Oona and W. S. Bickel, Nucl. Inst. Meth. 90 (1970) 223

Pe 35 R. Peierls, Proc. Roy. Soc. (London) A149 (1935) 467

Pe 70a D. J. Pegg, L. W. Dotchin and E. L. Chupp, Phys. Letters 31A (1970) 501

Pe 70b D. J. Pegg, E. L. Chupp and L. W. Dotchin, Nucl. Inst. Meth. 90 (1970) 71

Pi 69a E. H. Pinnington and Chii-Chan Lin, J. Opt. Soc. Am. 59 (1969) 717

Pi 69b E. H. Pinnington and Chii-chan Lin, J. Opt. Soc. Am. 59 (1969) 780

Pi 70 E. H. Pinnington, Nucl. Inst. Meth. 90 (1970) 93

Po 69 M. C. Poulizac, M. Druetta and P. Ceyzeriat, Phys. Letters 30A (1969) 87

Sm 69 P. L. Smith and W. Whaling, Phys. Rev. 188 (1969) 36

Sm 70 W. H. Smith, Nucl. Inst. Meth. 90 (1970) 115

Sm 71 W. H. Smith, J. Bromander, L. J. Curtis, H. G. Berry and R. Buchta, Astrophys. J. 165 (1971) 217

St 68 a. R. Striganov and N. S. Sventitskil, Table of Spectral Lines of Neutral and Ionized Atoms (IFI/Plenum, New York, 1968)

St 70 J. O. Stoner, Jr. and J. A. Leavitt (unpublished)

St 71 J. O. Stoner, Jr. and J. A. Leavitt, Appl. Phys. Letters, 18 (1971) 368

We 69a A. W. Weiss, Phys. Rev. 188 (1969) 119

We 69b P. Westhaus and O. Sinanoglu, Phys. Rev. 183 (1969) 56

Wi 66 W. L. Wiese, M. W. Smith and B. M. Glennon, Atomic Transition Probabilities, NSRDS-NBS 4-1 (U. S. Govt. Printing Office, Washington, D. C., 1966)

Wi 68a W. L. Wiese and A. W. Weiss, Phys. Rev. 175 (1968) 50

Wi 68b W. L. Wiese, Appl. Opt. 7 (1968) 2361

APPENDIX I

THE LEAST-SQUARES-CURVE-FITTING PROGRAM

Object

To fit the input data to a single or double exponential decay by a trial and error method. The program is to find the intensities and lifetimes for the components that minimize the quantity, D, given by

$$D = \sum_{i=1}^{N} \frac{(B(i) - S(i))^2}{B(i)}$$

where B(i) are signals calculated from the trial parameters and S(i) are the observed signals less the background noise.

Limitation on Parameters

Number of data points: $N \leq 40$

Number of sets of data: Unlimited

Order of Input

1. Beam velocity card

col. 1-5	Beam velocity (turns/nsec)	F5.3

2. Identification card

col. 1-6	Wavelength of the line	F6.1
col. 7-12	Number of data points	I6
col. 13-18	Estimated intensity I_1	F6.0
col. 19-24	Estimated lifetime τ_1	F6.2
col. 25-30	Estimated intensity I_2	F6.0
col. 31-36	Estimated lifetime τ_2	F6.2
col. 37-42	Averaged background	F6.0

$$\frac{}{}$$

3. Foil position cards

   Col. 1-5, 6-10 ... Foil positions 20I4

   (Two cards if number of data points is greater than 20)

4. Signal cards

   Col. 1-5, 6-10 ... Signals 20F4.0

   (Two cards if number of data points is greater than 20)

5. Repeat (2) to (4) for each set of data taken at the same beam velocity.

Output

Wavelength, intensities and lifetimes for the components as labeled on the top line of the output. The values for α and β as defined by Eqs. (5.9) and (5.10) are also printed.

The program

```
      DIMENSION A1(5),A2(5),T1(5),T2(5),X(40),S(40),NX(40)
   80 FORMAT(/'WAVELENGTH',15X,'A',10X,'T1',16X,'B',10X,
     1'T2',16X,DEVIATION'/)
  100 FORMAT(F6.1,I6,F6.0,F6.2,F6.0,F6.2,F6.0,F6.3)
  101 FORMAT(20F4.0)
  102 FORMAT(20I4)
      WRITE(6,80)
   10 READ(5,100,END=300) W,ND,AI1,TT1,AI2,TT2,BG,SPEED
      TT1=TT1*SPEED
      TT2=TT2*SPEED
      IF(ND.GT.20) READ(5,102) (NX(I),I=1,20)
      IF(ND.GT.20) READ(5,102) (NX(I),I=21,ND)
      IF(ND.LE.20) READ(5,102) (NX(I),I=1,ND)
      IF(ND.GT.20) READ(5,101) (S(I),I=1,20)
      IF(ND.GT.20) READ(5,101) (S(I),I=21,ND)
      IF(ND.LE.20) READ(5,101) (S(I),I=1,ND)
      DO 3 I=1,ND
      X(I)=NX(I)
      X(I)=X(I)/100.
    3 CONTINUE
      SUMS=0.
      DO 16 I=1,ND
```

```
      S(I)=S(I)-BG
      SUMS=SUMS+S(I)
   16 CONTINUE
      XND=ND
      KK=0
      DIVI=10000000.
      DA1=AI1/4.
      DT1=TT1/2.
      DA2=AI2/4.
      DT2=TT2/2.
   20 DO 40 J=1,5
      AJ=J
      A1(J)=AI1-DA1*0.5*(3.0-AJ)
      T1(J)=TT1-DT1*0.5*(3.0-AJ)
      A2(J)=AI2-DA2*(3.0-AJ)
      T2(J)=TT2-DT2*0.5*(3.0-AJ)
   40 CONTINUE
      IF(ABS(AI2).LT.50.) A2(1)=0.
      IF(ABS(AI2).LT.50.) MM=1
      IF(ABS(AI2).GT.50.) MM=5
      DO 60 M=1,MM
      DO 60 L=1,MM
      DO 60 K=1,5
      DO 60 J=1,5
      DIV=0.
      D0 50 I=ND
      V=A1(J)*EXP(-X(I)/T1(K))+A2(L)*EXP(-X(I)/T2(M))
      SB=AMIN1 (S(I),B,BG)
      DIV=DIV+(B-S(I))**2/B
   50 CONTINUE
      IF(DIV.GT.DIVI) GO TO 60
      IF(DIV.LT.DIVI) DIVI=DIV
      IF(DIV.EQ.DIVI) AI1+A1(J)
      IF(DIV.EQ.DIVI) TT1=T1(K)
      IF(DIV.EQ.DIVI) AI2=A2(L)
      IF(DIV.EQ.DIVI) TT2=T2(M)
   60 CONTINUE
      DA1=DA1*0.5
      DA2=DA2*0.5
      DT1=DT1*0.5
      DT2=DT2*0.5
      KK=KK+1
      IF(KK.LT.6) G) TO 20
      DIV1=DIVI/(SUMS*XND)**0.5
      DIV2=DIVI/XND
      TT1=TT1/SPEED
      TT2=TT2/SPEED
      IF(ABS(AI2).GT.50.) WRITE(6,200) W,AI1,TT1,AI2,TT2,
     1DIV1,DIV2
      IF(ABS(AI2).LT.50.) WRITE(6,201) W,AI1,TT1,DIVI,
     1DIV2
      GO TO 10
  200 FORMAT(F10.2,10X,2F10.2,10X,2F10.2,10X,2F10.5)
  201 FORMAT(F10.2,10X,2F10.2,40X,2F10.5)
  300 STOP
      END
```

APPENDIX II

THE ALLOWED TRANSITION PROGRAM

Object

To compute all allowed transitions between the listed energy levels according to the selection rules:

1. parity changed
2. $\Delta S = 0$
3. $\Delta L = 0, \pm 1, \pm 2$
4. $\Delta J = 0, \pm 1$ ($0 \rightarrow 0$ excluded)

Limitation on Parameters

Number of energy levels: NL $\leq$ 250

Number of sets of data: Unlimited

Order of Input

1. Number of energy levels card

col. 1-3	Number of energy levels	I3

2. energy level cards

col. 9	Value of 2S + 1	I1
col. 10	Value of L	I1
col. 11	Parity (Odd=1, even=0)	I1
col. 12-13	Value of J X 10	I2
col. 14-22	Level (cm^{-1})	F9.2

One card for each level

3. Repeat (1) and (2) for each ion

Output

Wavelengths of all allowed transitions and the upper and lower levels.

The Program

```
      DIMENSION DESIGN(250),JS(250),L(250),IP(250),
     1ELEVEL(250),J10(250)
      DIMENSION W(5000),ELVL(5000),ELV(5000)
   10 READ(5,100,END=300)NL
  100 FORMAT(I3)
      DO 50 I=1,NL
   50 READ(5,101) JS(I), L(I),IP(I),J10(I),ELEVEL(I)
      WRITE(6,102) JS(NL),L(NL),IP(NL),J10(NL),ELEVEL(NL)
  101 FORMAT(8X,3I1,I2,F9.2)
  102 FORMAT(10X,A8,3I1,I2,F9.2)
      LT=0
      NLI=NL-1
      D0 11 I=1,NL1
      I1=I+1
      DO 10 J=I1,NL
      IPD=IABS(IP (I)-IP(J))
      IF(IPD.NE.1) GO TO 10
      JSD=IABS(JS(I)-JS(J))
      IF(JSD.NE.0.AND.JSD.NE.1) GO TO 10
      LD=IABS(L(I)-L(J))
      IF(LD.NE.0.AND.LD.NE.1.AND.LD.NE.2) GO TO 10
      JD10=IABS(J10(I)-J10(J))
      IF(JD10.NE.0.AND.JD10.NE.10) GO TO 10
      IF(J10(I).EQ.0.AND.J10(J).EQ.0) GO TO 10
      LT=LT+1
      W(LT)=L./(ELEVEL(J)-ELEVEL(I))*10.**8
      ELVL(LT)=ELEVEL(I)
      ELV(LT)=ELEVEL(J)
   10 CONTINUE
   11 CONTINUE
      DO 20 K=2,LT
      K1=K-1
      IF(W(K).LE.W(K1)) GO TO 20
      IF(W(K).GE.W(1)) GO TO 16
      DO 14 KK=1,k1
      IF(W(K).LT.W(KK).AND.W(K).LT.W(KK+1)) GO TO 14
      M=KK+1
      GO TO 17
   14 CONTINUE
   16 M=1
   17 WW=W(K)
      EEI=ELVL(K)
      EEJ=ELV(K)
      KM=K-M
      DO 18 LL=1,KM
      LN=K-LL+1
      ELVL(LN)=ELVL(LN-1)
```

```
      ELV(LN)=ELV(LN-1)
   18 W(LN)=W(LN-1)
      ELVL(M)=EEI
      ELV(M)=EEJ
      W(M)=WW
   20 CONTINUE
      DO 60 I=1,LT,3
   60 WRITE(6,200) W(I),ELV(I),ELVL(I),W(I+1),ELV(I+1),ELVL
     1(I+1),W(I+2),ELV(I+2),ELVL(I+2)
      GO TO 10
  200 FORMAT(10X,9F12.2)
  300 STOP
      END
```